Systemic Bone Loss Following Myocardial Infarction

By

PRISCILLA MERCY TJANDRA

DISSERTATION

Submitted in partial satisfaction of the requirements for the degree of

DOCTOR OF PHILOSOPHY

in

Biomedical Engineering

in the

OFFICE OF GRADUATE STUDIES

of the

UNIVERSITY OF CALIFORNIA

DAVIS

Approved:

_____

Dr. Blaine A. Christiansen, Chair

_____

Dr. Crystal M. Ripplinger

_____

Dr. David P. Fyhrie

Committee in Charge

2023

ACKNOWELDGEMENTS

First and foremost, I would like to thank Dr. Blaine Christiansen, Dr. Crystal Ripplinger, and Dr. Dave Fyhrie for your invaluable advice and support throughout my PhD journey. Thank you for your patience and your commitment. Blaine, I would like to express additional gratitude. My progress through grad school has been non-linear in every way possible. The process of transitioning from the rigid structure of undergrad, through my own personal hurdles, and eventually through the pandemic was terrifying, complicated, and confusing. Thank you so much for your patience, your guidance when I got stuck, and for your trust in me to get to where I needed to be.

I would also like to thank my past and present lab mates for always being available whenever I needed extra support on my project, even during odd hours. Your generosity with your time has been invaluable to me. A special acknowledgement to Sophie for all your work in creating and fostering an inclusive and holistic lab environment. I can't begin to express how impactful it was to me.

The journey through graduate school was not an easy one for me. Beyond the work I have written in my thesis, I had many personal challenges of my own and I wouldn't have been able to face it alone. To the faculty and PhD students at the Asian American Studies department, thank you for being so welcoming to a BME PhD student from the other side of campus and connecting me to my community. You have pushed me to never lose sight of what we're fighting for. Thank you, Edgar, for inspiring me to continue activism regardless of whatever field I may end up.

To my friends Manali, Sara, and Lena, you've always been so willing to help me write intimidating emails, sit through practice presentations, and be a voice of reason when I was unreasonable. Thank you so much for always giving me new perspectives and for making my time here an enjoyable one.

To my family, thank you for doing everything you could to make my time here easier. I know it must have been difficult to support me from a different state, but you found a way and I'm forever grateful for it. Thank you especially, Phyll! I'm glad I got you into BTS because being able to share and experience their concerts, music, and messages with you has been a highlight of my 20's. Thank you for giving me an outlet to experience the world of K-pop because I really wouldn't have survived without it.

And of course, thank you Kelv for your unwavering support. You have been with me since the very beginning. You've been a great source of strength and safety through my hardest challenges and greatest wins. Thank you so much for being by my side. I may have felt like the world was falling apart at times, but I never felt alone.

Lastly, thank you Elliot, Jane, and Bucky and presently, Moody and Miri, for your unconditional love and companionship. I can't even begin to express how you were and continue to be one of my biggest sources of motivation and the reason I look forward to coming home.

TABLE OF CONTENTS

LIST OF FIGURES

List of Tables

ABSTRACT

Myocardial infarction (MI) and osteoporotic fracture are the two leading causes of morbidity and mortality worldwide. These events are etiologically linked but current theories are limited to correlation of advanced stages of their underlying disease, atherosclerosis and osteoporosis (OP). To effectively inform treatments post-MI, it is crucial to investigate the possibility of a causative relationship between MI and OP. It has been established that MI causes a strong inflammatory response, and that bone is sensitive to inflammation. This suggests that an acute, systemic inflammatory response could link adaptive responses of the cardiovascular and skeletal systems, but further investigation is necessary. Two post-injury responses have shown promise as potential mediators of MI and bone loss; the sympathetic nervous system (SNS) and the complement system. Both are primary mediators of inflammation after MI, and both can affect bone by the upregulation of osteoclastogenesis. However, no studies have established these systems as mediator if MI-induced bone loss. To address these issues, we investigated the effect of MI trauma on the skeletal response in the absence of any underlying conditions. Furthermore, we determined the role of the SNS and complement system in this response. The aim of the works was to establish a causative relationship between MI and bone loss, characterize the magnitude and time course of MI-induced bone loss, and determine if SNS or complement inhibition could attenuate bone loss.

In this study, we surgically induced MI in mice and analyzed systemic and localized bone changes across multiple time points. Analysis included quantifying whole body

bone mineral density using dual x-ray absorptiometry (DXA), assessing whole bone and mineral properties through 3-point bending, and measuring trabecular and cortical changes in the axial (L5 vertebra) and appendicular (femur) using micro-computed tomography (μCT). We also analyzed voluntary activity after operation to rule out any changes due to differences in mechanical loading. To determine the significance of the SNS, we used a β3-adrenoreceptor antagonist to inhibit SNS activity. To determine the role of the complement system we used transgenic mice that did not express the complement protein 5a receptor 1 (C5aR1-/-) as well as an additional group of B10.D2 C5a deficient mice.

We found that in the absence of underlying chronic conditions, MI directly causes systemic bone loss and that the bone loss peaks at 7 days post-MI and recovers to baseline at later time points. We further found changes in activity were not significantly different between MI and unoperated groups. Mechanistically, we determined that inhibiting the b3-adrenoreceptor attenuated bone loss. When comparing C5aR1-/-, B10.D2, and WT mice, we found baseline differences in trabecular and cortical bone morphology and that C5aR1-/- mice had less bone loss after MI compared to WT, but the B10.D2 C5a deficient mice did not. These results are the first of their kind to investigate the possibility of bone loss as a significant comorbidity of MI. Uncovering the etiology of this phenomenon will allow us to inform treatments aimed at preserving lifelong health following traumatic injury in more vulnerable patients.

CHAPTER 1: BACKGROUND

1.1. Significance – Myocardial Infarction and Osteoporosis

Myocardial infarction (MI) and osteoporotic fracture (Fx) are the leading causes of mortality and morbidity worldwide[1]. Over 20% of patients will die within 1 year following hip fracture[2,3] and over 30% will die within 5 years[4,5]. Similarly, within 5 years of a first MI, 36% of men and 47% of women will die due to MI-related complications[6]. In recent decades, the incidences of MI have shifted towards populations where OP is prevalent, particularly in post-menopausal women[7]. As a result, these diseases are often seen as comorbidities[8,9] and there has been emerging evidence that these diseases are linked to each other.

Epidemiological data show that MI is associated with increased risk of subsequent fragility fracture (Fx) and vice versa[10–12]. Chiang et al. followed patients 10 years after fracture and found that the fracture group had increased cumulative incidences of acute MI compared to the unfractured control[13] (**Figure 1.1A**). Similarly, a study done by Gerber et al. found the converse to be true. Within a 5 year follow up, patients with MI had lower fracture-free survival in comparison to the non-MI controls[10] (**Figure 1.1B**). These studies suggest that there is a link between MI and Fx.

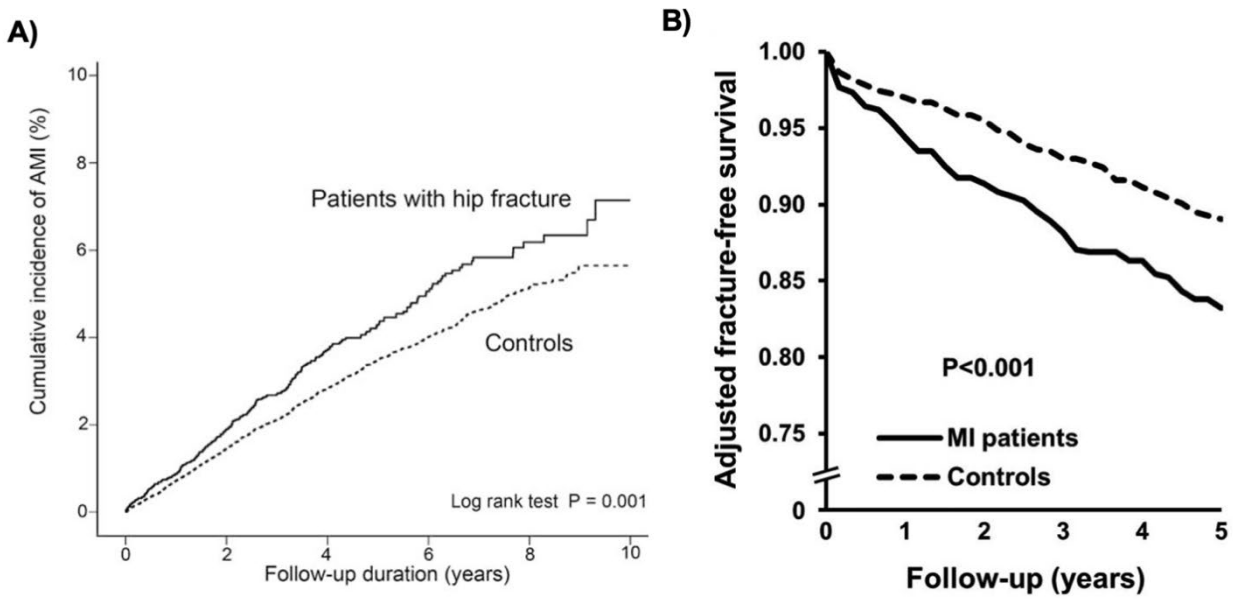

Figure 1.1 Correlations between MI and fracture in epidemiological studies. **A)** Steeper, increasing slope in patients with hip fracture indicates increased incidences of MI compared to control over 10 years[13]. **B)** Steeper, decreasing slope indicates lower fracture-free survival with patients after MI over 5 years[14].

1.2. Biology of MI and Bone Loss

To understand this link, it's important to first to define MI and Fx as acute events. Unlike chronic pathological states such as atherosclerosis or osteoporosis, which will be discussed in the following paragraphs, MI and Fx occur quickly, and the resulting damage occurs during that specific event.

1.2.1 Myocardial Infarction (MI)

MI is the trauma that occurs when a coronary artery is fully occluded, resulting in the total cessation of blood flow to the myocardium. The most common cause of MI is due to atherosclerosis, a chronic disease characterized by the hardening of arterial walls

due to plaque buildup. If left untreated, plaque in the coronary arteries can rupture and cause a blood clot that blocks blood flow to the surrounding tissue as shown in **Figure 1.2**. The resulting cardiac cell damage, or ischemia, will initiate a robust systemic inflammatory response to counteract the damage. However, if this response is prolonged, it can lead to adverse system effects. Clinically, this presents itself as impaired cardiac function leading to heart failure and, in some cases, cardiac rupture resulting in sudden death[14].

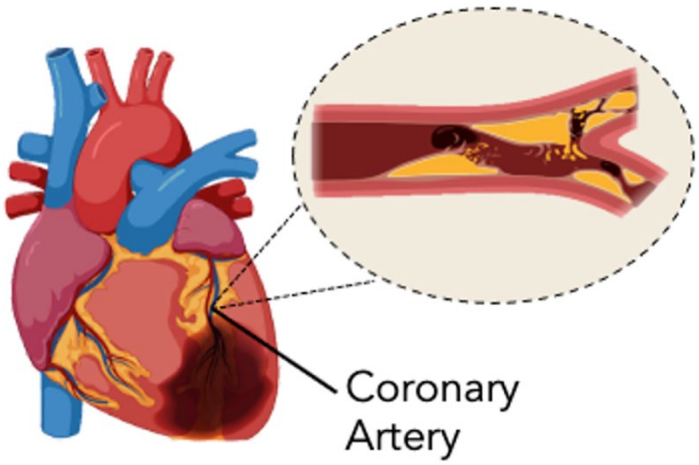

Figure 1.2 MI occurs when the coronary artery is completely occluded as is shown on the right. Cardiac cells surrounding the MI will die due to lack of oxygen.

1.2.2. Osteoporosis

Like MI and atherosclerosis, the trauma from fragility fractures (Fx) occurs due to an underlying chronic condition called osteoporosis. Osteoporosis is characterized by decreased bone mineral density and bone mass. This results in changes to the structure and strength of bone and ultimately increases the risk of fracture[15]. Mechanistically, osteoporosis occurs due to an imbalance in bone remodeling. Two

cells are integral in this process: osteoclasts for bone resorption and osteoblasts for bone formation. Proliferation and activation of these cells occur through cytokines, chemical factors secreted by cells leukocytes or by osteoblasts themselves. Specific cytokines will be discussed in later sections. During homeostasis, regulation and activity of osteoclasts and osteoblasts are balanced. However, during osteoporosis, a combination of these activities occurs and causes a bias towards lower bone mineral density, leading to increased bone fragility and risk of Fx[16,17].

1.3. Relationship Between Cardiovascular Diseases (CVD) and Osteoporosis

Although from seemingly exclusive systems, studies have shown cardiovascular diseases (CVD) and skeletal diseases have biological similarities that could explain the correlation between MI and osteoporosis incidences. Both diseases have shared risk factors such as smoking, alcohol intake, and menopause. However, an epidemiological studies review done by Farhat et al., found that the association between the two diseases were present even after adjusting for these etiological factors[11], suggesting that there are shared biological mechanisms that could explain the relationship between the two systems. Factors such as vitamin K, vitamin D, parathyroid hormone (PTH), and inflammatory cytokines have been shown to affect both bone and cardiovascular regulation and will be discussed in the following section[11,18].

1.3.1. Vitamin K

In bone, Vitamin K plays a role in regulating genetic transcription of osteoblast markers and bone reabsorption. Studies have found that low vitamin K levels in the serum is

associated with higher risk of fracture and lower BMD[19]. Alternatively, low levels of vitamin K were associated with markers of arterial stiffness and more severe atherosclerotic calcification[11,20] It's speculated that the contradictory calcification effects of low vitamin K in the skeletal and cardiovascular tissue is due to two vitamin K dependent proteins; osteocalcin and anti-calcific protein matrix Gla protein (MGP). The link between osteocalcin and osteoblast activity has been well-established, but the effects of osteocalcin and MGP together is not as well-known and could cause simultaneous calcification in the vasculature as well as decreased OB activity in the bone[11].

1.3.2. Vitamin D

Like vitamin K, low levels of vitamin D exacerbates the pathogenesis of osteoporosis and cardiovascular disease[11]. Vitamin D regulates calcium levels by stimulating absorption of calcium from the gut[21,22]. Clinically, low levels of vitamin D have been linked to lower BMD and increased risk of fracture whereas vitamin D supplementation decreased fracture incidences[21]. Vitamin D receptors are also found in the cardiovascular systems, primarily the endothelial and smooth muscle cells. It is proposed that vitamin D can regulate blood pressure through several mechanisms including the renin-angiotensin-aldosterone system activation or altered inflammatory pathways, but the literature is not well-established. Furthermore, deficiency of vitamin D could be predictors of cardiovascular disease and heart failure[23].

1.3.3. Parathyroid Hormone (PTH)

PTH is one of the main regulators of calcium homeostasis as it stimulates the release of calcium and phosphate from the bones. Its function is often coupled with vitamin D. Deficiency of vitamin D causes decreased calcium uptake and absorption from the gut. As a result, PTH levels increase to supply the body with calcium taken from the skeletal system instead. Elevated levels of PTH contribute to age-related bone loss and increased risk of fracture[11]. Increased levels of PTH have also been clinically linked to heart failure[24]. Although specific mechanisms haven't been well-established, there are multiple mechanisms that could explain this association. It has been found that higher PTH promotes endothelial dysfunction and increase aortic stiffness as well as being linked to arterial hypertension[24].

1.3.4. Pro-Inflammatory Cytokines

There are shared pro-inflammatory cytokines that have significant effects on both cardiovascular and skeletal regulation, including interleukin-1 (IL-1), tumor necrosis factor alpha (TNF-alpha), and interleukin-6 (IL-6). These three are integral in the regulation of bone resorption[25]. IL-1 and TNF-alpha are powerful initiators of bone resorption. TNF-alpha promotes bone resorption indirectly through osteoblasts by stimulating proliferation and differentiation of osteoclast precursors through RANK, which will be discussed in further detail below. TNF-alpha is also an inhibitor of bone formation and induces other pro-osteoclastogenic cytokines including IL-6[26,27]. Although not as powerful, IL-6 is able to effect bone resorption by increasing the number of osteoclast progenitors[27]. High levels of IL-6 have been found in diseased states with excessive bone resorption, suggesting that it could play a significant role in its

pathogenesis[25]. Epidemiologically, studies have found high levels of IL-1, TNF-alpha, and IL-6 in osteoporotic states[28]. In the cardiovascular system, IL-1, TNF-alpha, and IL-6 are found in abundance after MI[29]. They are essential in the cytokine cascade to increase leukocyte recruitment to areas of injury. Additionally, IL-6 levels are also a marker for subclinical CVD. Similarly, TNF-alpha has been associated with incidences of cardiovascular events. Among others, IL-1, TNF-alpha, and IL-6 have been found to be significant mediators in atherosclerotic states[30].

Another key regulator of osteoclast activity is the RANKL/RANK/OPG system. RANKL (receptor activator of NF-kappaB ligand (RANKL) and osteoprotegerin (OPG) are members of the TNF superfamily and secreted by osteoblasts. When RANKL binds to its receptor RANK on osteoclast precursors, it activates osteoclast differentiation and ultimately increases osteoclast activity. Conversely, OPG inhibits osteoclast differentiation by binding to RANKL and preventing its interaction with RANK[31] (**Figure 1.3**). Like TNF-alpha and IL-6, high levels of RANKL/OPG ratio in bone marrow are associated with diseases characterized by excessive bone resorption. Mechanistically, the pro-osteoclastic effect cytokines such as TNF-alpha and IL-6 is due to the modulation of the RANKL/RANK/OPG system[11,31]. Low levels of OPG have been associated with calcification of arteries and coronary artery disease. Although not well understood, studies have suggested that OPG has a protective effect from calcification in arteries[11].

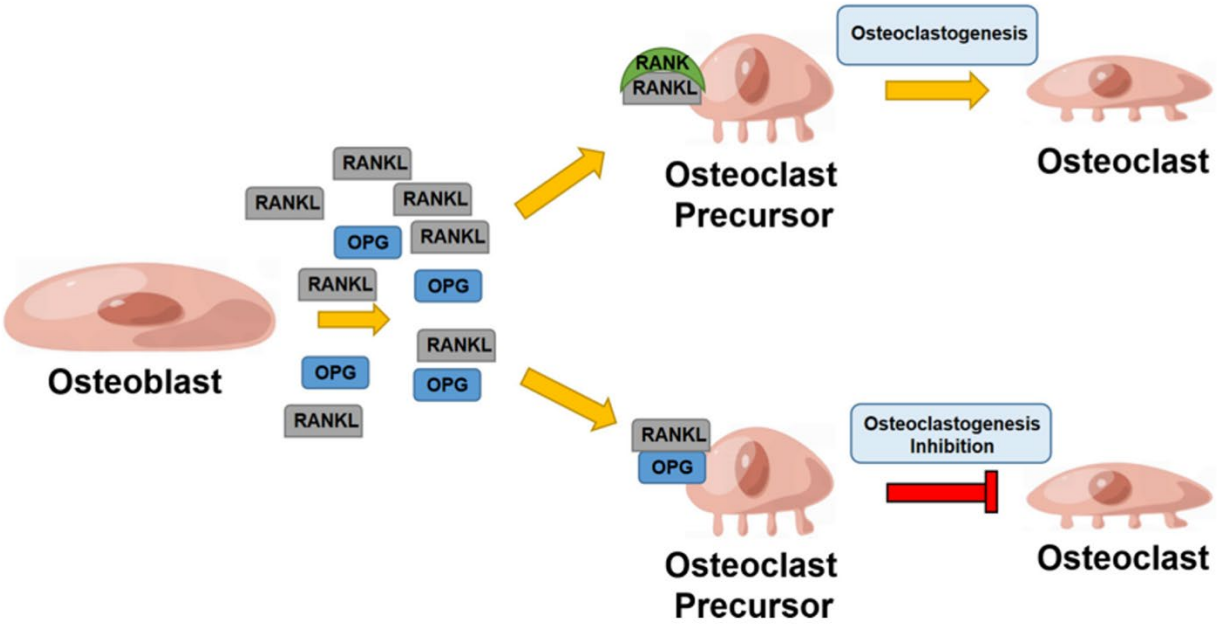

Figure 1.3 Osteoclastogenesis is activated or inhibited depending on whether RANKL binds to RANK on osteoclast precursors or to OPG[32].

1.3.5. Conclusion

These shared mechanisms in cardiovascular and bone regulation suggest that these systems are biologically linked. It is important to note that these shared biological mechanisms have systemic effects, particularly circulating cytokines. This suggests that any changes in cytokine levels could affect both systems simultaneously. Because catastrophic events such as MI and Fx will trigger systemic responses, it is reasonable to presume that the trauma in one system may affect the regulation of other systems in the body.

1.4. Inflammation After Trauma

The current theory is that the correlation in incidences of MI and Fx is reflective of advanced stages of their underlying chronic diseases, osteoporosis and atherosclerosis[11,32]. Atherosclerosis is a chronic inflammatory disease and chronic inflammation has been established to play a key role in bone resorption[11,32–34]. Patients with auto-immune diseases such as rheumatoid arthritis and lupus exhibit systemic bone loss and accelerated development of osteoporosis[35–37]. Accordingly, animal models of atherosclerosis, such as ApoE$^{-/-}$ mice on atherogenicdiet, have been found to have lower bone mineral density (BMD) compared to wild-type mice[38,39]. These studies establish that a systemic inflammatory state can induce systemic bone loss.

However, no studies have determined if acute inflammation after a traumatic event could cause a similar response. Inflammation is the body's response to cell death, damage-associated molecular patterns (DAMPs), or pathogens, pathogen-associated molecular patterns (PAMPs)[40,41]. After trauma, DAMPs are the primary activator of local immune cells to secrete mediators localized in the area of injury to counteract the cell damage. However, when the magnitude damage is too great, the immune cells will release mediators to enter circulation, resulting in system wide activation and recruitment of immune cells to the areas of damage. If the body is unable to restore homeostasis, systemic inflammatory response syndrome occurs which can lead to dysfunctional effects on other parts of the body. This is also known as multi-organ dysfunction syndrome (MODS). Severe traumatic events like MI trigger multiple mediators that all initiate inflammation simultaneously. Among these are the cytokine

cascade, the complement system, and the sympathetic nervous system (SNS), which have been implicated as important mediators of MODS. These systems will be discussed in greater detail in the following section[29,42].

A study by Dutta et al. demonstrated that MI created an inflammatory state that exacerbates atherosclerosis and increased risk of subsequent MI through the SNS (details of this study's SNS pathway will be discussed in later sections). After inducing permanent ligation (a severe model of MI) in mice, they found increased proliferation of monocytes in the spleen. This was followed by increased serum monocyte concentrations, known as monocytosis, which then increased the number of monocytes that was recruited to areas of plaque in other sections of the coronary arteries. As more monocytes are recruited, the plaque became more unstable and thus resulted in a greater risk of plaque rupture and ultimately, a second MI[43] as shown in **Figure 1.6**.

Emerging evidence from our lab suggests an association between inflammation after trauma and ***bone loss***. In previous studies, we have shown that femoral fracture in mice leads to greater bone loss in unassociated skeletal sites (e.g., the lumbar spine) when compared to sham and unoperated controls. Female mice aged 3 or 12 months were assigned into either fracture, placement of intermedullary pin into the femur followed by transverse fracture, sham, placement of intermedullary pin only, or unoperated groups. The study found that fracture groups had lower bone mineral density at 14 days post-injury with a trend to recovery at later time points in the 3-month group. The 12-month group showed the same peak bone loss at 14 days but did not

recover at later time points (**Figure 1.4A**). ELISA analysis of the serum followed a similar trend with peak levels of IL-6 at day 3 which coincided with OC numbers and activity peaked at the same time point. These results temporally correspond with bone loss. As IL-6 returns back to baseline, bone mass similarly increased before plateauing close to baseline levels as shown in (**Figure 1.4B)**[16,44]**.** Furthermore, a study done by Zhang et. al. found multiple fractures further increased the severity of bone loss. Similar to our lab's study, the investigators concluded from their findings that the mechanism behind it may be partly associated with increased osteoclast number and a more severe inflammatory response[45]. These studies suggests that trauma induces an acute systemic inflammatory response that may transiently initiate increased bone resorption.

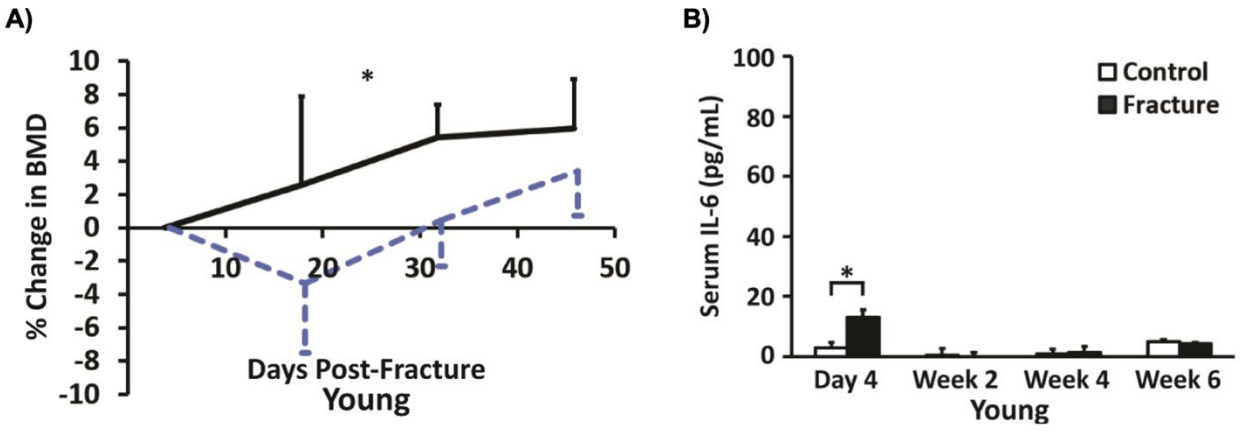

Figure 1.4 Results from systemic bone loss after fracture study. **A)** The magnitude and time course of whole-body BMD over time. Peak bone loss occurred 14 days post-fracture (blue). **B)** Levels of serum IL-6 in fractured mice peak at day 3 and returns to baseline in following weeks[16].

Interestingly, these studies investigating MI[43] and Fx[16] both characterized a similar positive-feedback loop where acute injury would result in exacerbation of its chronic

condition through inflammation. It is through this inflammatory response that we believe MI and OP can be ***causatively*** linked as proposed in **Figure 1.5**. However, little is known about whether injury-induced inflammation could act as a cross-link between two different systems. Because MI has a robust inflammatory response and because it has been shown that inflammation after trauma is associated with bone loss, it is likely that bone loss could be a significant co-morbidity after MI.

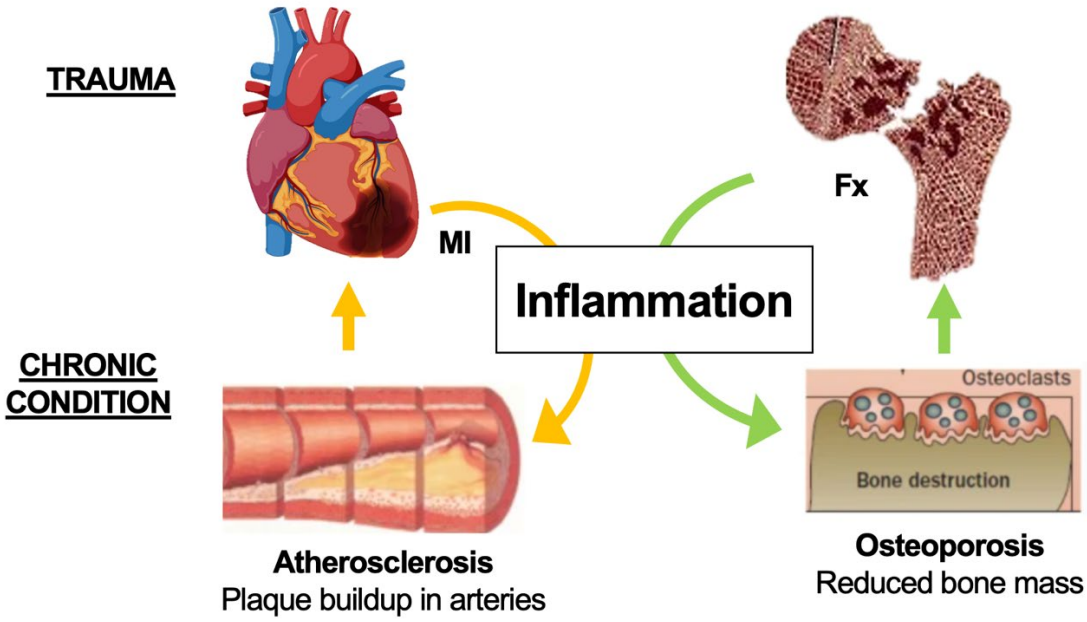

Figure 1.5 Traumatic injury, such as MI and fragility fracture, exacerbates its chronic condition through systemic inflammation.

As stated previously, inflammation after MI is initiated through multiple systems. For this study, two systems were of particular interest, the SNS and the complement system, which will be discussed in further detail in the following chapters. The mechanisms of both systems in initiating inflammation post-MI have been well-characterized in

literature. Furthermore, studies have shown direct effects of both systems on bone cells through the upregulation of osteoclastogenesis. As a result, these systems showed the most potential in linking MI and bone loss.

1.5. Sympathetic Nervous System (SNS)

The SNS, also known as the fight-or-flight response, is a response to physical and psychological threats including pain and stress. Triggering the SNS response causes the release of the adrenaline hormones, epinephrine and norepinephrine, from the adrenal glands. These hormones then signal multiple organs to increase organ activity to prepare the body for action such as increased heart rate and decreased digestion. The SNS response is especially robust for catastrophic traumatic events like MI. In addition to the cellular damage, MI creates pain and stress which will exacerbate SNS responses further[43]. SNS activation after MI has been well-established and its inhibition is a common therapeutic strategy[46,47]. It is activated through β-adrenergic receptors (β-AR) to initiate a global inflammatory response for remodeling damaged tissues. Excessive activation can, however, lead to pathological effects.

1.5.1. SNS-Activation After MI

As mentioned previously, a study by Dutta et al. demonstrated that MI activates the SNS through β_3-ARs resulting in exacerbation of atherosclerosis and increased risk of subsequent MI. After the first ischemic injury, activation of β3-AR releases hematopoietic progenitor cells from the bone marrow which in turn increases the proliferation of monocytes in the spleen. This results in increasing serum monocyte

concentrations, known as monocytosis, leading to plaque instability and greater vulnerability of a second MI as shown in **Figure 1.6**. When mice were treated with a β3-AR antagonist, accumulation of progenitors in the spleen decreased and overall reduction of monocytes in the serum, suggesting that β3-AR plays a significant role in the inflammatory response post-MI[43].

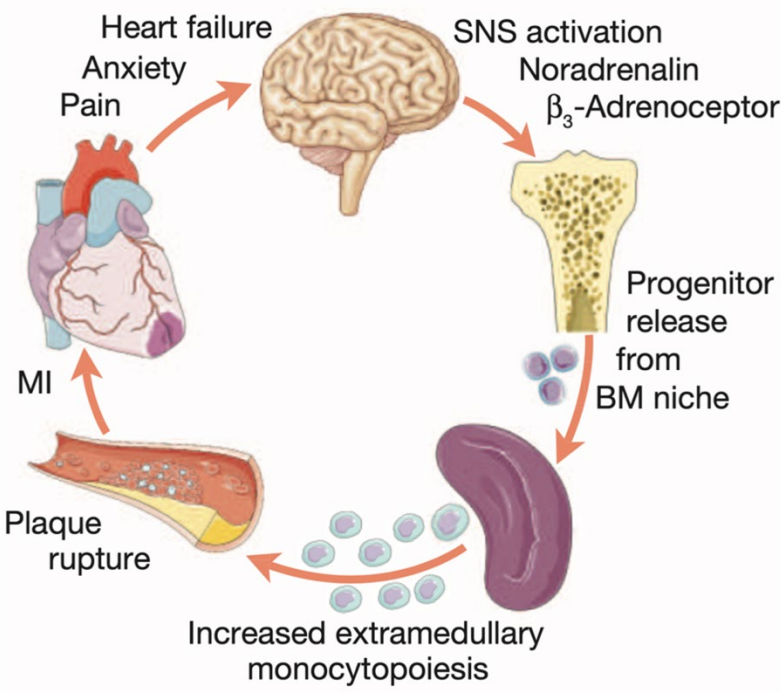

Figure 1.6 MI exacerbates atherosclerosis through an SNS-mediated pathway. MI activates SNS through β3-adrenoreceptors in the bone marrow. This releases hematopoietic progenitor cells from the bone marrow to proliferate in the spleen and increase levels of circulating monocytes. Monocytes are then recruited into areas of plaque, causing it to be more unstable and increases the risk of subsequent MI[43].

1.5.2. SNS-Mediated Bone Loss

It is possible that this SNS-mediated mechanism could also lead to bone loss post-MI. There are three types of β-ARs that are involved in cellular signaling in most areas of

the body: β1-AR, β2-AR, and β3-AR. Human osteoblasts express mostly β2-AR and it is believed that direct activation of osteoblast inhibits osteoblast proliferation and triggers osteoclast bone resorption[51]. However, another study found that although there were little to no β1-AR found on osteoblast surfaces, β1-ARs have a greater effect in bone regulation than β2-AR in humans. Selective inhibition of β1-AR had greater effect in increasing BMD in the ultradistal radius in women than propranolol, which has a lower ratio of β1-AR: β2-AR[50]. This suggests that although β1-AR are not abundantly expressed on bone cells, it plays a more dominant role in bone loss than β2-AR through an indirect mechanism.

Studies have shown that SNS activation can directly cause bone loss. A study by Jiao et al. found that the inclusion of psychological stress along with aberrant mechanical loading to the mandibular joint caused increases in RANKL and decreases in OPG as well as lower bone volume. They further found that an SNS inhibitor prevented lower bone density[48]. General β-AR antagonists have been shown to inhibit SNS-initiated bone loss. When mice were injected with risperidone (RIS), a drug that stimulates SNS activity, bone loss occurred due to increases in RANKL and other bone resorbing cytokines ultimately leading to increases in osteoclast activity. However, when propranolol, a non-selective β-AR blocker, was introduced, there was an increase in osteoblast activity that offset the SNS-initiated increase in osteoclasts[49]. A study done on human patients found similar results. In the study's sample population, those who took propranolol have a higher average bone volume content compared that those that do not[50]. From these findings, it is clear that β-AR's play some role in bone regulation

through modulation of osteoclast and osteoblast activity, but the specific cellular mechanisms are still not fully clear.

In contrast to the other types of β1-AR and β2-AR, comparatively little is known about the effect of β3-AR on bone. Like β1-AR, osteoblasts and osteoclasts exhibit no β3-AR and it does not seem likely that it would affect bone cells directly. However, as seen with the Dutta et al. study, β3-AR plays in important role in increasing monocyte numbers during inflammation and may have an indirect effect on bone[43]. Monocytes are share the same hematopoietic lineage to osteoclasts and are it precursors[52,53]. It is possible that modulating monocyte concentrations will affect osteoclast levels and therefore bone remodeling. Monocytes have been closely associated with postmenopausal osteoporosis and have been proven to be an appropriate model for bone related studies[54–56]. Furthermore, a study done by Ohtsuji determined that monocytes can regulate osteoclast activity and exacerbate bone loss in a mouse model of rheumatoid arthritis. When monocyte recruitment was inhibited, resulting levels of osteoclast numbers and activity as well as severity of arthritis decreased[36]. These studies suggest that MI may be able to cause SNS-mediated bone loss through β3-AR activation and monocytosis.

1.6. Complement System

Like the SNS, the complement system plays an integral role in initiating systemic inflammation after MI and has been shown to effect bone resorption. The complement system is the primary mediator of the inflammatory process. It enhances the roles of

phagocytic cells and induces inflammation in response to bacteria or trauma. In homeostatic conditions, the complement system consists of several inactive proteins circulating in plasma. However, once activated, the proteins will conformationally change in series and will interact with each other to initiate and mediate the inflammatory response. The complement system's effects are diverse and includes creating products with an opsonic function to coat bacteria for phagocytosis, creating a macromolecular complex cytotoxic to bacteria, tumor cells, etc.…, and most notably, activation leukocytes and chemotaxis through receptor-mediated mechanisms[57].

1.6.1. Complement System After MI

The complement system can be triggered through multiple pathways. These are the classical pathway (due to formation of an immune complex), the alternative pathway (due to chemical structures on target surfaces), and the lectin pathway (occurs when lectin proteins bind to certain carbohydrates on the surface of microbials or damaged cells)[58]. As shown in **Figure 1.7**, Regardless of initiation, both pathways create complement proteins 3a (C3a) and 5a (C5a). While both are crucial in recruiting leukocytes and inducing pro-inflammatory cytokines in the blood, C5a, has been shown to be a potent mediator in the inflammatory response after MI[57]. C5a levels are upregulated post-MI[59] for leukocyte recruitment and has direct effects on endothelial cells to promote adhesion of leukocytes to vasculature walls[57,60]. Like the SNS, complement activation is critical after trauma but excessive activation can lead to further damage and a systemic inflammatory response. One study found that the absence of C5a receptors (C5aR) in circulating leukocytes decreased the size of infarct after MI

and reperfusion associated with improved cardiac function and lower infiltration of neutrophils into the infarct area[61]. Another study found similar results with a C5a receptor antagonist, suggesting that specific inhibition of C5aR could be an effective therapy after MI[62].

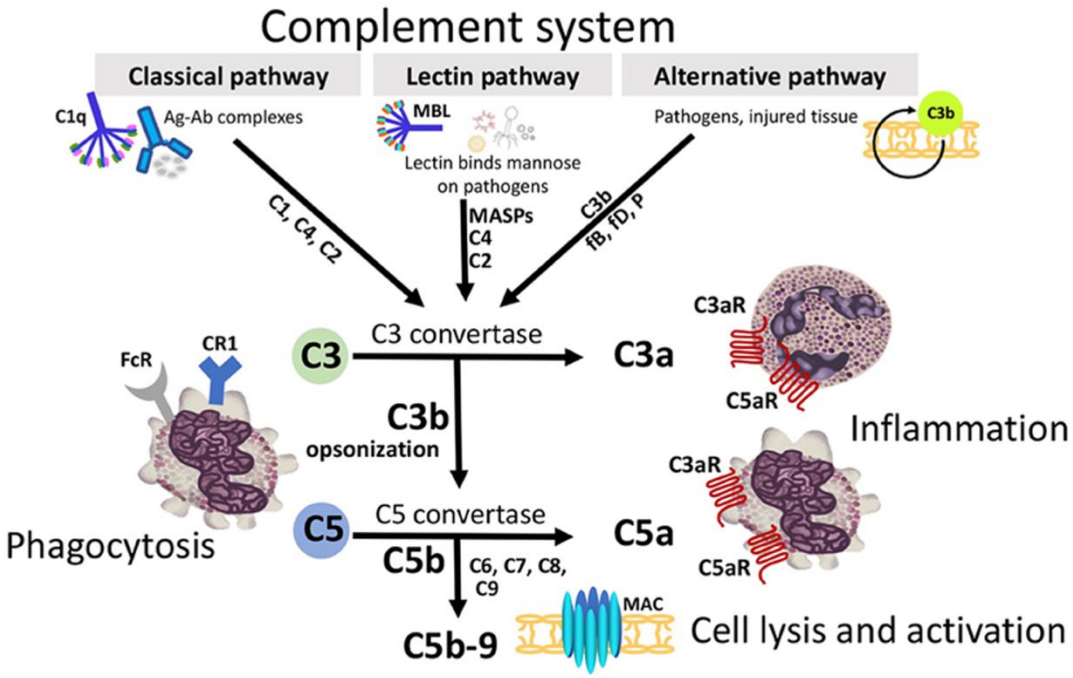

Figure 1.7 The complement system consists of multiple molecular pathways. All pathways converge in the creation of complement proteins 3a (C3a) and 5a (C5a), which are integral in initiating inflammation[62].

1.6.2. C5a as a Mediator Between Systems

As previously described, C5a plays a central role in initiating systemic inflammation. Due to its potency, it could serve as a bridge between the cardiovascular and skeletal systems. A recent study discovered that C5a levels are associated with heart damage after fracture. Investigators fractured the femur of porcine models and measured electrical and myocyte damage in the heart tissues. They found that the fracture group

had higher levels of troponin I, a marker for cardiac cell damage, the day of fracture compared to unfractured controls with slightly lower levels 14 days after as shown in **Figure 1.8A**. Systemic C5a levels followed the same trends with a peak the day of operation and lower levels at day 14 as described in **Figure 1.8B**. The investigators concluded that because C5a levels are known to contribute to cardiac dysfunction, it may have contributed to the cardiac alterations after femoral fracture . This suggests that C5a has the potential to mediate between cardiac and skeletal systems.

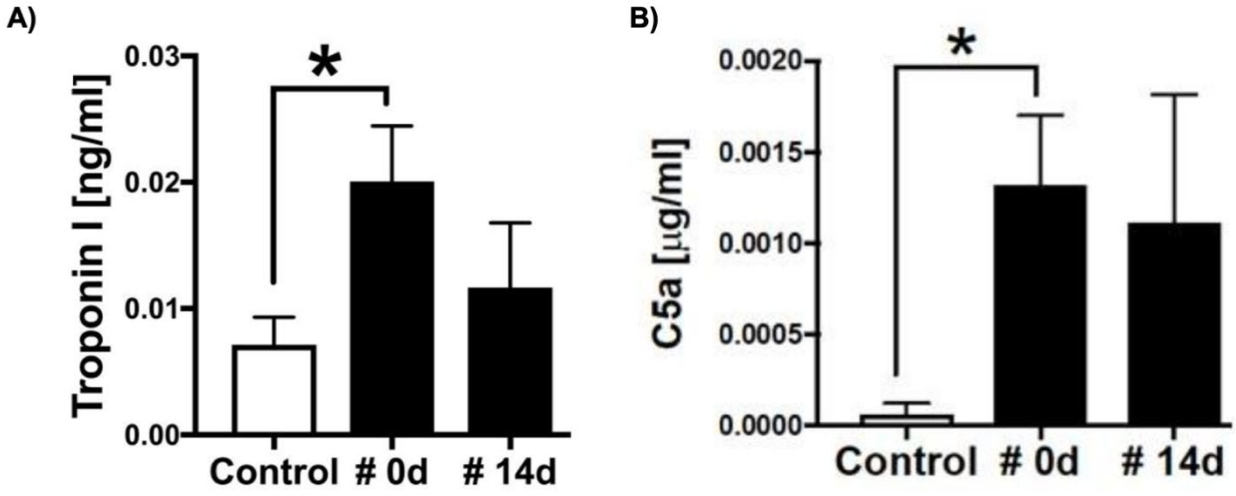

Figure 1.8 A) After femoral fracture, Troponin I levels (a marker for cardiac cell damage) are greatest the day of injury and remain elevated 14 days after. **B)** Serum C5a levels also peak the day of injury and remain elevated 14 days later[62].

1.6.3. C5a and Bone

Although not as well-established as the heart, the effect of C5a on bone has recently been investigated and was shown to play a role in bone resorption. Munenaga et al. found that mice infected with P.gingivalis, a model of inflammatory periodontal disease, had higher levels of serum C5a, greater osteoclast numbers, and greater bone loss[64].

Furthermore, two types of C5aR, C5aR1 and C5aR2, has been found on surfaces of osteoblasts, indicating that C5a has a direct role in regulating bone cell activity. A study done by Kovtun et al. demonstrates the necessity for C5a activation in bone turnover after trauma. After femoral fracture, C5aR1-/- and C5aR2-/- mice models had impaired fracture healing due to decreases in osteoclastogenesis, suggesting that C5aR activation increases osteoclast differentiation and bone resorption. Interestingly, this study found that C5aR1 exhibits a greater role in the inflammatory response in early phases of bone remodeling comparted to C5aR2[65]. Furthermore, another study found that overexpression of C5aR1 lead to increases in osteoclast differentiation and hinders bone healing, suggesting that C5aR1 would have greater role in regulation after trauma[66].

The cellular pathways in C5a-mediated bone loss are still under investigation. There is strong evidence that suggests C5a increases bone resorption through RANKL activation. When C5a binds to C5aR on osteoblasts, osteoblasts releases RANKL which will then induce osteoclastogenesis. Studies have shown that changes in RANKL levels and osteoclast numbers are directly affected by expression of C5aR[64,66] as described in **Figure 1.9**. It is also possible that C5a could have an indirect role in bone resorption through modulating inflammatory cytokine levels. As discussed previously, C5a can increase pro-inflammatory cytokine levels, including IL-6, a key cytokine in bone resorption. Some studies have suggested that activation of C5aR leads to increases in osteoclast activity and bone resorption through upregulation of local cytokines such as IL-6 from osteoblasts[67,68] and that inhibiting C5aR results in lower IL-6 levels and less

bone loss[65,66]. Although the specific cellular mechanisms of C5a-mediated bone loss are still being investigated, it is clear that C5a, through C5aR, is able to modulate bone resorption. Because C5a is upregulated after MI[59], it is possible that C5a-C5aR activation could play a mechanistic role in bridging MI and bone loss.

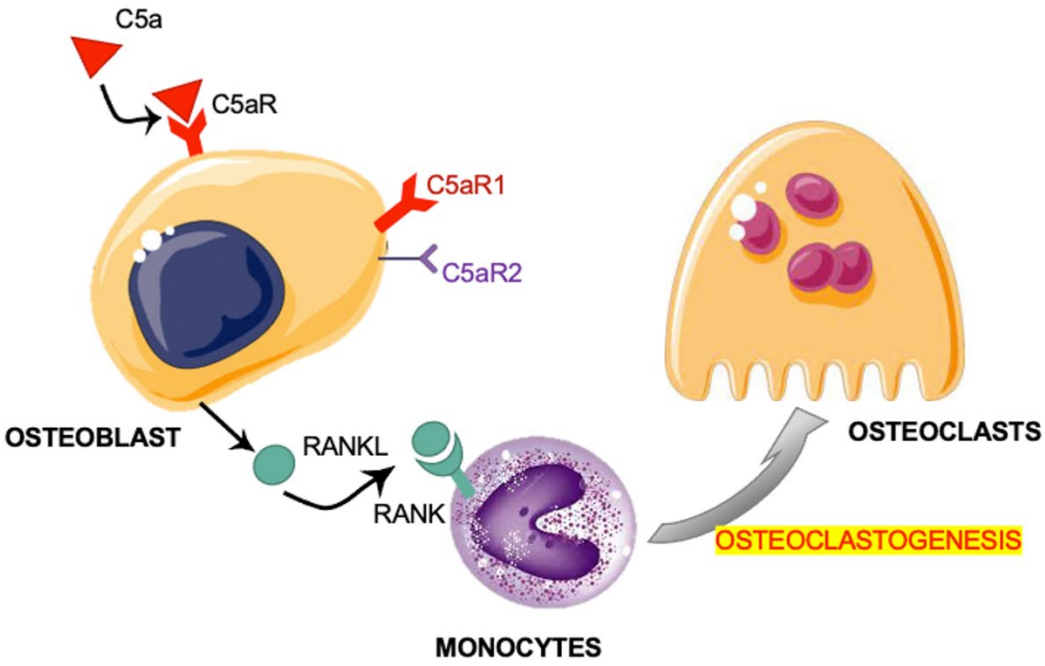

Figure 1.9 C5a initiates osteoclastogenesis by binding to C5aR1 on osteoblast surfaces and initiates the RANKL/RANK pathway. There are two types of receptors: C5aR1 and C5aR2. C5aR1 plays a greater role in the pro-inflammatory response after injury whereas C5aR2 is more imperative in mediating anti-inflammatory processes after the initial inflammatory response.

1.7. Conclusion

MI and Fx are leading causes of mortality and morbidity worldwide[1] and there is evidence of incidences of MI correlating to incidence of bone loss and subsequent Fx[10,11,13]. However, no investigation has been done to establish a causative link.

Research into MI initiating bone loss is still preliminary and evidence for a causative relationship has still not been explicitly established. However, there is strong evidence that inflammation system can act as a bridge between MI and bone loss.

Both the SNS and complement systems are integral to initiating a systemic inflammatory response after MI and the cellular mechanisms are well known in the field[43,57]. There has also been data showing that the same cellular mechanisms have effects on bone resorption. Bone loss is often associated with SNS activation, either through direct activation of β-ARs on bone cells or indirectly by influencing the cytokine levels known for promoting bone resorption such as TNF-alpha and IL-6[36,50]. Likewise, bone loss is also associated with C5a-C5aR activation, although it is unclear if the bone loss is primarily due to direct C5aR activation on osteoblasts and its release of RANKL or due to systemic C5aR activation on immune cells to release cytokines like IL-6[65]. In all cases, it is clear that activation of SNS and/or the complement system due to MI could have systemic effects on the bone. Establishing a causative relationship between the two would be integral in forming treatment plans after MI in order to develop proactive measures for Fx prevention, especially in at-risk populations such as elderly, post-menopausal women to reduce morbidity and ensure quality of life[7].

To address the hypotheses discussed above, these studies will investigate the relationship between MI and subsequent bone loss and the significance of acute systemic inflammation as an underlying mechanism. **Chapter 2** will quantify changes in bone mass and microstructure to examine bone loss after MI operation. It will also

determine the role of SNS and β3-activated monocytosis in bone loss after MI through β3-AR inhibition. **Chapter 3** will establish the magnitude and time course of systemic bone loss after MI and will determine the significance of the complement system and C5aR and investigate pro-inflammatory cytokines as a possible mechanistic pathway in the systemic bone loss response using global C5aR knockout mice.

CHAPTER 2: SYSTEMIC BONE LOSS FOLLOWING MYOCARDIAL INFARCTION IN MICE IS MITIGATED BY TREATMENT WITH β3 ADRENERGIC RECEPTOR ANTAGONIST

2.1. Abstract

Myocardial infarction (MI) and osteoporotic fracture (Fx) are leading causes of morbidity and mortality, and epidemiological evidence linking their incidence suggests possible crosstalk. MI can exacerbate atherosclerosis through sympathetic nervous system (SNS) activation and β_3 adrenoreceptor-mediated release of hematopoietic stem cells (HSCs), leading to monocytosis. We hypothesized that this same pathway initiates systemic bone loss following MI, since osteoclasts differentiate from monocytes. In this study, MI was performed in 12-week-old male mice (n=24) randomized to β_3-adrenergic receptor antagonist (SR 59230A) treatment or no treatment for 10 days post-operatively. Additional mice (n=21, treated and untreated) served as un-operated controls. Bone mineral density (BMD), bone mineral content (BMC), and body composition were quantified at baseline and 10 days post-MI using DXA; circulating monocyte levels were quantified and the L5 vertebral body and femur were analyzed with micro-computed tomography 10 days post-MI. We found that MI led to increases in circulating monocyte levels, which was further increased by β_3-antagonist treatment. BMD and BMC decreased at the femur and lumbar spine in MI mice (-6.9% femur BMD, -3.5% lumbar BMD); β_3-AR antagonist treatment diminished this bone loss response (-5.3% femur BMD, -1.2% lumbar BMD). Similarly, trabecular bone volume decreased in

MI mice compared to control mice, and this was partially attenuated by β_3-antagonist treatment.

Clinical Significance: These results suggests that MI leads to bone loss and that the SNS may be a modulator of this response; this bone loss and increased fracture risk may be important clinical co-morbidities following MI or other ischemic injuries.

2.2. Introduction

Osteoporotic fractures (Fx) and myocardial infarction (MI) are two of the leading cause of morbidity and mortality worldwide[1]. Over 20% of patients will die within 1 year following a hip fracture[2,3], and over 30% will die within 5 years[4,5]. Similarly, within 5 years of a first MI, 36% of men and 47% of women will die due to MI-related complications[6]. Interestingly, there is strong epidemiological evidence showing that MI is associated with increased risk of subsequent Fx. For example, Gerber *et al*. found that Fx incidence rates increased markedly over time (hazard ratio = 1.32) among those with previous MI compared to control patients[10]. A possible interpretation of these findings is that the incidence of Fx and MI is reflective of advanced stages of underlying chronic diseases such as osteoporosis and atherosclerosis, which are etiologically linked[11]. However, another contributing factor may be that MI initiates an adaptive healing response that actively initiates bone loss systemically, thus increasing subsequent risk of Fx.

Our previous study described a positive feedback loop between Fx and systemic bone loss in mice, which could lead to increased risk of subsequent fractures[16]. In that study,

Fx led to significant decreases in whole-body bone mineral density (BMD) in both young (3-month-old) and middle-aged (12-month-old) mice within 2 weeks post-injury. Fx also resulted in ~11-18% losses of trabecular bone volume in the L5 vertebral body at the same time point. These changes in BMD and bone microstructure were associated with decreased voluntary activity, increased systemic inflammation, and increased osteoclast number and activity at 3 days post-injury. These data demonstrate that acute skeletal injury (femur Fx) initiates a systemic response leading to loss of bone at distant skeletal sites. However, it is not known whether non-musculoskeletal injuries such as MI could also lead to systemic bone loss.

A similar positive feedback loop has been described for the cardiovascular system, wherein the systemic inflammatory response following MI in mice exacerbates underlying atherosclerosis[43]. This study demonstrated that activation of the sympathetic nervous system (SNS) after MI initiated the release of hematopoietic progenitor cells from the bone marrow, ultimately leading to monocytosis, accumulation of monocytes within atherosclerotic lesions, and exacerbated lesion formation. Treatment of mice with a β_3-adrenergic receptor antagonist after MI lowered protease activity and myeloid cell content, ultimately decreasing the severity of monocytosis. It is possible that a similar SNS-mediated pathway may also be a key mediator of systemic bone loss following Fx or other acute injuries since osteoclasts have a hematopoietic lineage and differentiate from monocytes. However, the role of the SNS in systemic bone loss following Fx or other injuries has not been described.

In the current study, we sought to determine if acute ischemic injury (MI) leads to a loss of bone systemically, and whether the SNS is a key regulator of this response. We hypothesized that systemic bone loss would occur after MI, and that blockade of β_3-adrenergic receptors would diminish or prevent this bone loss, implicating the SNS as a mediator of systemic bone adaptation following acute injury. These findings would describe a novel and potentially critical comorbidity associated with MI and other ischemic injuries and could inform future treatments that aim to preserve skeletal health in these patients.

2.3. Methods

2.3.1. Animals

Forty-four male C57BL/6 mice were obtained from the Jackson Laboratory (Bar Harbor, ME) at 10 weeks of age and were acclimated to the housing vivarium for 2 weeks prior to the start of experiments. At 12 weeks of age, mice were randomized to MI surgery (n=24) or anesthetized, un-operated controls (n=21). Twenty-one mice (11 MI, 10 control) were administered a selective β_3-adrenergic receptor (AR) antagonist (SR 59230A, Sigma-Aldrich, St. Louis, MO; twice daily IP injection, 5 mg/kg body weight) for 10 days post-operatively starting immediately post-surgery. All animals were maintained and used in accordance with National Institutes of Health guidelines on the care and use of laboratory animals, and all procedures were approved by the UC Davis Institutional Animal Care and Use Committee.

2.3.2. Myocardial Infarction Surgery

The left anterior descending (LAD) coronary artery was permanently ligated as previously described[69]. Briefly, mice were anesthetized with isoflurane, intubated, and continuously monitored with a 3-lead electrocardiogram (ECG). A small incision was made, oblique muscles were bluntly separated to expose the ribs, and a small opening was created in the muscle of the 4th intercostal space. The ribs were then separated, and the pericardium was opened. The LAD was identified and permanently ligated using an 8-0 Prolene suture. LAD ligation was confirmed by ST segment elevation on the ECG. The ribs and oblique muscles were closed using a 6-0 Ethilon suture and the skin was closed using wound clips. Approximately 150 μL of sterile saline and 0.1 mg/kg buprenorphine were injected subcutaneously before allowing the mouse to recover in its cage on a 35° C warmer for ~1 hour. Standard post-operative procedures were followed for 7 days, including analgesia (0.1 mg/kg buprenorphine) twice per day for 48 hours. Wound clips were removed after 7 days. Unoperated control animals were subjected to anesthesia for 30 minutes and followed the same analgesia schedule.

2.3.3. Measurement of Infarct Size

All mice were euthanized 10 days post-MI, and hearts were removed and placed immediately into cardioplegic solution (composition in mmol/L: NaCl 110, $CaCl_2$ 1.2, KCl 16, $MgCl_2$ 16, and $NaHCO_3$ 10) to prevent continued electrical activity and subsequent ischemic injury to myocytes. Hearts were frozen for 15 minutes, then sliced into 1 mm thick sections (Mouse Heart Slicer Matrix with 1.0 mm coronal section, Zivic Instruments, Pittsburgh, PA). Heart slices were stained with 1% 2,3,5-

triphenyltetrazolium (TTC) in PBS for 15 minutes at 35° C after which the slices were stored in PBS for 24 hours. Heart sections were gently blotted with a Kimwipe, then imaged with an office scanner (EPSON Perfection 4990 Photo, Suwa, Japan). Individual color images were taken at 1200 dpi resolution for each heart section, and images were analyzed using ImageJ[70,71]. To determine the area of ischemic tissue, a color filter was placed on the image to exclude all colors except for white. The filter was then manually adjusted until only the unstained ischemic tissue was highlighted. Total size of ischemic injury was quantified as the total area of ischemic (unstained) tissue in all transverse slices for each heart normalized by the total area of all slices (6-8 sections for each heart).

2.3.4. White Blood Cell Analysis

Whole blood was collected from the peritoneal cavity at the time of euthanasia for differential white blood cell count to determine the percentage of monocytes and neutrophils in blood. Approximately 0.5 – 0.75 mL of blood was slowly collected through the inferior vena cava using a 30-gauge needle and a 1 mL syringe. The needle tip was removed before the blood was placed directly from the syringe into the collection tube. All blood samples were placed in tubes coated with K_2EDTA (BD Microtainer®, Franklin Lakes, NJ) and were gently inverted ten times before storing at 4° C. Blood samples were transferred to the UC Davis Veterinary Clinical Labs (UC Davis, Veterinary Medical Teaching Hospital) for differential white blood cell count within 24 hours of collection.

2.3.5. Dual-Energy X-ray Absorptiometry (DXA) Analysis

Whole-body DXA imaging was performed at baseline (one day prior to surgery) and 9 days post-surgery (one day prior to euthanasia) to determine body composition, bone mineral density (BMD) and bone mineral content (BMC) of the whole body, lumbar spine, femoral diaphysis, and whole femur. Mice were anesthetized with isoflurane and placed in a cabinet x-ray system (Mozart®, Kubtec Medical Imaging, Stratford, CT). Whole-body analysis automatically excluded the head and wound clips, and BMD, BMC, bone area, lean mass area, and adipose tissue area were calculated using the manufacturer's software. For the lumbar spine region of interest (ROI), the L4 through L6 vertebrae were manually selected; the whole femur and femoral diaphysis were analyzed using the same method. The femoral diaphysis was determined as the middle third of the femur. The imaging system was calibrated before each use to ensure consistent data.

2.3.6. Micro-Computed Tomography Analysis

L5 vertebrae and both legs were collected following euthanasia and fixed in 4% paraformaldehyde for 3-4 days before preservation in 70% ethanol. L5 vertebrae and right femora were imaged with micro-computed tomography (SCANCO µCT 35, Brüttisellen, Switzerland) to determine trabecular bone microstructure of the L5 vertebral body and distal femoral metaphysis and cortical bone microstructure of the femoral mid-diaphysis. All bones were imaged according to the guidelines for µCT of rodent bone (energy = 55 kVP, intensity = 114 mA, 6 µm nominal voxel size, integration time = 900ms)[72]. Analysis of trabecular bone in the L5 vertebral body was performed by

manually contouring 2D transverse slices in the region between the cranial and caudal growth plates and excluded the vertebral processes. Analysis of the femoral metaphysis was similarly performed with manual contouring beginning at the convergence of the distal femoral growth plate and extending 1500 μm (250 slices) proximal. Trabecular bone volume fraction (BV/TV), trabecular thickness (Tb.Th), trabecular number (Tb.N), and other microstructural parameters were determined using the manufacturer's analysis software. Analysis of cortical bone in the femoral diaphysis was performed by contouring transverse slices centered on the midpoint of the femur including a total of 600 μm (100 slices). Bone area (B.Ar), cortical thickness (Ct.Th), bone tissue mineral density (TMD) and other microstructural parameters were determined using the manufacturer's analysis software.

2.3.7. 3-Point Bending Mechanical Testing of Femora

Mechanical testing was performed on femurs using 3-point bending to determine bone structural and material properties using a materials testing system (ELF 3200, TA Instruments, New Castle, DE, USA). Following μCT imaging, femurs were rehydrated for 10-15 minutes in PBS solution before mechanical testing. The span length of the lower supports was 8 mm, and the femur was positioned so that the posterior aspect of each bone was downward (loaded in tension). The upper loading platen was positioned in the middle of the bone perpendicular to the long axis of the femoral shaft. The bone was preloaded to 1-2 N to ensure contact with the upper platen. Loading was applied at a displacement rate of 0.01 mm/sec until fracture, and displacement and resultant force were recorded at 50 Hz.

Whole-bone structural properties were determined from force-displacement curves using standard methods[73]. Stiffness was calculated as the slope of the linear pre-yield region. Post-yield displacement was determined as the displacement difference between the yield and fracture displacements. Material properties were calculated using previously established beam theory equations[73]. Elastic modulus, yield stress, and ultimate stress were determined using bending moment of inertia (I) and bone radius (c) determined from μCT analysis of the femoral mid-diaphysis.

2.3.8. Statistical Analysis

All results are expressed as mean ± standard deviation. Cross-sectional data were analyzed by two-way analysis of variance (ANOVA) stratified by operation (MI or Control) and treatment (β_3-AR antagonist or untreated) to determine main effects and interactions. DXA data were longitudinal and were analyzed using repeated measures ANOVA to determine differences in the time course of outcomes. Post hoc analyses were performed using Tukey's Honest Significant Difference test. Two-way ANOVA was performed using JMP Pro 14.2.0 (SAS Institute Inc., Cary, NC, USA). Repeated measures ANOVA values were through jamovi (version 0.9). Statistically significant differences were identified at $p \leq 0.05$; trends were noted at $p \leq 0.10$.

2.4. Results

2.4.1. Measurement of Infarct Size

Presence of ischemic (unstained) tissue was consistently observed in the left ventricle and areas inferior to the ligation site, confirming successful MI (**Figure 2.1B**). When infarct areas were normalized by total heart area (IA/TA), there was no significant difference between the infarct sizes of the β_3-AR antagonist treated mice and that of untreated mice (**Figure 2.1A**).

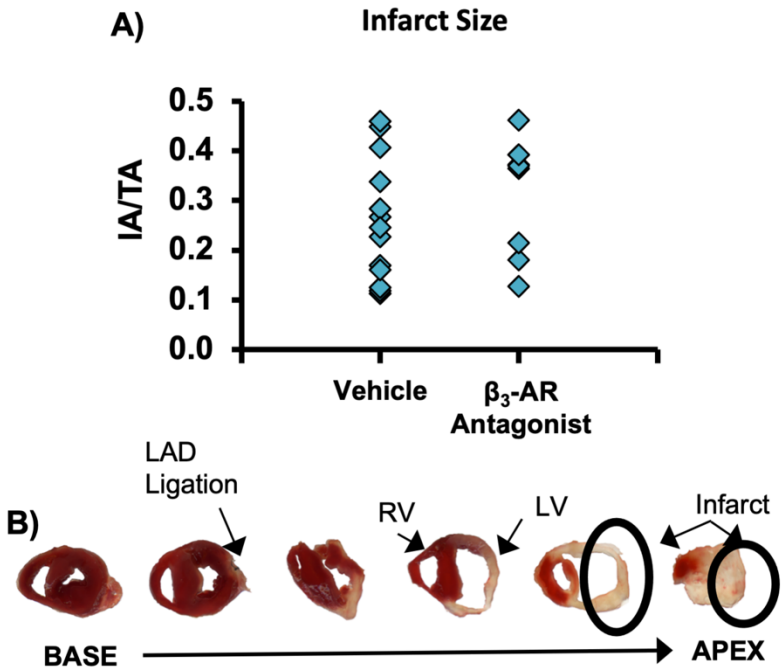

Figure 2.1 A) Infarct sizes normalized by total heart area for mice following surgical creation of MI. No differences were observed between untreated mice and mice treated with a β3 adrenergic receptor antagonist (IA/TA = Infarct Area/Total Area). **B)** Representative 1 mm thick cross-sections of a mouse heart 10 days after MI surgery.

2.4.2. White Blood Cell Analysis

At 10 days post-MI, circulating monocyte levels were significantly greater in MI mice than in Control mice (**Figure 2.2A**; main effect of MI: $p = 0.007$), and mice treated with the β_3-AR antagonist had a higher percentage of monocytes in the serum than untreated mice (main effect of treatment: $p = 0.033$). Similarly, neutrophil levels in MI mice were higher than in Control mice (**Figure 2.2B**; main effect of MI: $p = 0.0003$), though there was no significant effect of treatment on neutrophil levels. No significant interaction was observed between MI and β_3-AR antagonist treatment for either monocyte or neutrophil levels.

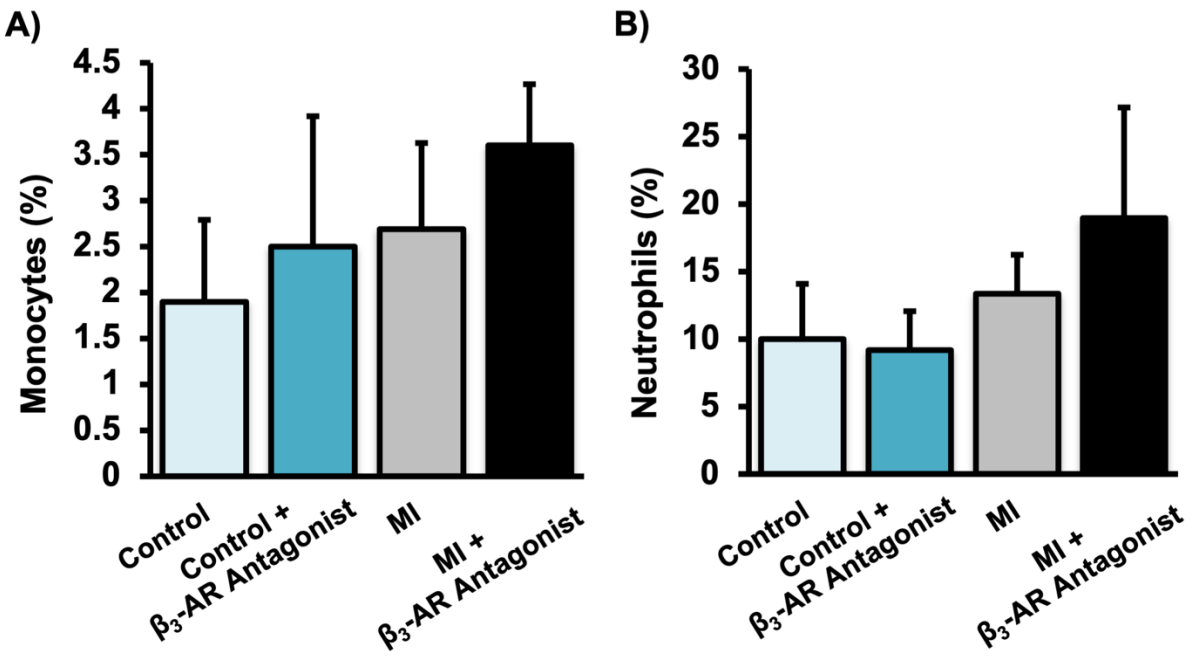

Figure 2.2 Percent of **A)** monocytes and **B)** neutrophils in blood 10 days post-MI. Monocyte levels were significantly increased by MI (main effect of MI: $p = 0.007$), and by treatment with a β_3-AR antagonist (main effect of treatment: $p = 0.033$). Similarly, neutrophil levels were significantly increased by MI (main effect of MI: $p = 0.0003$).

2.4.3. Dual-Energy X-ray Absorptiometry (DXA) Analysis

Whole-body DXA of mice revealed few significant changes from baseline to 9 days post-MI in any of the experimental groups, and no statistically significant differences based on MI or treatments (**Figure 2.3**). Generally, whole-body BMD decreased in MI mice from baseline to 9 days post-MI (though not statistically significant), while BMD of Control mice increased significantly during this time period. Whole-body BMC followed similar trends, with MI mice exhibiting less of an increase from baseline than Control mice on average.

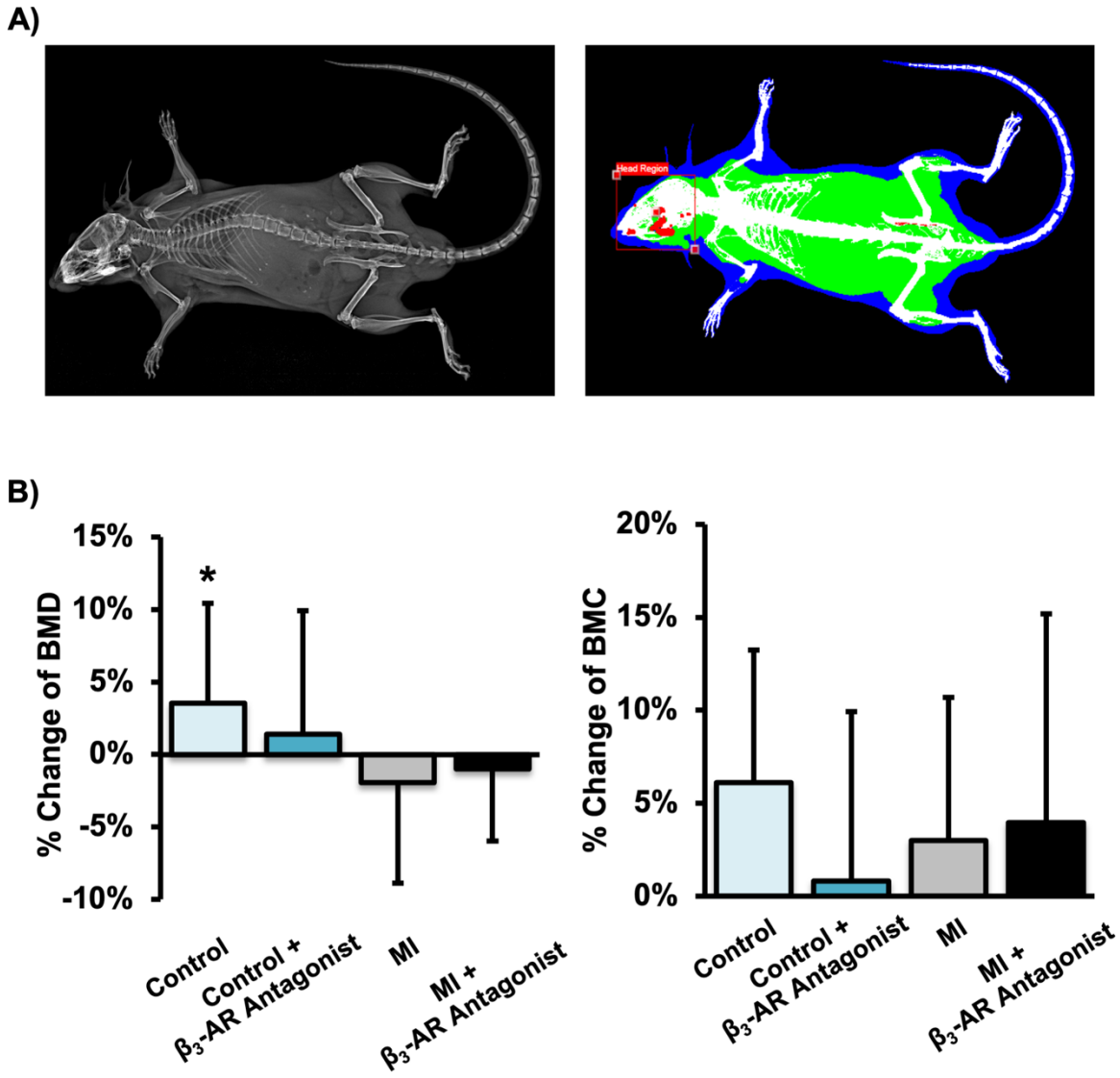

Figure 2.3 A) X-ray *(left)* and DEXA (*right)* images of the whole mouse. **B)** Average change of whole-body BMD *(left)* and BMC *(right)* from baseline to 9 days post-MI. * denotes significant change ($p \leq 0.05$) from baseline to 9 days post-MI.

Results from analysis of BMD and BMC in the lumbar spine were more definitive (**Figure 2.4**). At this skeletal site, Control mice generally showed an increase in BMD and BMC, while MI mice showed decreases in BMD and BMC from baseline to 9 days post-MI. Additionally, untreated mice exhibited greater changes from baseline (+2.5% BMD and +6.0% BMC for Control mice, -3.5% BMD and -4.2% BMC for MI mice) compared to β_3-AR antagonist treated mice (+0.4% BMD and +3.7% BMC for Control mice, -1.2% BMD and -2.5% BMC for MI mice).

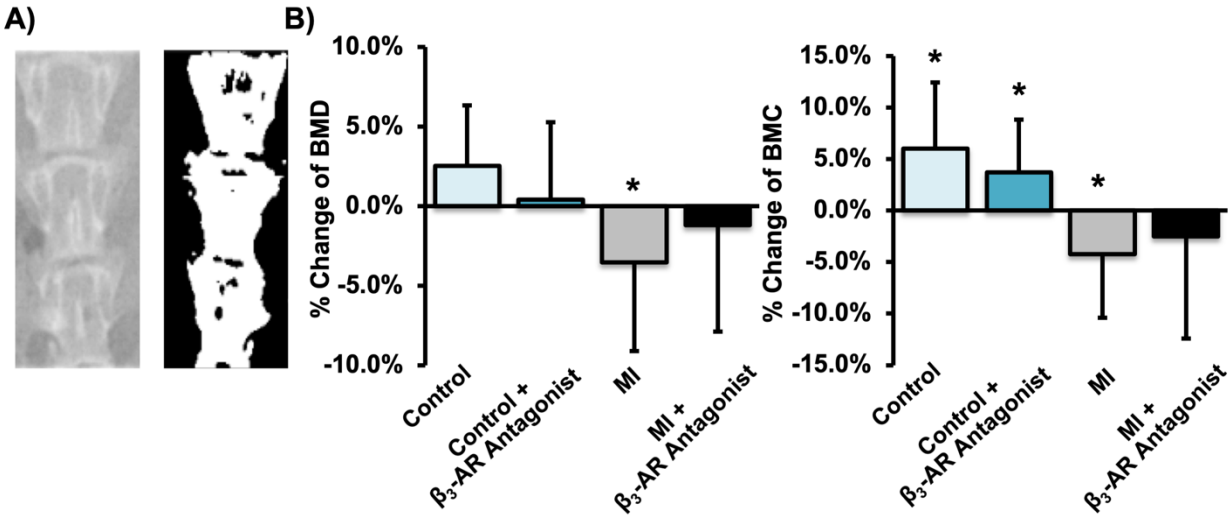

Figure 2.4 A) X-ray (*left*) and thresholded (*right*) images of the lumbar spine (L4-L6). **B)** Average change of lumbar BMD (*left*) and BMC (*right*) from baseline to 9 days post-MI. * denotes significant change ($p \leq 0.05$) from baseline to 9 days post-MI. Overall, average lumbar BMD and BMC of MI mice decreased from baseline to 9 days post-MI, and untreated mice exhibited greater changes than β_3-AR antagonist treated mice.

Results from analysis of BMD and BMC of the femur followed similar trends to those from the lumbar spine. For both the whole femur and femoral diaphysis (**Figure 2.5A and 2.5C**), BMD in the MI groups decreased significantly, and this decrease was greater for untreated mice (-6.9% whole femur, $p = 0.017$; -5.6% diaphysis, $p = 0.040$) than for β_3-AR antagonist treated mice (-5.3% whole femur, $p = 0.034$; -4.5% diaphysis, $p = 0.081$). No significant differences were observed between β_3-AR antagonist treated Control mice and untreated Control mice. BMC of the whole femur showed similar results, with BMC of untreated MI mice decreasing from baseline to 9 days post-MI (-5.2% whole, $p = 0.018$; -6.5% diaphysis, $p = 0.012$); this change in BMC was mitigated in β_3-AR antagonist treated MI mice.

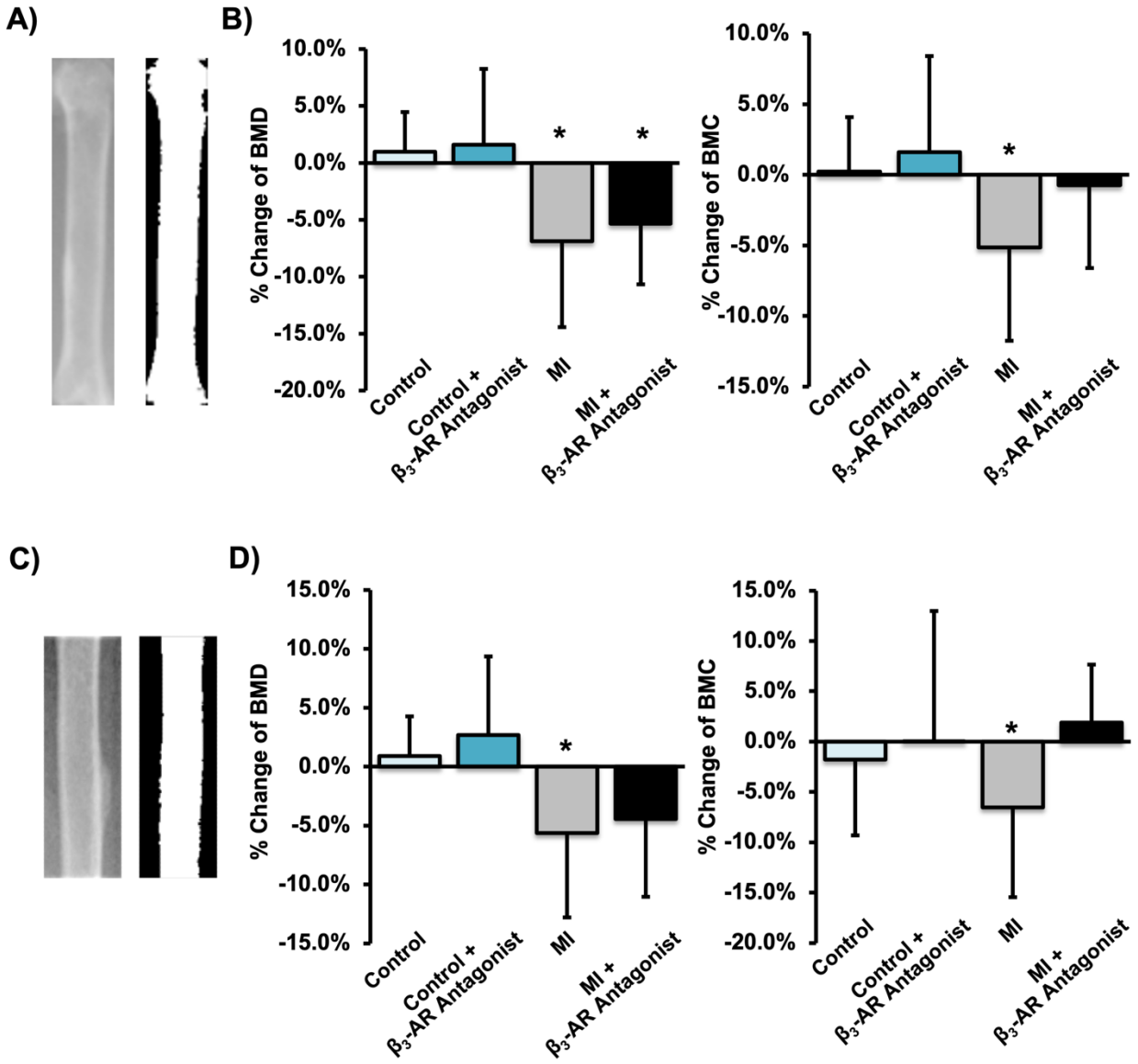

Figure 2.5 A, C) X-ray and thresholded images of the whole femur A) and the femoral diaphysis C). **B, D)** Average change of femoral BMD (*left*) and BMC (*right*) from baseline to 9 days post-MI for the whole femur and femoral diaphysis. * denotes $p \leq 0.05$ between baseline and 9 days post-MI. Both BMD and BMC decreased significantly in MI mice, and this decrease was greater for untreated mice than for β_3-AR antagonist treated mice.

Whole-body adipose tissue area decreased from baseline to 9 days for all groups (**Figure 2.6A**), though this change was not statistically significant for untreated Control mice. Whole-body lean tissue area, however, decreased only in MI mice (main effect of MI: $p < 0.001$), and this change was greatest for β_3-AR antagonist treated MI mice (-18.3%, $p = <0.001$).

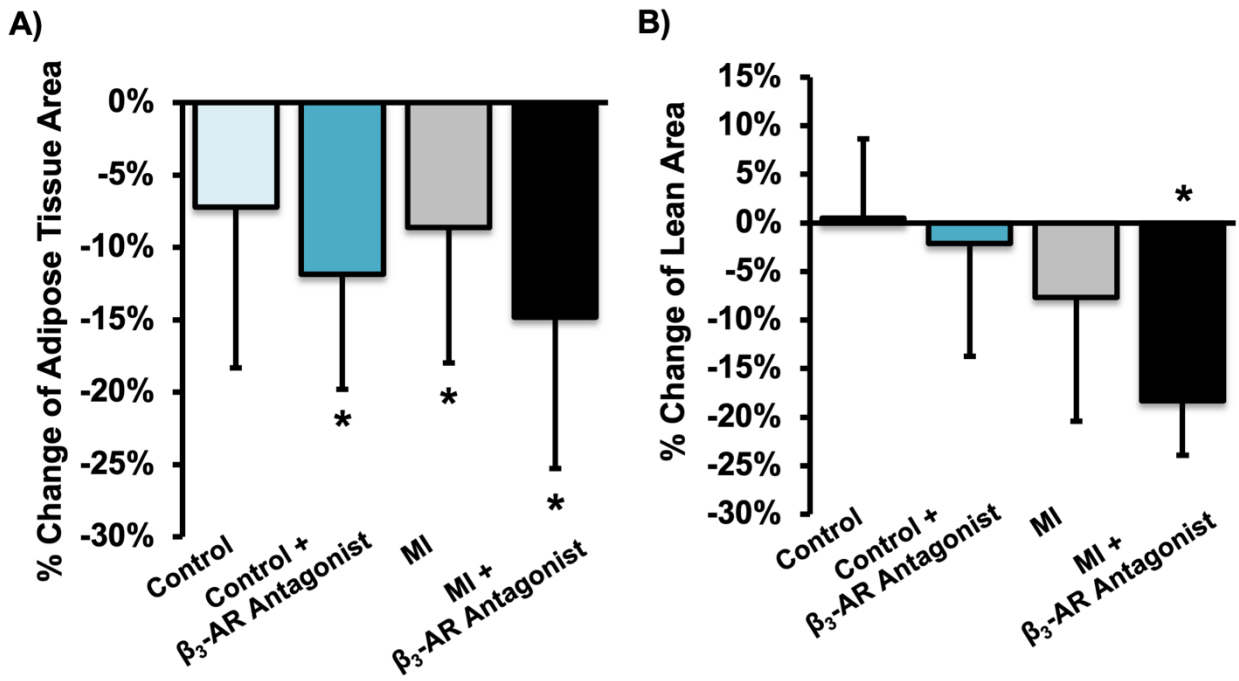

Figure 2.6 Average change in **A)** whole-body fat area and **B)** whole-body lean tissue area between baseline and 9 days post-MI. * denotes $p \leq 0.05$ between baseline and 9 days post-MI. Fat area decreased all groups, but lean tissue area decreased only in MI mice (main effect of MI: $p < 0.001$), and this change was greatest for β_3-AR antagonist treated MI mice (-18.3%, $p = <0.001$).

2.4.4. Micro-Computed Tomography Analysis

Trabecular bone analysis of the axial (L5 vertebral body) and appendicular (distal femoral metaphysis) skeleton yielded results that were generally consistent with those from DXA analysis (**Figure 2.7**). At the L5 vertebral body we observed several statistically significant main effects of β_3-AR antagonist treatment, with treated mice exhibiting decreased BV/TV ($p < 0.001$), Tb.N ($p = 0.003$), Tb.Th ($p = 0.045$), and apparent BMD ($p < 0.001$), and increased Tb.Sp ($p = 0.001$) relative to untreated mice. At the distal femoral metaphysis, we observed a significant main effect of β_3-AR antagonist treatment on Tb.N ($p = 0.028$) only, with treated mice exhibiting decreased Tb.N relative to untreated mice.

Untreated MI mice exhibited an 8.2% lower BV/TV in the L5 vertebral body than untreated Control mice ($p = 0.103$); untreated MI mice also exhibited an 11.4% lower BV/TV ($p = 0.051$) and a 6.6% lower Tb.Th ($p = 0.094$) in the distal femoral metaphysis than untreated Control mice. These MI-associated differences were largely mitigated in β_3-AR antagonist treated mice, though this may be in part due to β_3-AR antagonist treated Control mice having lower BV/TV and Tb.Th than untreated Control mice. No significant differences were observed between any experimental groups for cortical bone microstructural outcomes at the femoral diaphysis.

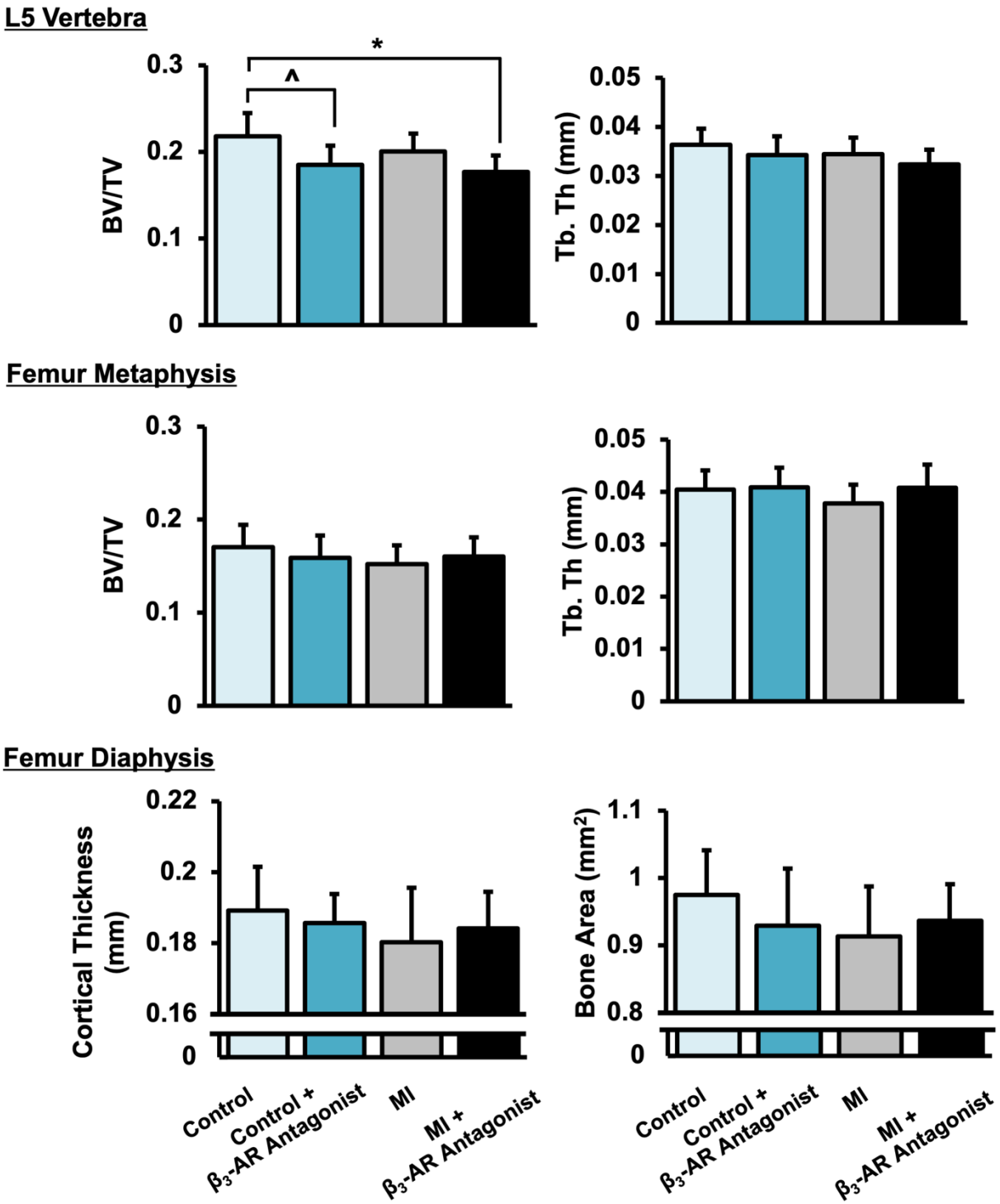

Figure 2.7 Trabecular bone volume fraction and trabecular thickness of trabecular bone in the L5 vertebral body (top) and distal femoral metaphysis (center); cortical thickness and cortical bone area of the femoral mid-diaphysis (bottom) 10 days post-MI. BV/TV and Tb.Th were lower in MI mice, and these MI-associated differences were largely mitigated in β_3-AR antagonist treated mice. p-values < 0.05 are marked by lines between groups.

2.4.5. 3-Point Bending Mechanical Testing of Femora

Mechanical testing of femurs in 3-point bending revealed no significant differences between groups in tissue material properties such as modulus of elasticity and ultimate stress (**Table 2.S1**). Similarly, we observed no significant differences in structural properties such as stiffness, ultimate force, and post-yield displacement. However, we observed significant interactions between MI and β_3-AR antagonist treatment for yield force ($p = 0.004$) and yield stress ($p = 0.046$).

	Control	Control + β3-AR Antagonist	MI	MI + β3-AR Antagonist
Stiffness (N/mm)	126.9 ± 20.2	126.8 ± 9.0	123.0 ± 13.4	115.0 ± 26.6
*** Yield Force (N)**	14.0 ± 2.2	11.3 ± 1.6	12.1 ± 1.6	12.6 ± 1.4
Ultimate Force (N)	18.4 ± 2.5	17.2 ± 1.8	17.9 ± 1.9	16.8 ± 1.8
Post-Yield Displacement (mm)	0.17 ± 0.09	0.17 ± 0.10	0.24 ± 0.18	0.13 ± 0.07
Modulus of Elasticity (kPa)	7789 ± 1491	8573 ± 1144	8344 ± 1258	7841 ± 2154
*** Yield Stress (kPa)**	112.9 ± 14.9	97.2 ± 13.6	103.7 ± 19.6	108.7 ± 14.1
Ultimate Stress (kPa)	148.5 ± 15.3	148.0 ± 8.2	153.8 ± 22.1	143.9 ± 17.2

***** Significant interaction between MI and β3-AR Antagonist treatment ($p < 0.05$)

Table 2.S1 Results from 3-point bending mechanical testing of femurs.

2.4.6. Correlations of Bone Outcomes with Infarct Size

No significant correlations were observed between infarct size and monocyte or neutrophil levels, or between infarct size and DXA data for whole-body or regional measurements. However, we observed significant negative correlation between infarct size and L5 BV/TV of untreated MI mice and femoral metaphysis BV/TV of β_3-AR antagonist treated MI mice (**Figure 2.S1**).

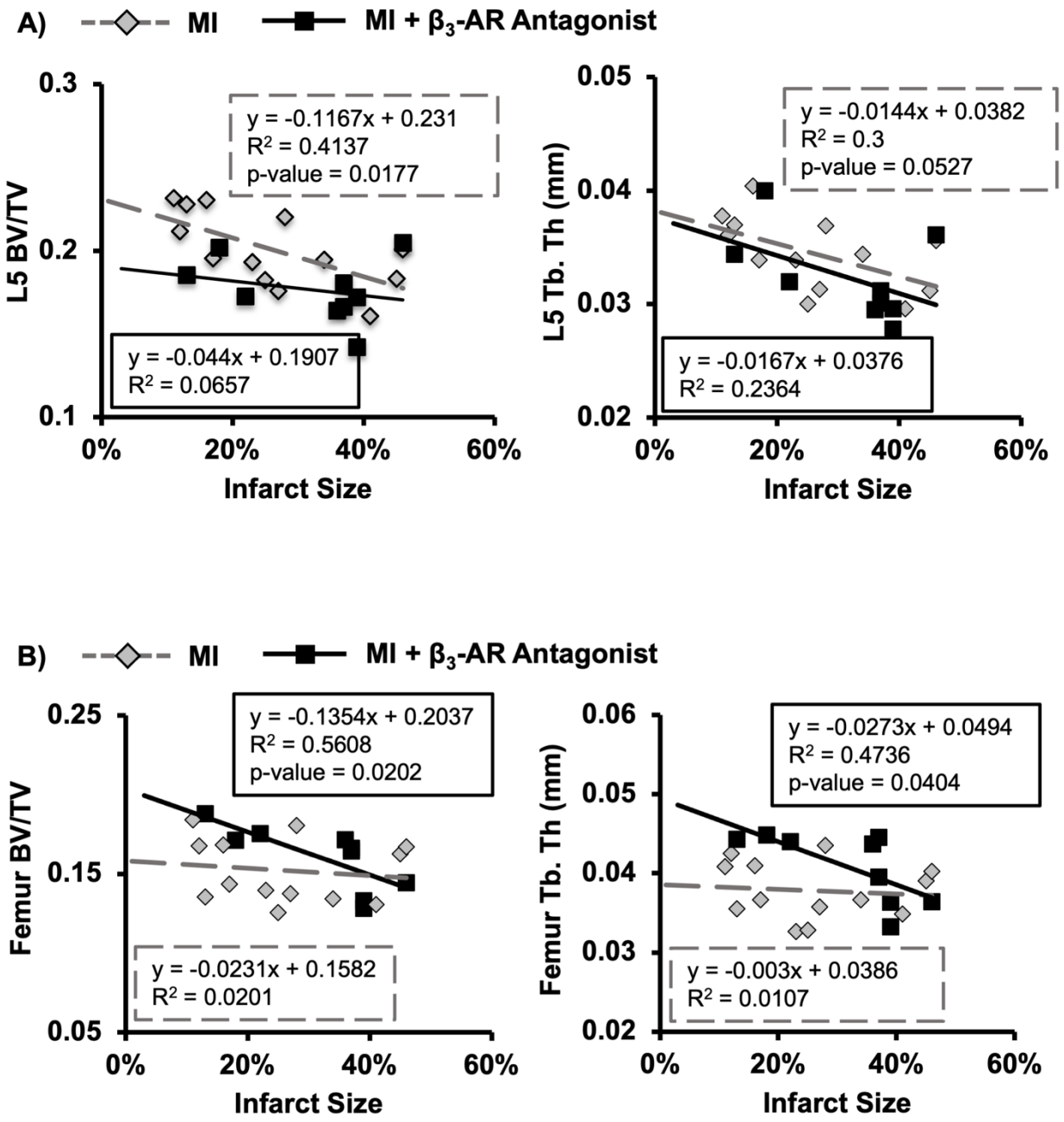

Figure 2.S1 Correlations between ischemic tissue area and **A)** L5 BV/TV and **B)** femur metaphysis BV/TV. Infarct size was significantly negatively correlated with BV/TV of untreated MI mice at the L5 vertebral body and BV/TV of β_3-AR antagonist treated MI mice at the distal femoral metaphysis.

2.5. Discussion

In this study, we investigated bone loss in the whole-body and at axial and appendicular skeletal sites following MI in mice. Consistent with our hypothesis, MI mice had a lower BMD and BMC in the axial and appendicular skeletal sites and lower BV/TV and Tb.Th at the same skeletal sites compared to Control mice. BMD and BMC changes in β_3-AR antagonist treated mice showed a muted effect compared to untreated mice. These results are the first to show a causative effect of MI leading to systemic bone loss, and these data suggest that the sympathetic nervous system may be an important regulator of this response.

The magnitude of systemic bone loss we observed in this study following MI is consistent with our previous study of bone loss following femoral fracture in mice[16]. In both cases, whole body BMD and BMC decreased in injured mice compared to age-matched control mice within 2 weeks post-injury. Additionally, trabecular bone microstructure was diminished in the L5 vertebral body and distal femur in both injured groups. Our previous study also included quantification of other variables such as bone formation rate, osteoclast number and activity, voluntary activity, and levels of interleukin 6 (IL-6) in serum. These parameters were not measured in the current study, but we anticipate that we would observe similar trends in these outcomes following MI in mice.

The SNS acts through signaling via three types of β-adrenergic receptors (β_1, β_2, and β_3). Activation of the SNS via adrenergic neurotransmitters generally inhibits osteoblast

proliferation[74] and triggers osteoclastic bone resorption[75]. Several studies showed that treatment with non-specific SNS inhibitors increased bone mass[51,76], and stimulation of the SNS decreased bone mass[77]. While all three β-adrenergic receptors are present in the skeletal system, β_2 is prevalently expressed in both osteoblasts and osteoclasts[51,78–85]. The specific role β_2 plays with these two cell types have not been thoroughly investigated, but there is evidence that β_2 stimulation has a significant deleterious effect on bone[51]. In contrast, relatively little is known about the role of β_3 receptors in the skeletal system. β_3 has been shown to increase osteoclastogenesis and subsequent bone resorption *in vitro,* but there is no consensus of its effect *in vivo*[78,86]. Beta-blockers have been investigated as a potential treatment for the skeletal system in several studies. Daily treatment with a β_1/β_2 agonist triggered an osteoclastic response[51,87,88] with increases in RANKL and IL-6 expression; another study determined that treatment with a general beta-blocker lead to a high bone mass phenotype[89]. In the current study we utilized the same β_3 adrenergic receptor antagonist (SR 59230A) that was able to lower protease activity, myeloid cell content, and mRNA levels of inflammatory cytokines in atherosclerotic plaques following MI in mice[43], thus allowing us to determine if the same underlying mechanisms contributed to bone loss following MI.

Our findings using β_3-AR antagonist treatment in mice following MI yielded somewhat inconsistent results. In the study by Dutta et al.[43], treatment with the same β_3-AR antagonist decreased the inflammatory response through increased withdrawal of stem cell retention factors by β_3 expressing cells. Four days post-MI, blood HSPC's levels and inflammatory markers were lower in treated groups[43]. In contrast, we observed

greater monocyte and neutrophil levels in the blood of treated mice, although this could be largely due to the time point when blood was collected (day 4 in Dutta et al. vs. day 10 in the current study). Additionally, our results suggest that β_3-AR antagonist treatment generally led to decreased bone volume and diminished systemic bone loss after MI; these data are consistent with a previous study investigating β-adrenergic blockade in rats during hindlimb unloading[90]. In this study, hindlimb unloading resulted in a 20% decrease in cancellous vBMD, but this bone loss was halved in rats treated with a general β-blocker (propranolol) through stimulation of osteoblastic activity and suppression of osteoclastic activity. This study similarly showed that β-blocker treatment of cage activity control rats resulted in net trabecular bone loss at the proximal tibia relative to vehicle-treated controls. We also observed effects of β_3 inhibition on changes in lean tissue area and adipose tissue area. While it was expected that MI may decrease lean tissue and adipose tissue mass due to post-operation recovery, treatment with the β_3-AR antagonist exacerbated the loss of both lean and adipose tissue. These findings are contrary to previous studies that showed that β_3 agonists promote weight loss, especially in obese mice and rats[91–94].

This study established, for the first time, a novel mechanistic relationship between acute cardiac injury and subsequent remodeling in bone. Despite some epidemiological evidence supporting a link between Fx and MI, this is the first study to show a causal relationship between these two seemingly unrelated events. Interestingly, the epidemiological evidence linking incidence of Fx and MI suggests this link is bidirectional, therefore Fx may also exacerbate atherosclerosis, leading to increased

risk of subsequent MI. This is supported by a study by Chiang et al., which reported significantly higher risk of subsequent MI following hip fracture (hazard ratio = 1.29)[13]. Further studies are required to establish this relationship mechanistically.

The current study has some limitations that must be acknowledged. First, quantification of monocytosis was performed by drawing blood through a needle, which allows for the possibility of cell lysing and subsequent inaccuracy in results. Furthermore, our method of measuring monocytosis was a more general assessment of blood cell composition than in Dutta's study, which looked at many markers of inflammation in more specific areas such as the bone marrow and the spleen, two important areas for monocyte proliferation. Secondly, the β-blocker we used was specific to β_3 receptors, where its interaction with the skeletal system is not as well-known as the other types of β-adrenergic receptors. As a result, it is possible the effects we see with treatment could be due to the minimal presence of β_3 receptors in bone cells. It is possible that a general β-blocker would be more successful in preventing bone loss following MI. Third, many of our variables were measured only at one time point (10 days post-MI). While we have previously established that peak bone loss occurs between 7-14 days after fracture[16], it is possible that 10 days post-MI is not the optimal time point to assess bone loss following this type of injury, and we did not quantify recovery of bone at later time points. Additionally, the animals used for this study were young, male mice, while MI and Fx occur more commonly in the older population. We have also shown that bone remodeling after fracture differs between young and middle-aged mice[16]. However, we chose to study young male mice as it allows for minimal confounding factors from

existing comorbidities and for their higher survival rate following MI. Finally, we did not directly quantify bone formation or bone resorption rates in these mice, therefore it is difficult to determine the biological mechanisms underlying the observed changes in bone mass and microstructure.

2.6. Conclusions

This study is the first to establish a causal relationship between MI and bone loss at multiple skeletal sites and suggests that the SNS may have a governing role in this adaptation. This injury-induced response may also be operative in human subjects after MI and may be a potentially catastrophic co-morbidity in post-MI patients. Further delineating the relationship and mechanisms governing this crosstalk could inform future treatments aimed at preventing injuries and preserving skeletal health following ischemic injuries.

2.7. Acknowledgements

We would like to thank Dr. Heike Wulff for her valuable input on this project. Research reported in this publication was supported by the National Institute of Arthritis and Musculoskeletal and Skin Diseases, part of the National Institutes of Health, under Award Number AR071459. The content is solely the responsibility of the authors. The funding bodies were not involved with design, collection, analysis, or interpretation of data, or in the writing of the manuscript. The authors have no conflicts of interest to disclose.

CHAPTER 3: CHARACTERIZATION OF BONE LOSS AFTER MI AND THE ROLE OF C5a-C5aR1

3.1. Abstract

Myocardial infarction (MI) and osteoporotic fracture (Fx) are leading causes of morbidity and mortality, and epidemiological evidence linking their incidence suggests possible crosstalk. We have previously established that the event of MI alone is able to directly cause systemic bone loss. We further found that the sympathetic nervous system, through β-adrenoreceptors, play a limited role in this pathway. However, systemic inflammation after trauma is mediated by multiple systems and no studies have investigated the role of one of the main mediators driving multiple organ dysfunction after trauma, the complement system and its primary complement protein 5a (C5a). In this study, MI was performed on 12-week old C57BL/6 male mice (n = 12-16) as well as C5aR1-/- (n = 6-13) and C5a deficient B10.D2 (n = 13) mice. Additional mice (n=7-13) from each group served as un-operated controls. L5 vertebra and femur were analyzed with micro-computed tomography and bone mechanical properties were quantified using three-point bending mechanical testing of the femora at days 7, 14, and 28 post-MI. Furthermore, activity was measured at 3, 14, and 24 days after operation. We found that MI led to peak bone loss 7 days after injury in the L5 vertebra and 28 days in the femoral metaphysis and diaphysis. We also determined that the C5aR1-/- mice had smaller levels of bone loss but the B10.D2 did not compared to the wild-type control. **Clinical Significance:** These results suggests that MI leads to bone loss and that C5aR1 may be a modulator of this response; this bone loss and increased fracture risk may be important clinical co-morbidities following MI or other ischemic injuries.

3.2 Introduction

3.2.1. Background Significance

Osteoporotic fractures (Fx) and myocardial infarction (MI) are two of the leading cause of morbidity and mortality worldwide[1]. Over 20% of patients will die within 1 year following a hip fracture[2,3], and over 30% will die within 5 years[4,5]. Similarly, within 5 years of a first MI, 36% of men and 47% of women will die due to MI-related complications[6]. Interestingly, there is strong epidemiological evidence showing that MI is associated with increased risk of subsequent Fx. For example, Gerber *et al*. found that Fx incidence rates increased markedly over time (hazard ratio = 1.32) among those with previous MI compared to control patients[10]. An interpretation of these findings is that the incidence of Fx and MI is reflective of advanced stages of underlying chronic diseases such as osteoporosis and atherosclerosis, which are etiologically linked[11]. However, our previous study has established a causative relationship between MI and bone loss. Our results show that the event of MI alone, without any underlying chronic condition, can cause bone loss at multiple skeletal sites 10 days after MI, suggesting that bone loss and increased fracture risk may be an important comorbidity in MI patients[95].

3.2.2. Systemic Inflammation After Trauma

Inflammation plays an important role in healing after trauma. While the inflammatory response primarily targets the site of local injury, injuries with high magnitudes of damage initiates a systemic response. After an MI, serum levels of pro-inflammatory cytokines such as tumor necrosis factor alpha (TNF- α) and interleukin 6 (IL-6) increase

[43,96,97]. A study by Dutta et al. demonstrated that MI resulted in an inflammatory state that exacerbated atherosclerosis and increased risk of subsequent MI through the sympathetic nervous system (SNS). MI activates β3 adrenergic receptors (β3-AR) and induces higher concentrations of monocytes in the serum, thus increasing risk for subsequent MI[43]. Our lab observed a similar positive feedback loop after skeletal trauma. Our previous studies found that bone loss occurred at distant skeletal sites after femoral fracture and was associated with decreased voluntary activity and increased systemic inflammation at 3 days post-injury[16]. These studies further support the findings that sustained systemic inflammation after acute trauma can result in multi-system disruption and increased risk of adverse events systemwide.

3.2.3. C5a-C5aR1

Several systems are key regulators of the inflammatory response after MI. Our previous study investigated the role of the sympathetic nervous system through β3-AR activation. We found that inhibiting β3-AR resulted in partial attenuation of bone loss, suggesting that β3-AR plays a limited role in MI-induced bone loss[95]. However, systemic inflammation after trauma is mediated by multiple systems. One of the main mediators in driving multiple organ dysfunction after trauma is the complement system. In homeostatic conditions, the complement system consists of a series of inactive proteins circulating in serum. Once activated, the proteins will conformationally change and interact with each other for multiple inflammatory processes including leukocyte activation, upregulating the release of pro-inflammatory cytokines, and chemotaxis through receptor mediated mechanisms[57]. Triggering the complement system results in

the initiation of multiple pathways, but all lead to the cleaving of complement protein 5 (C5) into C5a. In comparison to the other complement proteins, C5a has been shown to be a potent mediator in the inflammatory response after MI[57]. Studies have found that the absence of C5a receptors (C5aR) decreased infarct size after MI, suggesting that specific inhibition could attenuate systemic damage post-MI [98,99].

Due to its systemic effects, C5a may serve as a bridge between the cardiovascular and skeletal systems. A study done by Weber et. al. demonstrated that increased C5a levels were associated with heart damage after fracture. Fracture groups had higher levels of troponin I, a marker for cardiac cell damage, than unoperated controls and these levels were sustained for 14 days post-injury. Serum C5a levels showed a similar trend. The investigators concluded that because C5a is known to directly contribute to cardiac dysfunction, it may have played a role in the cardiac alteration seen after femoral fracture[63]. This suggests that C5a has the potential to mediate between different systems.

C5a has also been shown to play a role in bone resorption. Studies have found that C5a activation is necessary for bone healing after fracture. Mice models showed impaired healing due to decreases in inflammation and osteoclastogenesis, suggesting that C5aR activation increases osteoclast differentiation and bone resorption[65]. There is strong evidence that indicates C5a modulates bone through RANKL activation. The binding of C5a to C5aR on osteoblasts initiates the RANK-RANKL pathway which will in turn induce osteoclast differentiation. Studies have shown that changes in RANKL

levels and OC numbers are directly affected by expression of a specific form of C5aR called C5aR1[64,66]. Because C5a is upregulated after MI[59], it is possible that C5a-C5aR1 activation could play a mechanistic role in bridging MI and bone loss. Further investigation is needed to determine if C5aR1 activation plays a central role in MI-induced bone loss.

To address these issues, we sought to determine first, the time course and magnitude of bone loss and recovery following MI and second, whether C5a is a key regulator of bone loss after MI. We hypothesized that systemic bone loss after MI will follow a similar trend as bone loss after Fx, with peak bone loss at day 14 and partial recovery at later time points. We further hypothesized that the absence of the C5a-C5aR1 axis in genetically modified mice would diminish or prevent this bone loss, implicating C5a and C5aR1 as a mediator of systemic bone adaptation following acute injury. These findings would further characterize a novel and potentially critical comorbidity associated with MI and other ischemic injuries and could inform future treatments that aim to preserve skeletal health in these patients.

3.3. Methods

3.3.1 Animals

72 male C57BL/6, wild-type (WT) mice and 24 B10.D2-*Hc^0 H2^d H2-T18^c*/oSnJ mice[100–104] (JAX stock #000461) were obtained from Jackson laboratory (Sacramento, CA). B10.D2 mice carry the *Hc^0* allele from DBA/2J, making them completely serum C5 deficient. Additionally, we obtained 2 male and 4 female homozygous C5aR1-/- mice[105]

from the Jackson Laboratory (JAX stock #033903) for breeding in our animal facility. Mice from the resulting colony were genotyped at UC Davis Mouse Biology program to confirm the absence of C5aR1 mRNA. All purchased animals were obtained at 10 weeks of age and were acclimated to the housing vivarium for 2 weeks prior to the start of experiments. Mice from each genotype group were randomized to MI surgery (n=7-15) or anesthetized, un-operated controls (n=7-13). 17 B10.D2, 26 C5aR1-/-, and 22 WT mice were euthanized at 7 days post-MI surgery. 19 WT and 13 C5aR1-/- mice were euthanized at day 14 post-injury. C5aR1-\- were used for days 7 and 14 timepoints because changes in the L5 vertebra was only present in early time points. B10.D2 mice were used only for day 7 as the mortality rate for these mice was higher than expected and we wanted to focus on the L5 vertebra at that time point. Finally, 23 WT mice were sacrificed 28 days after injury. All animals were maintained and used in accordance with National Institutes of Health guidelines on the care and use of laboratory animals, and all procedures were approved by the UC Davis Institutional Animal Care and Use Committee.

3.3.2. Myocardial Infarction Surgery

The left anterior descending (LAD) coronary artery was permanently ligated as previously described. Briefly, mice were anesthetized with isoflurane, intubated, and continuously monitored with a 3-lead electrocardiogram (ECG). A small incision was made, oblique muscles were bluntly separated to expose the ribs, and a small opening was created in the muscle of the 4th intercostal space. The ribs were then separated, and the pericardium was opened. The LAD was identified and permanently ligated using

an 8-0 Prolene suture. LAD ligation was confirmed by ST segment elevation on the ECG. The ribs and oblique muscles were closed using a 6-0 Ethilon suture and the skin was closed using wound clips. Approximately 150 μL of sterile saline and 0.1 mg/kg buprenorphine were injected subcutaneously before allowing the mouse to recover in its cage on a 35° C warmer for ~1 hour. Standard post-operative procedures were followed for 7 days, including analgesia (0.1 mg/kg buprenorphine) twice per day for 48 hours. Wound clips were removed after 7 days. Unoperated control animals were subjected to anesthesia for 30 minutes and followed the same analgesia schedule.

3.3.3. Activity Analysis

WT mice were taken to the IDDRC Rodent Behavioral Core at the UC Davis Medical Center to assess voluntary movement. Mice were individually placed in enclosed chambers (40 cm x 40 cm x 30.5 cm) interfaced with VersaMax detection software (AccuScan, Omni-Tech Electronics, Columbus, OH) with photocell detectors for 30 minutes at 3, 14, and 24 days. Horizontal activity, vertical activity, and time spent at the center of the cage was measured by photobeam breaks.

3.3.4. Measurement of Infarct Size

Hearts were removed after euthanasia and were placed immediately into cardioplegic solution (composition in mmol/L: NaCl 110, $CaCl_2$ 1.2, KCl 16, $MgCl_2$ 16, and $NaHCO_3$ 10) to prevent continued electrical activity and subsequent ischemic injury to myocytes. Hearts were frozen for 15 minutes, then sliced into 1 mm thick sections (Mouse Heart Slicer Matrix with 1.0 mm coronal section, Zivic Instruments, Pittsburgh, PA). Heart

slices were stained with 1% 2,3,5-triphenyltetrazolium (TTC) in PBS for 15 minutes at 35° C after which the slices were stored in PBS for 24 hours. Heart sections were gently blotted with a Kimwipe, then imaged with an office scanner (EPSON Perfection 4990 Photo, Suwa, Japan). Individual color images were taken at 1200 dpi resolution for each heart section, and images were analyzed using ImageJ[70,71]. To determine the area of ischemic tissue, a color filter was placed on the image to exclude all colors except for white. The filter was then manually adjusted until only the unstained ischemic tissue was highlighted. Total size of ischemic injury was quantified as the total area of ischemic (unstained) tissue in all transverse slices for each heart normalized by the total area of all slices (6-8 sections for each heart). Because white tissue is present in hearts without ischemic injury, unoperated hearts were also quantified to use as a baseline control.

3.3.5. Micro-Computed Tomography Analysis

L5 vertebrae and right legs were collected following euthanasia and fixed in 4% paraformaldehyde for 3-4 days before preservation in 70% ethanol. L5 vertebrae and right femora were imaged with micro-computed tomography (SCANCO μCT 35, Brüttisellen, Switzerland) to determine trabecular bone microstructure of the L5 vertebral body and distal femoral metaphysis and cortical bone microstructure of the femoral mid-diaphysis. All bones were imaged according to the guidelines for μCT of rodent bone (energy = 55 kVP, intensity = 114 mA, 6 μm nominal voxel size, integration time = 900ms)[72]. Analysis of trabecular bone in the L5 vertebral body was performed by manually contouring 2D transverse slices in the region between the cranial and caudal

growth plates and excluded the vertebral processes. Analysis of the femoral metaphysis was similarly performed with manual contouring beginning at the convergence of the distal femoral growth plate and extending 1500 μm (250 slices) proximal. Trabecular bone volume fraction (BV/TV), trabecular thickness (Tb.Th), trabecular number (Tb.N), trabecular separation (Tb. Sp), connectivity density (Conn.D), and other microstructural parameters were determined using the manufacturer's analysis software. Analysis of cortical bone in the femoral diaphysis was performed by contouring transverse slices centered on the midpoint of the femur including a total of 600 μm (100 slices). Bone area (B.Ar), cortical thickness (Ct.Th), and other microstructural parameters were determined using the manufacturer's analysis software.

3.3.6. 3-Point Bending Mechanical Testing of Femora

Mechanical testing was performed on femurs using 3-point bending to determine bone structural and material properties using a materials testing system (ELF 3200, TA Instruments, New Castle, DE, USA). Left femurs were -20°C immediately after collection and rehydrated for 10-15 minutes in PBS solution before mechanical testing. The span length of the lower supports was 8 mm, and the femur was positioned so that the posterior aspect of each bone was downward (loaded in tension). The upper loading platen was positioned in the middle of the bone perpendicular to the long axis of the femoral shaft. The bone was preloaded to 1-2 N to ensure contact with the upper platen. Loading was applied at a displacement rate of 0.01 mm/sec until fracture, and displacement and resultant force were recorded at 50 Hz.

Whole-bone structural properties were determined from force-displacement curves using standard methods[73]. Stiffness was calculated as the slope of the linear pre-yield region. Post-yield displacement was determined as the displacement difference between the yield and fracture displacements. Material properties were calculated using previously established beam theory equations[73]. Elastic modulus, yield stress, and ultimate stress were determined using bending moment of inertia (I) and bone radius (c) determined from μCT analysis of the femoral mid-diaphysis.

3.3.7. Statistical Analysis

All results are expressed as mean ± standard deviation. Because data from activity analysis was longitudinal, repeated measures analysis of variance (ANOVA) stratified by operation (MI or Control) and time point (3,14,24 days post-MI) with Šídák post hoc test was used. Comparisons of WT mice from different time points were analyzed by two-way ANOVA stratified by operation and time point (7,14,28 days post-MI) with post hoc analysis using unpaired t-test. Differences in genotype was also analyzed using two-way ANOVA, but stratified by operation and genotype (WT, C5aR1-/-, B10.D2) with Tukey's Honest Significant Difference post-hoc test. Correlations were evaluated using Pearson's correlation coefficient. All statistical tests were performed using Prism 9.5.0 for Mac, Graphpad Software, San Diego, California USA, www.graphpad.com. Statistically significant differences were identified at $p \leq 0.05$; trends were noted at $p \leq 0.10$.

3.4. Results

3.4.1. Activity Analysis

Activity analysis at day 3 indicated 12.4% less total activity, -16.8% less horizontal activity, and -32.2% less vertical activity in the MI group than in the unoperated group (**Figure 3.1**). There were no significant differences between operated and unoperated groups at later time points. As expected, total activity level decreased at later time points as the enclosure was no longer “novel” for the mice (significant effect of time: p-value = 0.01 horizontal; 0.008 vertical).

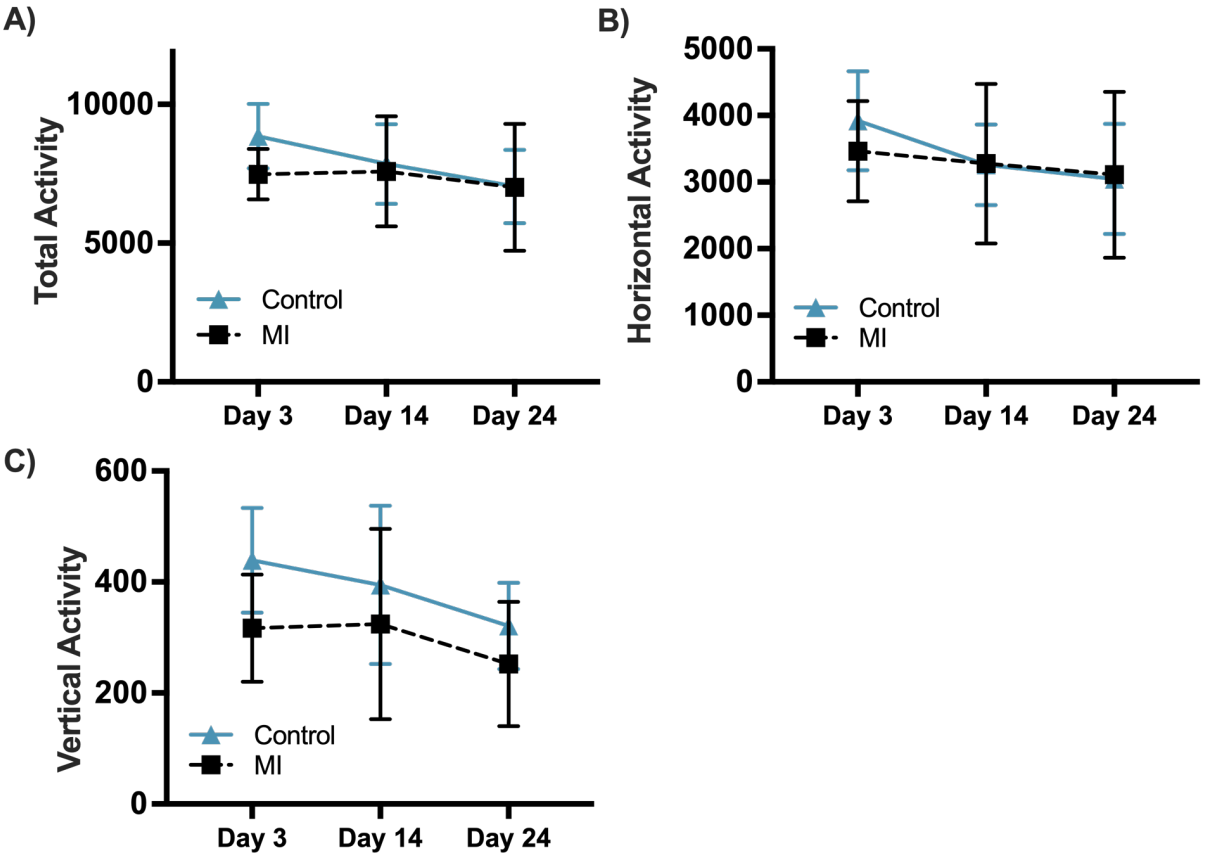

Figure 3.1 A) Total **B)** horizontal and **C)** vertical activity of MI operated and unoperated mice measured in sensor breaks. Main effects of time and subject were significant in horizontal and vertical activity.

3.4.2. Measurement of Infarct Size

Presence of ischemic tissue was consistently observed in the left ventricle inferior to the ligation site as was seen in **Figure 2.1b**, confirming successful MI. Infarct size (IA/TA) had no significant differences although there was an increasing trend between infarct size and time (**Figure 3.2A**). Furthermore, C5aR1-/- was found to have a protective effect in infarct severity. WT mice had increases in infarct size from day 7 to day 14 post-MI. In comparison, C5aR1-/- did not. Additional statistical analysis found that genotype was a significant effect at day 14, suggesting that C5aR1-/- may have a role in infarct size at that time point (**Figure 3.2B**).

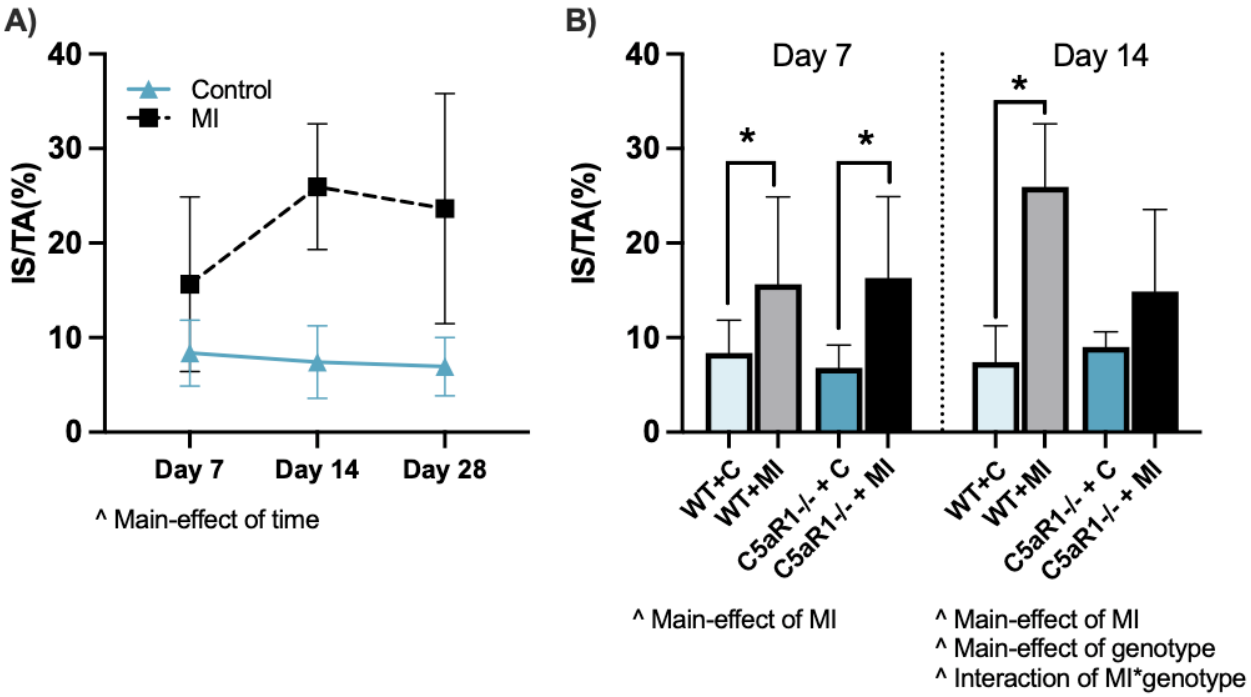

Figure 3.2 A) Infarct size quantified as infarct area over total area of the heart (IA/TA) of WT mice at days 7, 14, and 28 post-MI. There were no significant differences over time. **B)** IA/TA of WT and C5aR1-/- mice at days 7 and 14. * denotes p-value < 0.05 using unpaired t-test between operated and unoperated groups. ^ denotes p-value < 0.05 of main effects.

3.4.3. Micro-Computed Tomography Analysis

3.4.3.1. Time Course of Bone Loss and Recovery Following MI in Wild-Type Mice

MI operation resulted in peak bone loss at different time points at different skeletal sites. In the L5 vertebra, peak bone loss was found at 7 days post-MI. MI operated mice had 12.3% less BV/TV (p-value = 0.020) and 8.3% less Tb.th. (p-value = 0.047) compared to unoperated controls at each time point (**Figure 3.3)**. BV/TV data also had trends towards significance for main effect operation and main effect of time while Tb. Th showed significant main effect of time (p-value = 0.0015) but not operation. The Conn dens. and structure model index (SMI) were also significantly greater in MI groups (not shown). Later time points showed recovery as there were no significant differences at days 14 and 28 post-injury.

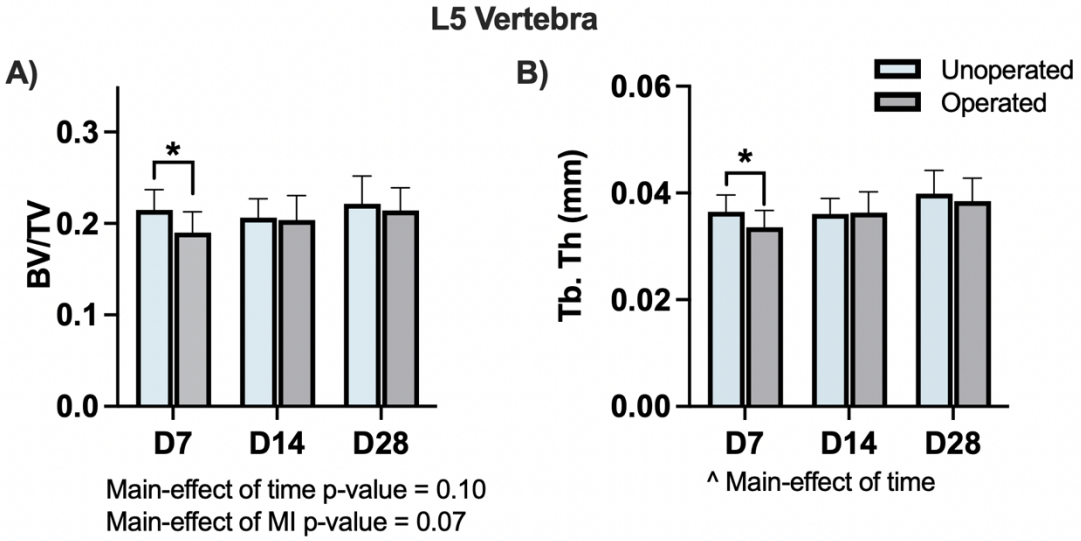

Figure 3.3 μCT analysis of WT mice at 7, 14, and 28 days post-MI. **A)** BV/TV was significantly different at Day 7 between operated and unoperated groups when analyzed with unpaired t-test. Main effects were statistically trending. **B)** Similarly, differences in Tb. Th was statistically significant at day 7 when analyzed with unpaired t-test with significant effect of time.

In comparison, bone loss did not occur in the distal femoral metaphysis until 28 days post-MI. There was 4.5% less Tb. N. (p-value = 0.034; unpaired t-test) and 4.6% more Tb. Sp. (p-value = 0.033; unpaired t-test) relative to unoperated controls with a decreased trend for Tb. Th (**Figure 3.4 B-D**). There was also 14.1% less BV/TV, but this was not statistically significant. The main effect of time was significant (p-value = 0.036) at this time point (**Figure 3.4 A**).

Analysis of the cortical bone in the femoral diaphysis yielded similar trends. There were no significant differences until 28 days after MI operation where Ct. Th. was 5.1% less in the MI group (p-value = 0.037; unpaired t-test). There were also trends towards lower B. Area at this time point, but these were not statistically significant (**Figure 3.4 E-F**).

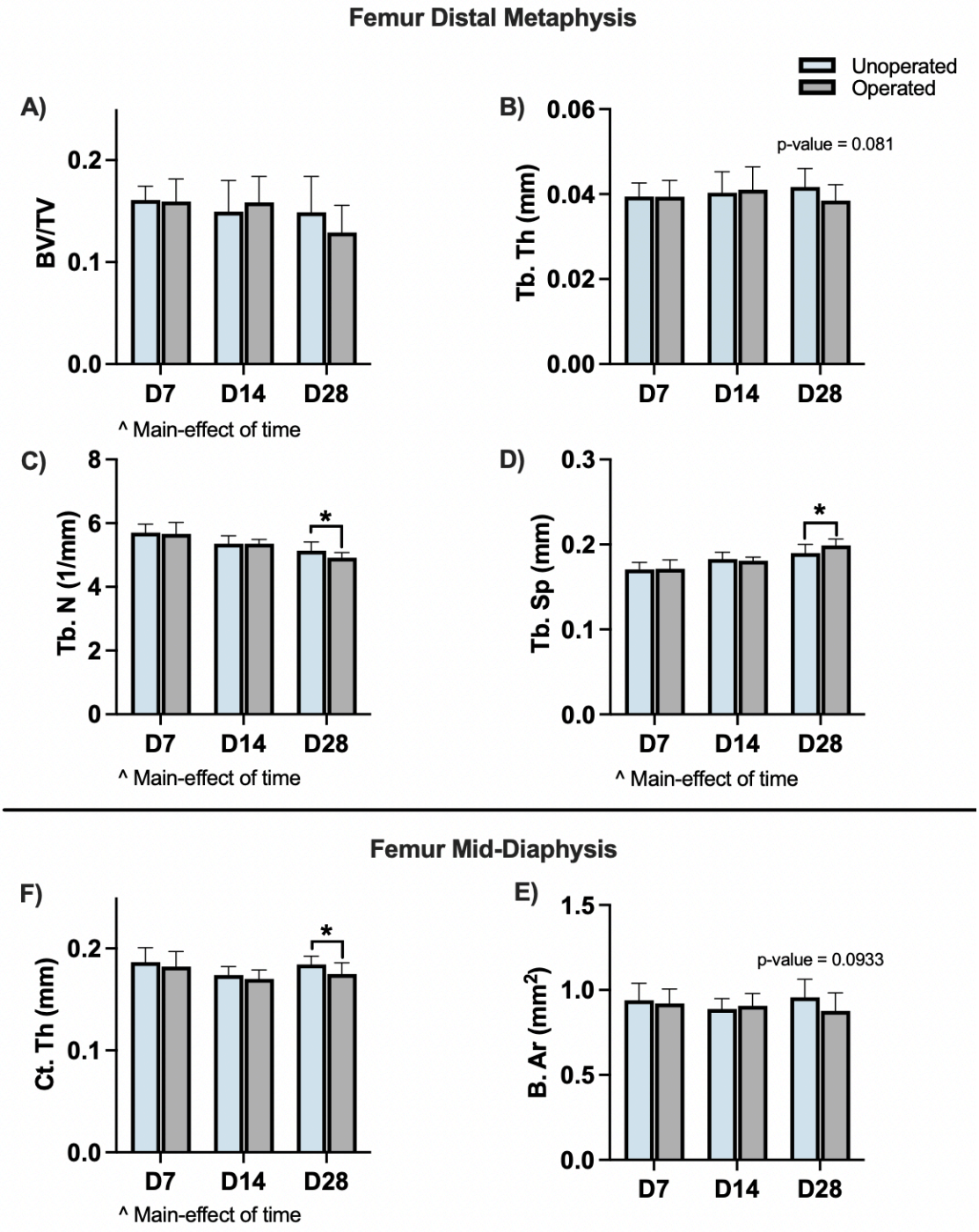

Figure 3.4 μCT analysis of WT mice at 7, 14, and 28 days post-MI. **A-D)** Trabecular bone analysis in the femur metaphysis showed significant main effect of time in BV/TV. **E-F)** Cortical thickness and bone area at the femur mid-diaphysis. Like the metaphysis, there are no differences until day 28. The main effect of time was significant in the Ct. th.

3.4.3.2. Effect of C5a Deficiency on Post-MI Bone Loss

3.4.3.2.1. L5 Vertebra

C5a deficiency effected baseline bone phenotypes in the L5 vertebra. C5aR1-/- had consistently more bone mass. For example, BV/TV was 12.7% greater at day 14 (p-value = 0.073). BV/TV was also 10.2% greater at day 7, but this was not statistically significant (**Figure 3.5 A**). In comparison, B10.D2 mice had consistently less bone. At day 7, B10.D2 mice had 13.5% lower Tb. N (p-value = <0.0001) and 23.5% greater Tb. Sp. (p-value = 0.003) relative to WT mice (**Figure 3.5 C-D**). The main effect of genotype on BV/TV and Tb. Th was significant for all time points.

However, C5a deficiency did not affect bone loss after MI. WT, C5aR1-/-, and B10.D2 mice had similar percent differences between MI and unoperated groups for both BV/TV and Tb. Th, although, C5aR1-/- had a smaller magnitude of bone loss. For example, BV/TV for WT and B10.D2 mice were 12.3% and 10% lesser than their unoperated control. In comparison, C5aR1-/- had 6.7% lesser BV/TV but these changes were not statistically significant (**Figure 3.5 A**). The main effect of operation on BV/TV and Tb. Th was significant for day 7 only.

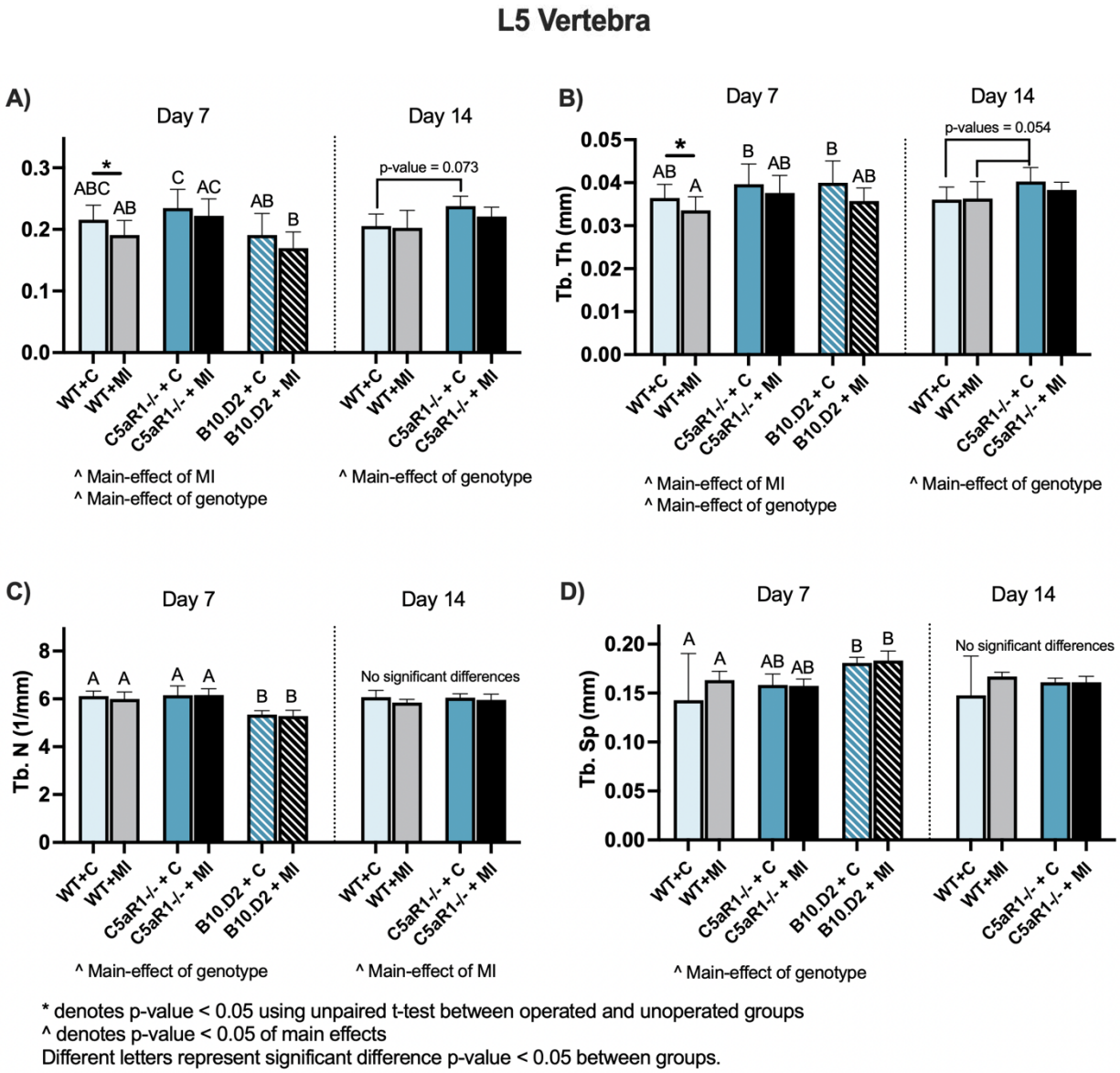

Figure 3.5 μCT analysis of L5 vertebra in WT, C5aR1-/-, and B10.D2 C5a deficient mice at 7 and 14 days post-MI. **A-B)** Bone volume fraction and trabecular thickness were higher in unoperated C5aR1-/- mice respective to WT control. Bone loss after MI was present for all genotype groups. **C-D)** Trabecular number was lower and trabecular separation was higher in B10.D2 C5a deficient mice.

3.4.3.2.2. Femur Metaphysis and Diaphysis

Similar trends were observed in the femoral metaphysis. C5aR1-/- had greater bone mass at baseline. At day 7, there was 15.8% greater BV/TV and 13.4% greater Tb. Th respective to WT. These differences were similar at day 14 at 15.7% greater and 11.6% greater respectively (**Figure 3.6 A-B**) although these differences at both time points were not statistically significant. Conversely, B10.D2 mice had significantly lower bone mass. There was 34.2% less BV/TV (p-value = 0.026), 23.2% less Tb. N), and 24.6% more Tb. Sp (p-values < 0.0001) compared to WT (**Figure 3.6 A, C-D**). The main effect of genotype was significant for all variables at all time points.

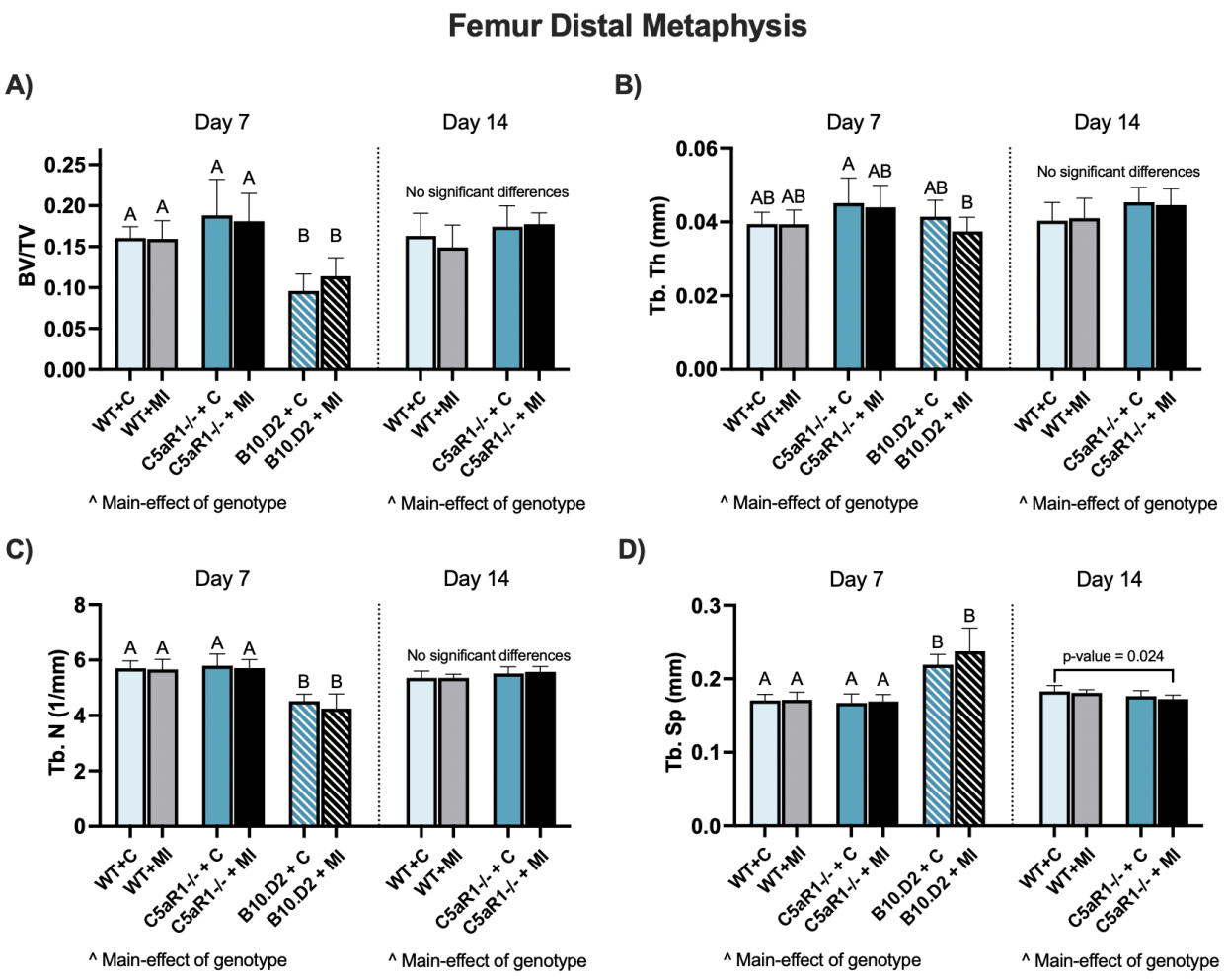

Figure 3.6 μCT analysis of femur in WT, C5aR1-/-, and B10.D2 C5a deficient mice at 7 and 14 days post-MI. In the femur distal metaphysis, **A-B)** bone volume fraction and trabecular thickness were higher in unoperated C5aR1-/- mice respective to WT control. **C-D)** Trabecular number was lower and trabecular separation was higher in B10.D2 C5a deficient mice.

The diaphysis of C5aR1-/- mice had similar differences. At day 14, B. area and Ct. Th were greater by 9.5% and 11.1% respectively (p-values = 0.018, 0.001) (**Figure 3.7**). There were no other significant differences in cortical thickness between C5aR1-/-, B10.D2, or WT mice at day 7. The main effect of genotype was only significant for B.area at each time point.

As expected, C5a deficiency did not affect bone loss in the femoral metaphysis or diaphysis as significant bone loss in the femur did not occur until 28 days post-MI. There were no statistical differences between unoperated and operated groups for any genotypes (**Figure 3.6 & 3.7**).

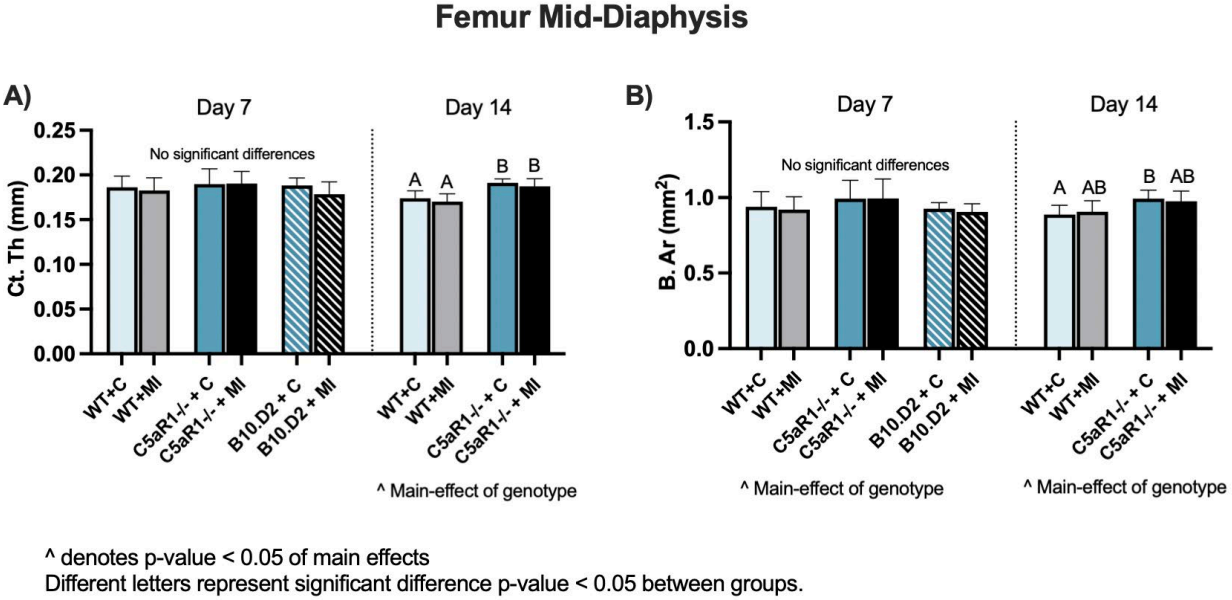

Figure 3.7 μCT analysis of femur in WT, C5aR1-/-, and B10.D2 C5a deficient mice at 7 and 14 days post-MI of the femur diaphysis. **A-B)** Ct. Th and B. Ar was greater in C5aR1-/- mice.

3.4.4. 3-Point Bending Mechanical Testing of Femora

Mechanical properties of the femoral diaphysis partially corresponded with the results of μCT analysis. There were no significant differences after MI in all groups for all time points (not shown). At baseline, only C5aR1-/- showed any differences relative to WT. Stiffness was significantly greater in C5aR1-/- groups on day 7 (19.2%, p-value = 0.004). There was also significant increase in stiffness by 40.8% (p-value = 0.014) and fracture load by 22.9% (p-value = 0.042) 14 days post-MI (**Figure 3.8)**. There were no differences between B10.D2 and WT mice.

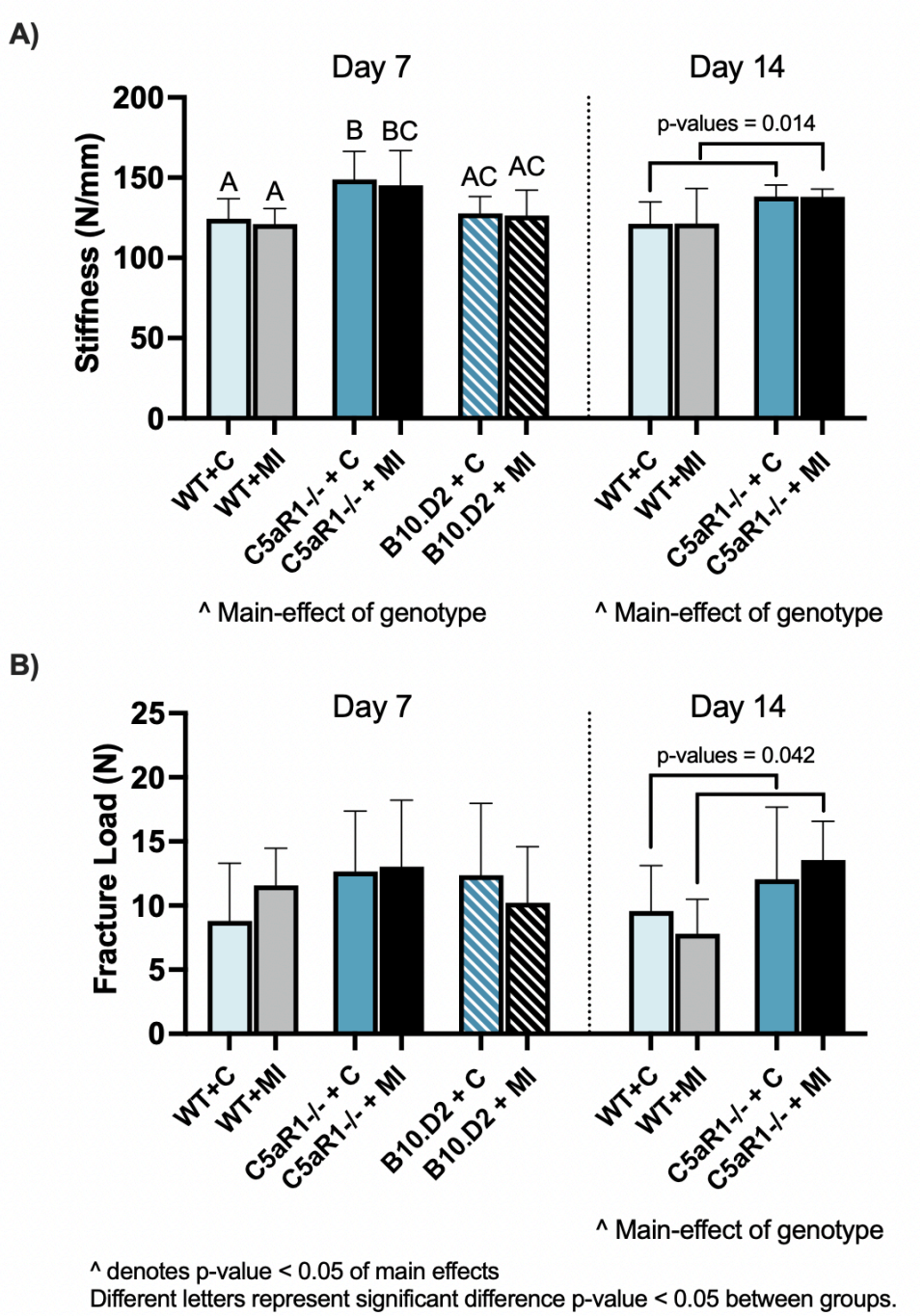

Figure 3.8 3-point bending analysis of femur. At baseline, C5aR1-/- had **A)** greater stiffness (day 7 and 14) and **B)** fracture load (day 14 only) compared relative to WT control.

3.4.5. Correlations

There were no significant correlations between infarct size (IA/TA) and BV/TV in the L5 vertebra and femoral metaphysis or between IA/TA and Ct. Th in the diaphysis. However, there is a trend towards a negative slope in all groups with the exclusion of D28WT, although this is not statistically significant (**Figure 3.9**)

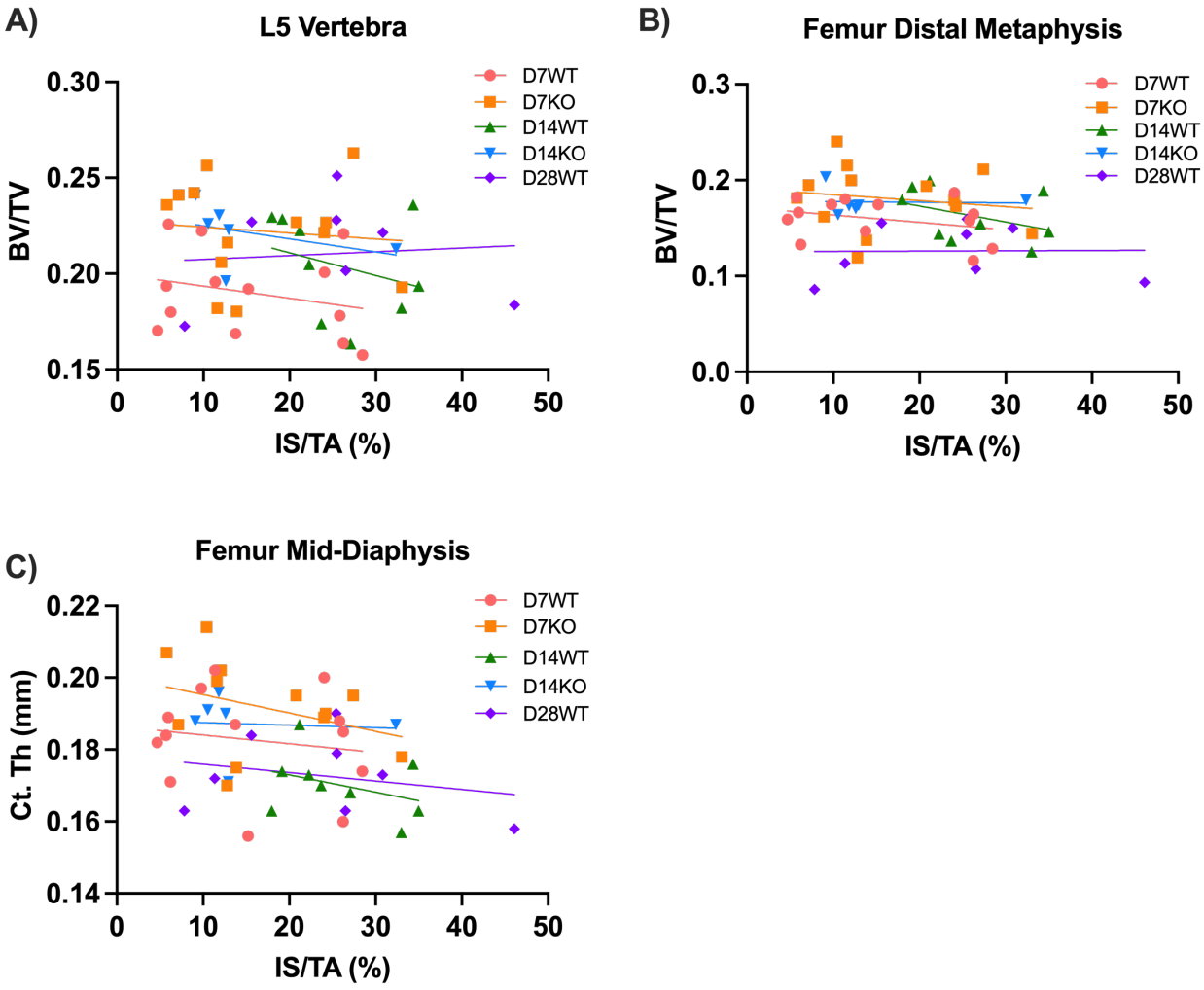

Figure 3.9 Correlations between ischemic area (IA/TA) vs **A)** BV/TV in the L5 vertebra, **B)** BV/TV in the femoral metaphysis, and **C)** Ct. Th in the femoral diaphysis.

3.5. Discussion

In this study, we characterized the time course of bone loss after MI in mice and investigated the role of C5a and C5aR1 in this process. Our results partially support our original hypothesis. MI mice showed significant loss of trabecular bone volume in the L5 vertebra at day 7 with recovery at later time points. In contrast, peak bone loss in the femoral metaphysis and diaphysis was at day 28 post-MI. Furthermore, C5aR1-/- mice had less bone loss due to MI compared to WT, although this was not statistically different. These results are the first to determine the time course of MI-induced bone loss mice and show that C5a-C5aR1-/- may serve as a partial regulator of this response.

3.5.1. Heart Infarct Sizes

While infarct sizes were significantly greater than the unoperated control for each genotypic group, the day 14 C5aR1-/- group had smaller IA/TA differences and was not statistically significant. These results suggest that the severity of MI to the heart increases over time until an eventual plateau. It also suggests that C5aR1 may play a role in regulating the severity of the heart attack and that inhibiting C5aR1 could mitigate the damage to the heart. These results are consistent with existing literature. Studies have shown that administration of treatments inhibiting the creation of C5a or inhibition of its receptor resulted in infarct reduction after reperfusion[98,99].

3.5.2. Differences in Time Points at Different Skeletal Sites

Contrary to our hypothesis, bone loss occurred at different time points at different skeletal sites. While the trabecular bone in the L5 vertebra decreased at 7 days post-MI, both trabecular and cortical bone in the femur had no changes until day 28. The L5 vertebra is part of the axial skeleton whereas the femur is categorized as the appendicular. The femur is considered to be more of a weight bearing site so it could be more responsive to changes in mechanical loading. Furthermore, we speculate that differences in blood flow to the axial versus appendicular skeleton could cause these differences. Studies have showed increased vascularization leads to altered levels of bone remodeling[106,107]. Furthermore, a study done by Nobuto et. al. found that changes in the periosteum vasculature could alter the transport of factors in bone remodeling[108]. Because the vertebra is more vascularized than the femur (and closer to the heart), it could be possible that the differences we see in the timing of bone loss is due greater changes in factors for bone remodeling[109,110]. However, additional studies are needed to make a conclusion.

The magnitude of bone loss observed in this study is consistent with our previous study of bone loss following femoral fracture, however the time course was not[16]. Peak bone loss after fracture occurred 2 weeks post-injury. However, our study found that peak bone loss at the L5 vertebra 1-week post-injury, suggesting that there are different mechanisms regulating these processes. The magnitude of bone loss in the femur was also similar, however, this difference was seen at four weeks post-MI compared to the two weeks post-fracture. Furthermore, this study saw less cortical thickness in the injured group at four weeks post-MI where there were no differences in the cortical

thickness after fracture for any time points. Analysis of voluntary activity were also similar after both types of injuries. The greatest difference in activity between injured and uninjured groups were at early time points with no differences at later ones[16]. Given these results, it is likely that the cellular mechanisms mediating bone loss after fracture are not the same as after MI. While the mechanism driving bone loss after fracture is unknown, a theory has been proposed that fracture healing requires greater mineral need to the local bone for repair and this mechanism is not present after MI[44].

3.5.3. Complement System

As mentioned previously, the complement system is one of the primary initiators of the inflammatory response after injury. Although well-characterized after MI, the effects of the complement system on bone after injury are not as well-known. Studies have found that osteoblasts and osteoclasts are able to produce and cleave C5 into C5a. Furthermore, activation of C5aR1-axis induces an immune response in osteoblasts that could be exacerbated in inflammatory states. There are two types of C5aR receptors found on osteoblast surfaces, C5aR1 and C5aR2[65]. Our study focused on the role of C5aR1 because it was shown to be critically responsible in osteoclastogenesis after fracture while C5aR2 did not[65]. Furthermore, a study found that C5aR1 and C5aR2 played antagonistic roles in the inflammatory response. C5aR1 was found to be pro-inflammatory while C5aR2 was anti-inflammatory[65].

Our findings were inconsistent between C5aR1-/- and C5a deficient B10.D2 mice. At baseline, C5aR1-/- had greater BV/TV and Tb. Th than WT control, which suggests its

role in osteoclastogenesis. This is consistent with the literature[65,66]. Conversely, B10.D2 mice had lower Tb. N and greater Tb. Sp. Considering the roles of C5aR1-/- and C5aR2-/-, this response is not unexpected. C5aR2 is considered a scavenger receptor for C5a; directly competing with C5aR1[111,112]. Without C5a, both C5aR1 and C5aR2 cannot be activated. It is possible that because of this, there wasn't a protective effect of C5aR2 against bone resorption.

The effects of C5aR1 and C5a on MI-induced bone loss partially supported our hypothesis. While both groups had bone loss after operation, the C5aR1-/- had less bone loss compared to either WT or B10.D2 mice. This suggests that C5aR1-/-, not C5a plays a role in bone loss after MI. The attenuating effect of C5aR1-/- on bone loss was supported in literature. A study found that C5aR1-/- had lower levels of Il-6 and neutrophil recruitment after femur fracture, suggesting that other pro-inflammatory mechanisms such as IL-6 mediated signaling could also play an important role[65]. Furthermore, the B10.D2 group had a high mortality rate in comparison to either WT or C5aR1-/- groups. C5a is a powerful recruiter of monocytes and neutrophils to areas of damage after MI. Monocytes and neutrophils have been thought to be essential in healing as they can be both pro- and anti-inflammatory. Along with phagocytosis of damaged tissues, these leukocytes have also been shown to have pro-reparative effects by upregulating fibroblast activity[113,114]. It is possible that C5a deficiency disrupted healing, leading to an increased mortality rate.

3.5.4. Limitations

The current study has some limitations that must be acknowledged. First, with the exception of activity analysis, data was taken at terminal time points rather than a longitudinal study. An added longitudinal bone measurement such as dual x-ray absorptiometry (DXA) would further characterize the time course of bone loss after MI. Furthermore, bone was characterized up until 28 days post-MI in wild-type mice. Longer time points will be needed to determine whether bone in the femur would recover as it did in the L5 vertebra. Secondly, C5aR1-/- and C5a deficient B10.D2 mice were only used at earlier time points. Because femoral changes weren't seen until 28 days after MI, it is difficult to predict if C5a-C5aR1-/- had effects at later time points there. Additionally, the genetic mice models used to measure the effects of C5a inhibition was not consistent. Unlike C5aR1-/- mice, B10.D2 mice were not specifically genetically targeted. It is possible that the B10.D2 mice had a compensatory mechanism that could contribute to bone loss after MI. Lastly, only male mice were used in this study. Studies have shown that the inflammatory response differ between male and female in humans[115–117]. Further investigation is needed to determine differences in MI-induced bone loss between sexes.

3.6. Conclusions

This study is the first to characterize bone loss after MI at different skeletal sites at multiple time points. Reduced bone loss in C5aR1-/- mice compared to WT controls suggests that the complement system may play a regulatory role in this adaptation. This injury-induced response may also be operative in human subjects after MI and may potentially be a co-morbidity in post-Mi patients. Further delineating the relationship and

mechanisms governing this crosstalk could inform future treatments aimed at preventing injuries and preserving skeletal health following ischemic injuries.

3.7. Acknowledgements

Research reported in this publication was supported by the National Institute of Arthritis and Musculoskeletal and Skin Diseases, part of the National Institutes of Health, under Award Number AR071459. The content is solely the responsibility of the authors. The funding bodies were not involved with design, collection, analysis, or interpretation of data, or in the writing of the manuscript. The authors have no conflicts of interest to disclose.

APPENDIX

4.1. DETAILED PROTOCOLS

4.1.1. BLOOD COLLECTION

4.1.1.1. Retro-Orbital – for Complete Blood Count (CBC)

Supplies

1. Pipet-aid
2. Pasteur Pipet
3. Small well of PBS
4. 0.5mL PBS of SC Injection
5. Heparinized tubes (EDTA)
6. Plastic pipettes

Procedure

1. Place mouse in nose cone with stomach-side down (prone). Hold head firmly with the right eye angled up.
2. Angle Pasteur pipette so that it's parallel to the mouse and table and put the tip into the medial side of the right eye.
3. Push and twist gently, but firmly until blood comes out. Immediately angle the needle downward.
4. Pull back and forth in small movements and keep twisting until blood reaches the wide end.
5. Immediately attach to the pipet-aid and deposit into the heparinized tubes. Gently invert tube 10x and place in 4C° until all mice are finished.
6. Close the cover until it snaps. Gently invert up and down ten times. Place in the fridge.
7. Kimwipe the eye to dab it. Put a small drop of saline onto the eye and dab again.
8. Inject 0.5 mL PBS SC
9. Throw the eye needle into the sharps container.
10. Submit heparinized tubes to the UC Davis VMTH Clinical Laboratory Services

4.1.1.2. Inferior Vena Cava – for Serum Collection

Supplies

- Scissors and tweezers
- 30-gauge needle
- 1mL syringe

Procedure

1. Open peritoneal cavity by pulling the skin on the stomach up and cutting. Move organs to the side.
2. Identify inferior vena cava.
    a. Look for a large blood vessel close to the bladder and running parallel and near to the spine.

3. Insert needle parallel, but at a small angle up into the vena cava.
4. Slowly pull syringe. There should be a flash of blood if pulled correctly. Allow blood to fill the syringe before pulling the stopper again.
5. Work slowly and allow the blood to fill up with every pull of the stopper. If blood stops flowing, twist the stopper to allow blood to continue filling the syringe.
6. On average, one mouse usually gives 500-750 μL.
7. Take needle out of syringe and deposit blood into tube.

4.1.2. HEART INFARCT SIZE ANALYSIS

4.1.2.1. Heart Collection and TTC Staining

Supplies

- Scissors, coarse tweezers, fine tweezers
- PBS
- 1% 2,3,5-Triphenyltetrazolium chloride (TTC) in PBS
    - 1g dissolved in 100mL PBS
- Cardioplegia
    - Must be cold
- 6x4 Wells
- Kimwipes
- Mouse heart slicer matrix
    - Stainless steel 1.0mm coronal section slice intervals (Zivic)
- Single edge razor blade

Procedure

1. Pull up sternum and cut through. Cut through both sides of diaphragm. Cut through both sides of ribs underneath the shoulder to expose the chest.
2. Identify one of the lungs and pull up. Angle your scissor down and cut.
3. Keep pulling the lung up as you continue cutting down. Be gentle.
4. Place immediately in PBS. “Swish” the heart around to get rid of any excess blood inside the heart.
5. Using two fine tweezers, pry apart any extra tissues away from the heart. If it rips easily, then it’s not supposed to be there. If there is resistance, it’s part of the heart.
6. Place in one of the wells in PBS and place in 4C° fridge until ready to section.
7. When ready to section, pipette out the PBS and place in the freezer for 10-15 minutes.
    a. 15 minutes is the MAX. Do not let it stay in the freezer for longer than that.
8. At 15 minutes, place the heart in a kimwipe and dab gently to get rid of any excess moisture.
9. Place heart in the slicer matrix as flat as possible. Fill the wells with TTC.
10. Place one blade at the first slot near the base of the heart.
11. Place a second blade near the apex. Ideally, it’s about the 9^{th} or 10^{th} slot from the apex depending on how enlarged the heart has become.
12. Place a third blade in the slot in the middle of the heart. Press down as consistent as possible.
13. From there, place two more blades halfway between the middle and the end blades.
14. Place two more blades in the most middle slots. This ensures the infarct area is at least cut thin enough.
15. Place the remaining blades in a symmetrical manner until the slots next to the ends are the only ones left.
16. Take the end blades out. Hold the heart in place with fine tweezers. Place the blades into the remaining slots.

17. Slide the blades back and forth as much as possible.
18. With fine tipped tweezer, gently scrape the heart away from the blade and place in wells.
19. Repeat with remaining hearts in the tray. After it is finished, place on heater, 30-35 degrees C, for 15 minutes.
20. Pipette out the TTC and fill the wells with PBS instead.

4.1.2.2. Heart Imaging

Supplies

- Epson scanner (Epson Perfection 4990 Photo)
    - Any scanner would work.

Procedure

1. Dry heart pieces for one heart on a kimwipe. Place in a single file across the width of the scanner surface.
    a. Prop the scanner open to ensure heart shapes are altered.
2. Set resolution to 1200 dpi.
3. Hit *Preview.*
4. Create a box over one of the heart pieces. Change the size of the box to 0.58 x 0.58 inch by changing the values in the pop-up window in *Document Size*.
5. Hit *Scan…*Wait for it to finish scanning.
6. Hit *Save File.*
7. Move the box to the next heart section and repeat until all are done.
8. Wipe the scanner surface with an alcohol wipe followed by a kimwipe.
9. Repeat for all hearts.

Note: The images taken will be mirrored. Infarct will be in the left ventricle, but the scan taken will have the infarct on the right. It doesn't affect finding IS/TA, but it is something to keep in mind.

4.1.2.3. Infarct Size Quantification on Image J

Naming

1. Slices are named (Mouse #)000(slice #)
2. Slice #1 = base of the heart. Increasing numbers head towards the apex (bottom of the heart).

Removing Background

1. Select freehand tool.
2. Draw around the outer outline of the slice. Click 'Edit' -> 'Clear Outside'.
3. Draw around any holes within the slice. Click 'Edit' -> 'Clear'.
4. Save file.

Measuring Infarct Size (IS) and Total Area (TA)

1. Click 'Image' -> 'Adjust' -> 'Color Threshold'.
2. Pop-up window with 3 colored boxes and 6 sliding scales will appear.

a. Make sure the following settings are as follows:
    i. Thresholding method → Default
    ii. Threshold color → Red
    iii. Color Space → HSB
    iv. Dark background is checked.

3. To measure Infarct Size (IS)
    a. The sliding scales will filter out colors/hues. For IS, we want to filter out the red stain. We can do so by adjusting creating a threshold for how "red" and how "dark" areas of the heart are.
    b. Adjust the sliding scales to the following:
        i. 1st = 0 (keep as is)
        ii. 2nd = 255 (as is)
        iii. 3rd = 0 (as is)
        iv. 4th = 145
        v. 5th = 145
        vi. 6th = 245
    c. Click 'Select" at the bottom of the window. This will create an outline.
    d. Click 'Analyze' on the main tool bar. Then, click 'Measure'.
        i. You can also use "Ctrl+M"
    e. Enter the value under 'Infarct Area' under the appropriate mouse and slice number.
4. To measure Total Area (TA)
    a. Adjust the sliding scales to the following:
        i. 1st = 0 (keep as is)
        ii. 2nd = 255 (as is)
        iii. 3rd = 0 (as is)
        iv. 4th = 255
        v. 5th = 1
        vi. 6th = 245
    b. Click 'Select' and then 'Measure' as before.
    c. Enter the value under "Total Area".

4.1.2.4. Calculating Infarct Size Over Total Area of the Heart (IS/TA)

1. To determine the severity of the MI, infarct size (IS) is corrected by the total area (TA) of the whole heart.
2. Whole heart IS/TA = Total Infarct Sizes of ALL slices of the heart/Total Area of ALL slices of the heart in %.

4.1.3. BONE MINERAL DENSITY ANALYSIS – CABINET X-RAY

4.1.3.1. Calibrating

1. Turn monitor on, then the key switch, and then the power switch to the cabinet.
2. Click Digicom 11 3D icon or Kubect NC BMD depending on which image you want to acquire. Open the BMD first because Digicom 11 3D doesn't minimize.
3. Making sure there is nothing (including the magnification tray) in the cabinet, select **NEXT** for the Calibration Wizard. This calibrates Offset and Gain.
4. Once complete, click **Back to Main Window**

4.1.3.2. Whole-Body Bone Mineral Density

4.1.3.2.1. Scan

1. If the cabinet x-ray does not have isoflurane set-up inside the system, anesthetize the mouse from ~2 minutes before placing in cabinet.
2. Position mouse on its stomach (prone) with legs stretched out.
3. Place aluminum filter
4. Click New Case
   a) Fill in the info.
5. Click Optical Camera
6. Click BMD Acquire
   a) Fill in mouse number.
7. Calculate BMD after images are done.

4.1.3.2.2. Analysis

1. You can edit the image to get rid of the skull or see difference between axial and appendicular skeleton (definitions of regions of interest in following section).
   a) ROI BMD on the top menu → Select ROI → Crop to ROI → hit BMD
   b) ROI Type → if speckle or lines → make sure enough leading tissue → Calculate
2. Get BMC and BMD for both → get bone area. You're able to get BMD from there.
3. Click "Export to .csv" for analysis.

4.1.3.3. ROI Analysis

4.1.3.3.1. L5

1. Starting from the top of the hip, include three full vertebrae above it.

4.1.3.3.2. Whole Femur

1. Include from the top of the femoral head to the bottom of the condyles. You want to include all areas of the femur.

4.1.3.3.3. Femoral Diaphysis

1. Select the middle 2/3 of the femur. You want to be sure to exclude the metaphysis.

4.1.4. MICROCT ANALYSIS: L5, FEMUR METAPHYSIS, & FEMUR DIAPHYSIS

*Protocol modified from Armaun Emami

4.1.4.1 To Start…

4.1.4.1.1 - Loading, Naming, and Saving the Scan of Interest

1. Using the 3rd button on the SCANCO computer control panel, open desired file
    a. Type in **File Number** in the search bar from the excel sheet.
    b. Click appropriate **Scan #** from the window on the right from the excel sheet.
    c. The bone will be positioned as indicated in the **Position** column of the excel sheet.
2. Draw a random circle on the file, click **Save As.** Save as the **C00xxx** file defaulted by the system. *This file is the "default" file and needs to be saved before you name your file. It will be used to analyze the contours later.*
3. Click **Save As** again. Replace **C00xxx** with the name of your choice. *I notate my bones as follows…*

    Femoral Metaphysis → Sample#_ME_Initial of person analyzing
    Femoral Diaphysis → Sample#_DIA_Initial of person analyzing
    L5 Vertebra (trabecular bone) → Sample#_L5_Initial of person analyzing

4.1.4.1.2. - Basic controls

- Zooming in/out
    - Click **Zoom** in the menu above and select desired view.
    - OR
    - Click the **scroll pad on the mouse and hold**. Drag the cursor down to zoom in and up to zoom out.

- Moving the image
    - Left click on the image and hold. Drag cursor to the left and right to move image.

- Shortcuts
    - **Save →** Alt + S
    - **Undo →** ctrl + Z
    - **Copy →** ctrl + C
    - **Paste →** ctrl + V

4.1.4.2 Selecting ROI - Femoral Metaphysis

4.1.4.2.1 - Identifying the Femoral Metaphysis

1. Using the scroll bar, identify the beginning of the metaphysis using the following instructions.
    a. Starting from the bottom of the femur, scroll up until you see the growth plate form and then disappear.
    b. The first slice you see a break in the growth plate where you able to draw a full 4-point shamrock/cross is the beginning of the metaphysis.

2. In the excel sheet in the **Start of Meta** column, input slice number from Step 2. The **End of Meta** column will give you the last scan you need to analyze for the metaphysis.

3. Type this number into the white box indicated with the blue arrow below.

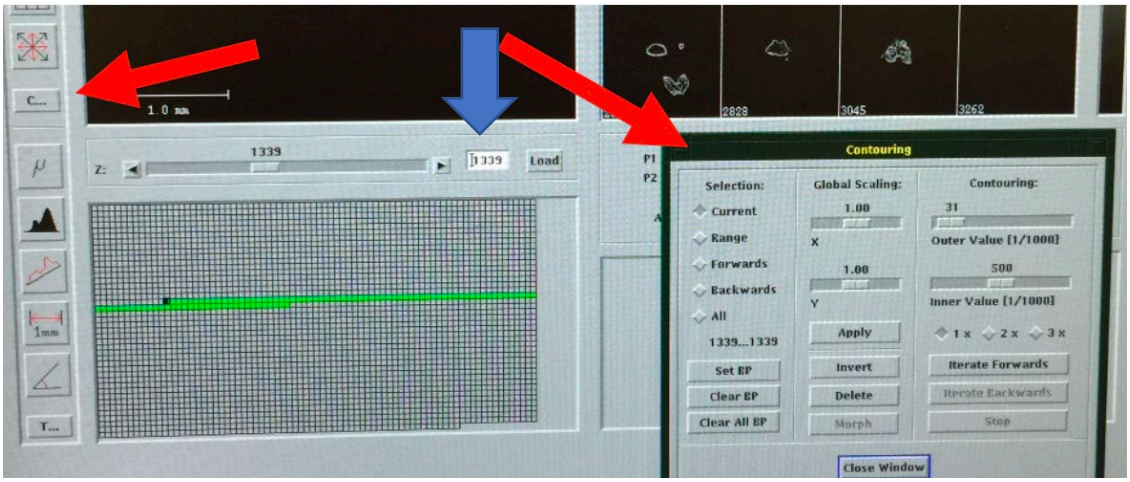

4.1.4.2.2 - Contouring trabecular bone in femur

4. Select the counterclockwise green contouring icon.

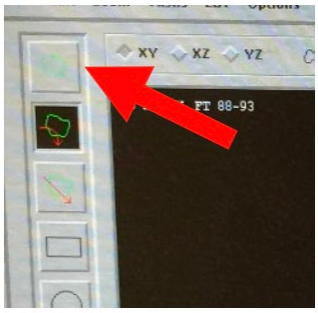

5. Open the contouring tool window by pressing **C…** and it will open the contouring window the right.

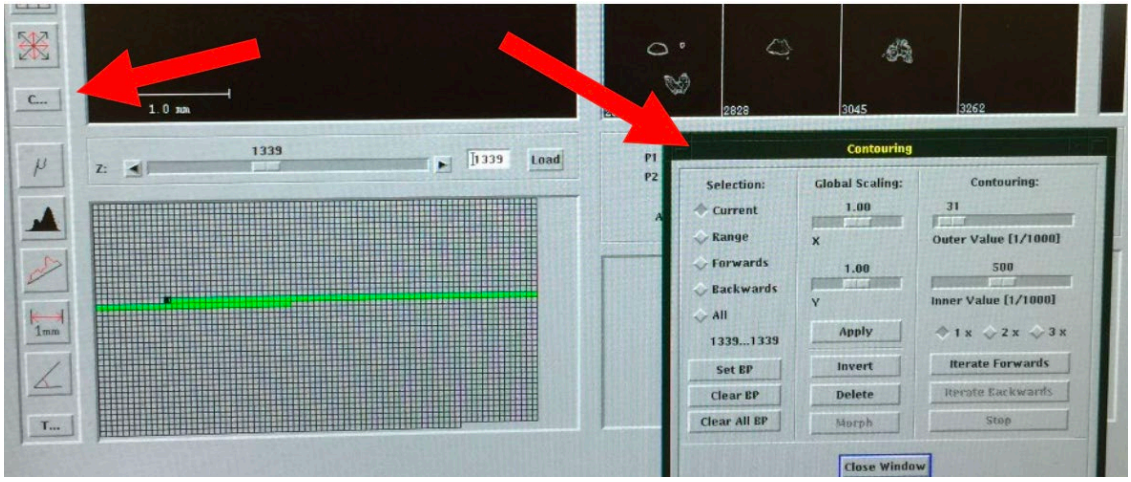

6. Circle the region of interest ***COUNTER-CLOCKWISE.*** You want to include the outline of the trabecular bone as shown below.
    a. You want to be sure to follow the outline of the cortical bone, but leaving enough of a gap to ensure the cortical bone is not included (Figure C).

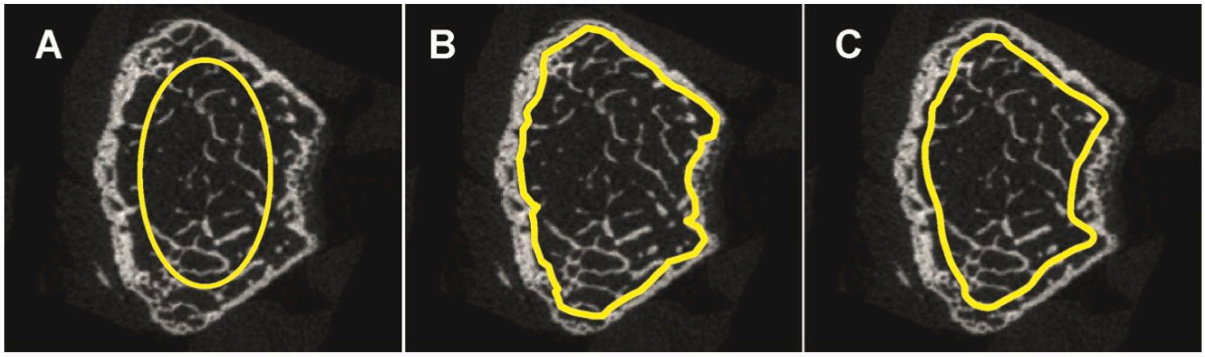

Figure A shows too little bone included and figure B shows too much.

    b. **Important!!!** Be sure to ONLY contour in the counterclockwise direction as this will include the region of interest *inside* the outline. Clockwise will analyze the area *outside* of the outline.

7. Skip 20 slices by clicking the right of the scroll bar twice (indicated by blue square and blue arrow). Outline the bone as you did for **Step 9**. *Clicking the left and right arrows will advance you once. Clicking the bar itself will advance you 10 slices*.

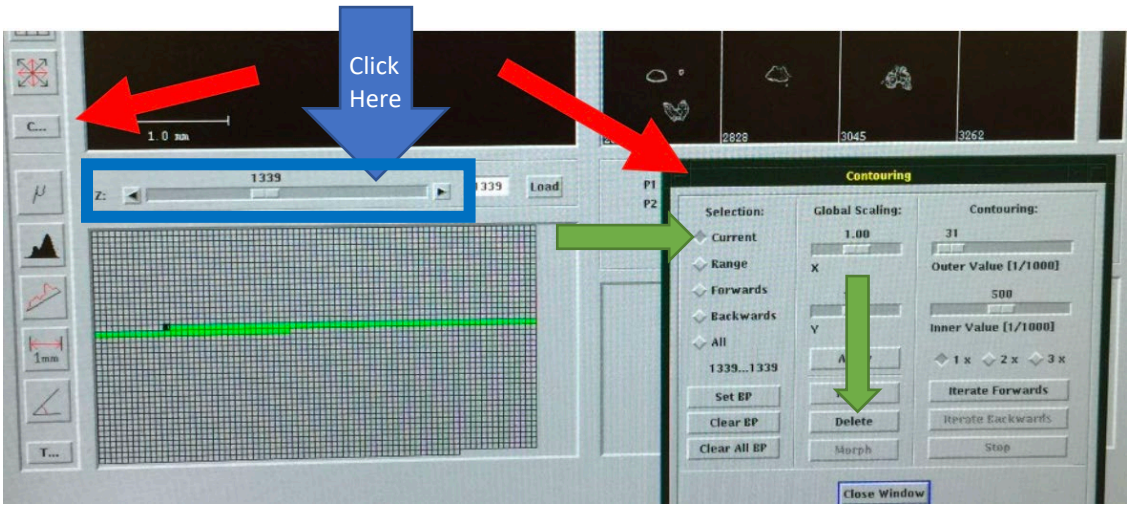

8. Click **Range** in the contour window on the right. Then click **Morph.** Both are indicated in green arrows in the figure above.
    a. *This will take the average shape between the two green contours you manually drew in. It works best when the bone doesn't change too drastically in shape.*

9. Scroll through each slice one by one making sure the outline follows the trabecular bone well. If not, click the modify tool icon below the contour tool icon

indicated below.

10. In a ***counterclockwise*** direction, modify the shape of the contour to best follow the outline of the bone. *This tool works by creating a line in between two intersections in the original outline. In order to use this, you need to be sure to cross at least two points of the original outline with your cursor.* As you modify, be consistent and outline the trabecular bone as you did in **Step 6**.

11. Once you've determined all contours adequately follow the outline of the trabecular bone. Repeat **Steps 6-11** until you begin seeing part of the growth plate. Exclude the growth plate from you contours.

12. Skip 10 slices by clicking the right of the scroll bar once. Contour the trabecular bone and exclude the growth plates. Click **Morph** and modify the contours as you did in **Steps 8-10.**

13. Repeat **Step 12** until you reached the beginning of the metaphysis. *This is the slice you identified in Step 1 and inputted in the **Start of Meta** column in the excel sheet.*

14. Be sure to save as *Sample#_ME_Initial of person analyzing.* For analysis, refer to **Running Analysis** section below.

    ***NOTE: If you find modifying the contours easier than drawing it by hand, you can hit **Ctrl+C; Ctrl+V** to copy and paste your previous contours to the new slice. This works well for **Step 7**.

    ***NOTE: Be sure to save often. A shortcut is to use hit **Alt+S**. Be sure this saves into your named file and not the default C00xxx file.

4.1.4.3 Selecting ROI – L5 Vertebra

4.1.4.3.1 - Identifying the L5 Vertebra

Starting from **Scan #1**, scroll to the **last scan #.**..

If the vertebral processes move ***towards the center*** (see figure to the right)→ the spine is ***right-side up.***

i. Analyze the ***last intact bone.***

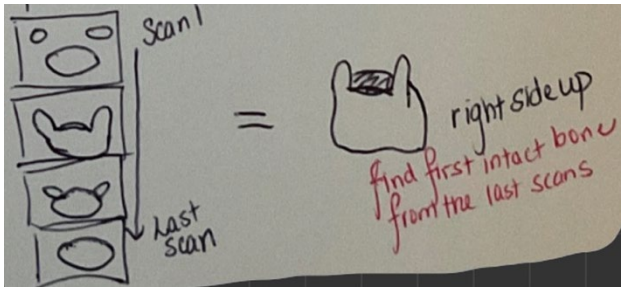

If the vertebral process moves **away from the center** (see figure to the right) → the spine is ***upside down.***

ii. Analyze the **first intact bone.**

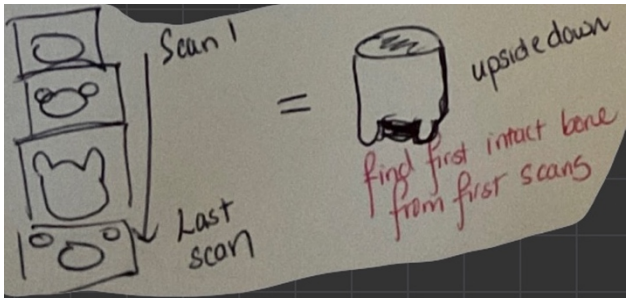

4.1.4.3.2 – Contouring trabecular bone in L5

1. You want to analyze the areas between the growth plates.
2. Exclude the vertebral processes. Analyze on in the vertebral body (see figure below).
3. Eval task Name: 161 BC AE tibia
   Threshold: 340

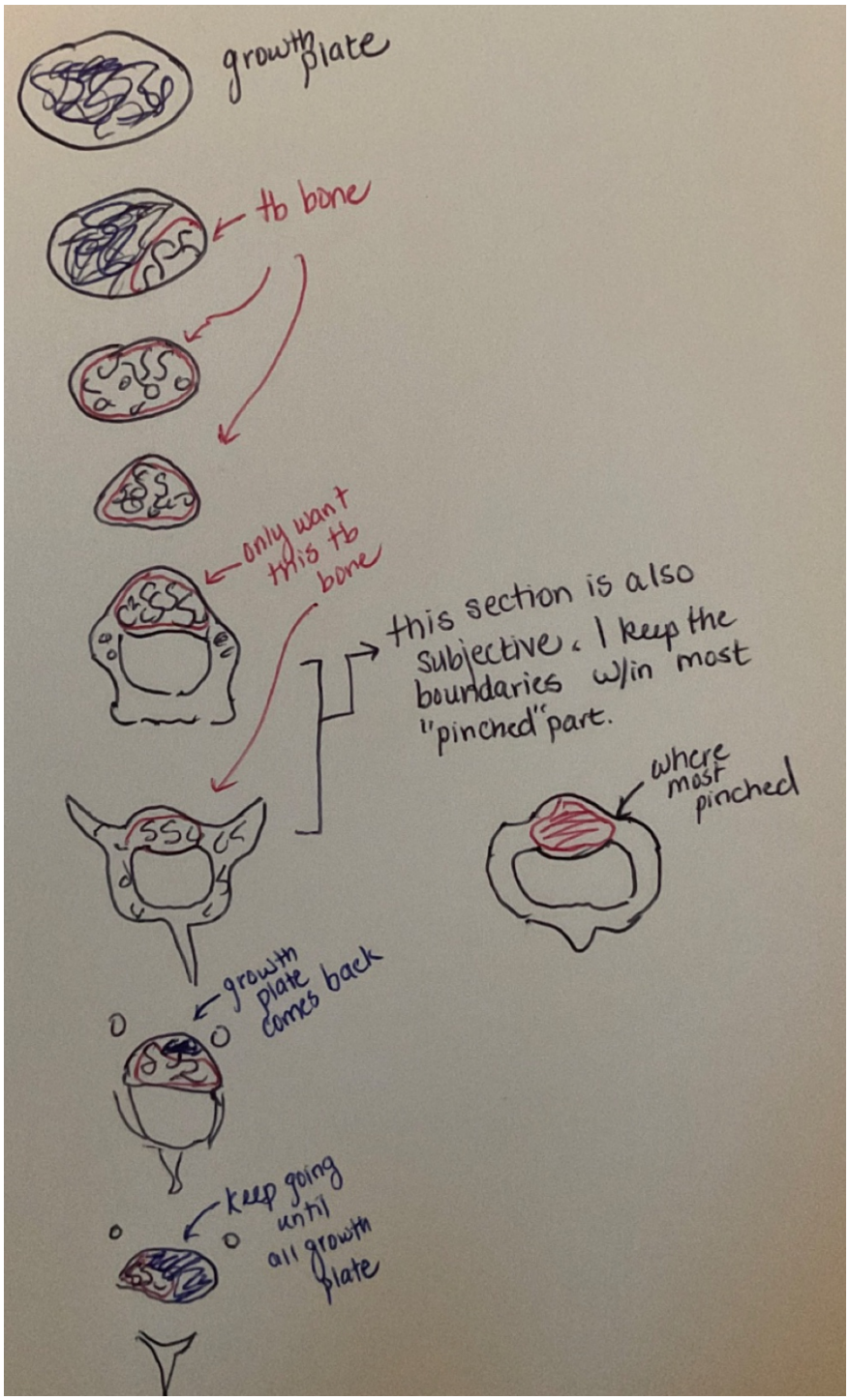

4.1.4.4 Selecting ROI - Femoral Diaphysis

1. Using the scroll bar, identify the bottom of the femoral condyle. This the slice where the condyle is first seen.

2. Type this slice number into the **End of Condyle** column in the excel sheet.

3. Type the **Midpt Slice #** from the excel sheet into the white box by the scroll bar (blue arrow).

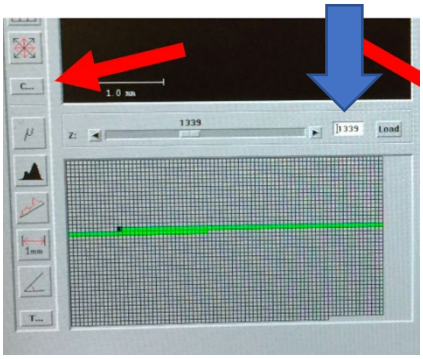

4. In the contouring window, change **Inner Value** to **400** (indicated in blue box).

5. Draw a circle ***COUNTER-CLOCKWISE*** around the cortical bone. Double-click on the screen so that the contour snaps into the outer outline of the bone. *If it does not snap well, double-click again. You can also try modifying the contour to better fit the bone, then double-clicking again.*

6. Click **Backwards** in **Selection: >** Click **Iterate Backwards** (green arrows)

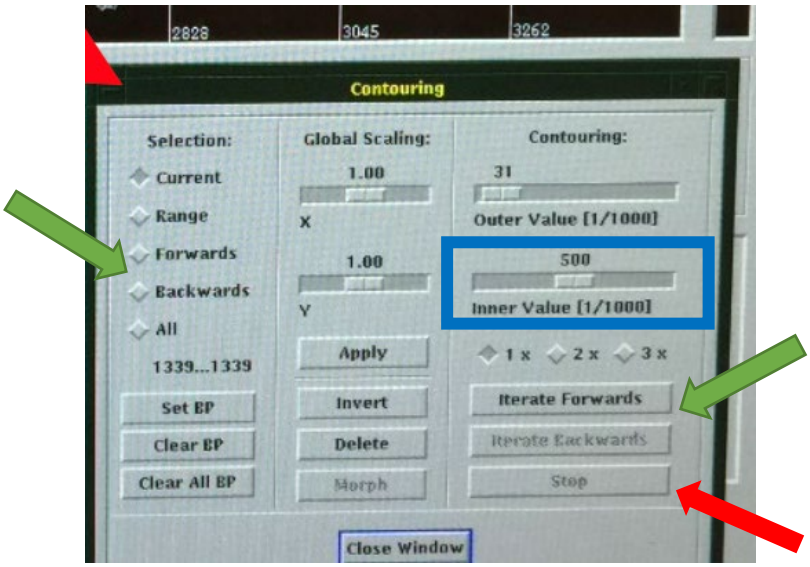

7. The program will automatically outline the outer rim of the cortical bone. *It may occasionally outline incorrectly. If it does, click **Stop** (red arrow) and modify accordingly.*

8. Click **Stop** (red arrow) once the program reaches the slice number indicated in the **Iterate Backward** column on the excel sheet.

9. Repeat **Steps 6-8** except by clicking **Forwards** and **Iterate Forwards**. Continue until it reaches the slice number indicated in the **Iterate Forward** column on the excel sheet.

10. Be sure to save as *Sample#_DIA_Initial of person analyzing*! For analysis, refer to **Running Analysis** section below.

4.1.4.5 Running Analysis

1. Save file as the default file **C00xxx.**

2. Click **Tasks** in the bar at the top. Then **Eval 3D** > **Select…** > Type in desired file number below > **Select.**

   *Femoral Metaphysis → **140: BC tibia mouse***
   *Femoral Diaphysis → **9: Bone Midshaft Evaluation***
   *L5 Vertebra (trabecular) → **140: BC tibia mouse***

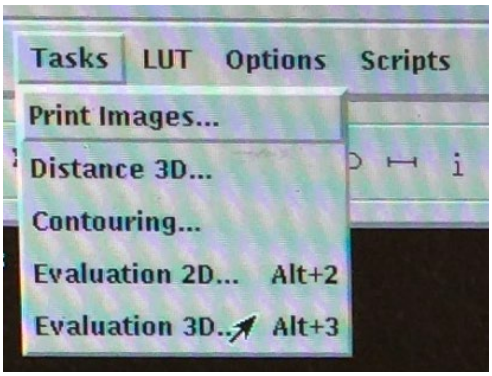

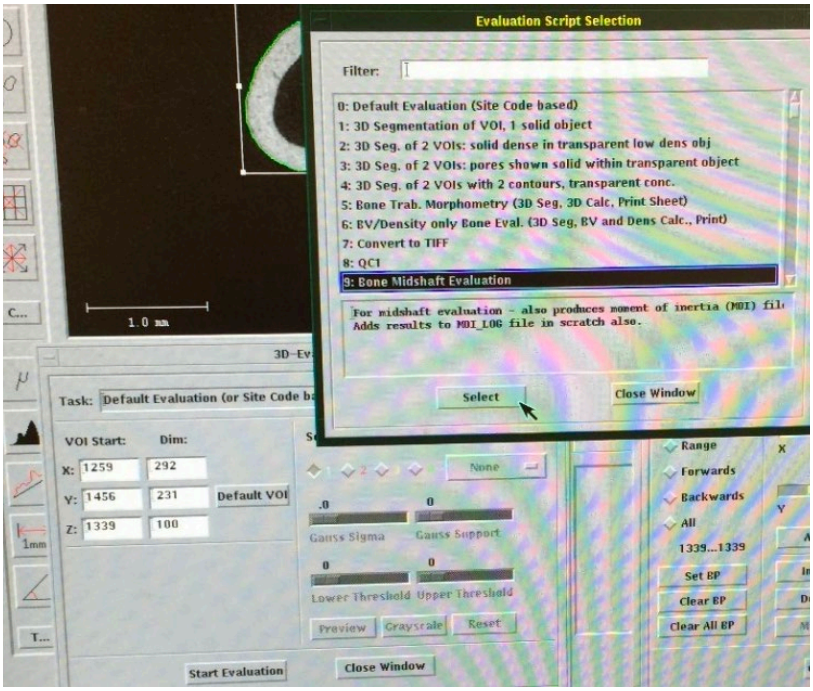

3. Click **Default VOI** to make sure the white box snaps to the correct bone. *The femoral meta and femoral dia will have a Z Dim value of 250 and 100 respectively. The L5 will vary.*

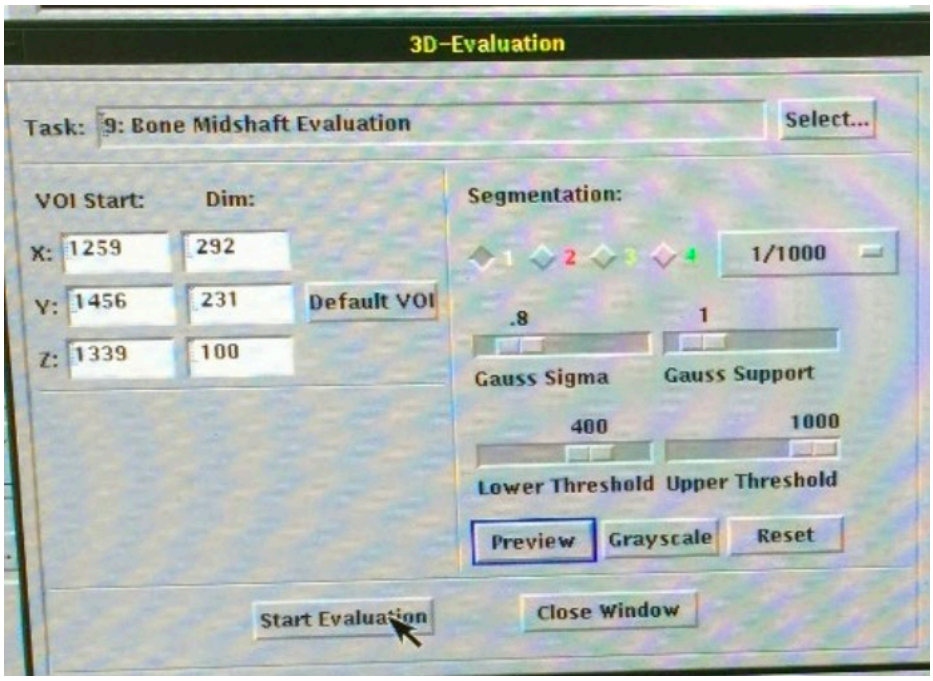

4. In **Lower Threshold**, set to the appropriate threshold. *The set threshold is determined at the beginning of the study. Unless otherwise notes, all bones will be analyzed with the same threshold.*
   *Femoral Metaphysis → **340***
   *Femoral Diaphysis → **400***
   *L5 Vertebra (trabecular) → **340***

5. Click **Start Evaluation.**

6. Wait for evaluation to finish. You can check the queue in the white window manager on the computer to determine if the analysis is done. If finished, the window will state “FILE #_ SCAN #_COMPLETED”

7. After completed, go to SCANCO website. *There is usually a **SCANCO** icon in the bottom right of the computer screen which you can double click.*

8. Click **Show Current Measurement on Disk**

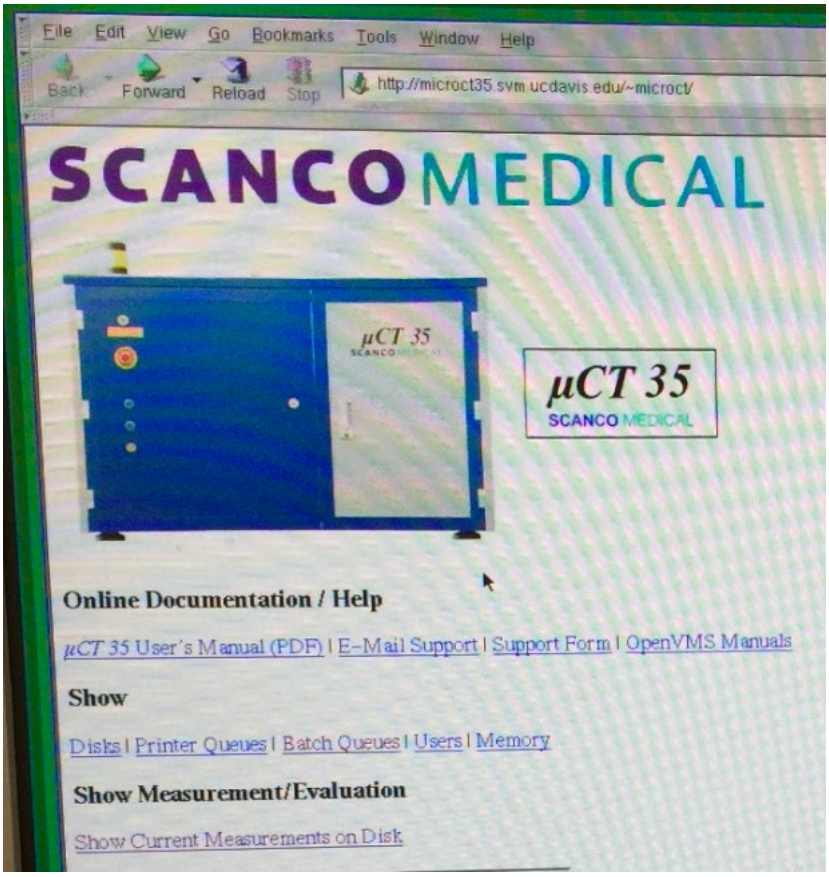

9. Scroll until you find the File # and Scan # you ran.

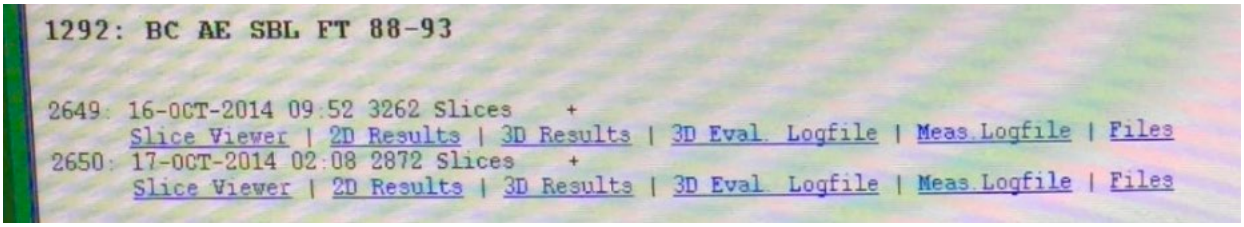

10. For *Femoral Metaphysis* and *L5 vertebra*
    a. Click **3D results.**

11. For *Femoral Diaphysis*

a. Click **Files > C000XXXX_MOI_RESULTS_MIDSHAFT.TXT**

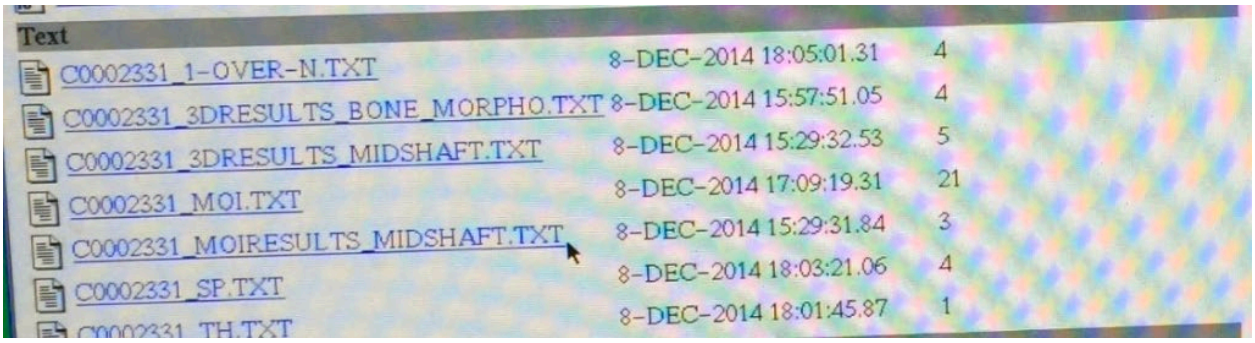

12. Record the numbers of the desired variables into the excel sheet.

Femoral Metaphysis & L5 Vertebra	• BV • BV/TV • Conn. Dens • SMI • Tb. N & Std Dev • Tb. Th & Std Dev • Tb. Sp & Std Dev • Mean 1 & Std Dev • Mean 2 & Std Dev
Femoral Diaphysis	• pMOI • Imax • Imin • Imin/cmin • Barea • Tarea • TRI-CT.th • Mean 1 • Mean 2

REFERENCES

1. Murray CJ, Richards MA, Newton JN, et al. UK health performance: findings of the Global Burden of Disease Study 2010. *The Lancet*. 2013;381(9871):997-1020. doi:10.1016/S0140-6736(13)60355-4

2. Jiang HX, Majumdar SR, Dick DA, et al. Development and Initial Validation of a Risk Score for Predicting In-Hospital and 1-Year Mortality in Patients With Hip Fractures. *J Bone Miner Res*. 2005;20(3):494-500. doi:10.1359/JBMR.041133

3. Schnell S, Friedman SM, Mendelson DA, Bingham KW, Kates SL. The 1-Year Mortality of Patients Treated in a Hip Fracture Program for Elders. *Geriatr Orthop Surg Rehabil*. 2010;1(1):6-14. doi:10.1177/2151458510378105

4. Lee YK, Lee YJ, Ha YC, Koo KH. Five-Year Relative Survival of Patients With Osteoporotic Hip Fracture. *J Clin Endocrinol Metab*. 2014;99(1):97-100. doi:10.1210/jc.2013-2352

5. Peterson MGE, Cornell CN, Paget SA, Allegrante JP. Five-Year Survival in a Cohort of Hip Fracture Patients: The Predictive Role of Pre-fracture Health Status. *HSS J*. 2008;4(1):43-47. doi:10.1007/s11420-007-9074-z

6. Benjamin EJ, Blaha MJ, Chiuve SE, et al. Heart Disease and Stroke Statistics—2017 Update: A Report From the American Heart Association. *Circulation*. 2017;135(10). doi:10.1161/CIR.0000000000000485

7. Ji M, Yu Q. Primary osteoporosis in postmenopausal women. *Chronic Dis Transl Med*. 2015;1(1):9-13. doi:10.1016/j.cdtm.2015.02.006

8. Roger VL, Jacobsen SJ, Weston SA, et al. Trends in the Incidence and Survival of Patients with Hospitalized Myocardial Infarction, Olmsted County, Minnesota, 1979 to 1994. *Ann Intern Med*. 2002;136(5):341. doi:10.7326/0003-4819-136-5-200203050-00005

9. Yeh RW, Selby JV. Population Trends in the Incidence and Outcomes of Acute Myocardial Infarction. *N Engl J Med*. Published online 2010.

10. Gerber Y, Melton LJ, Weston SA, Roger VL. Association Between Myocardial Infarction and Fractures: An Emerging Phenomenon. *Circulation*. 2011;124(3):297-303. doi:10.1161/CIRCULATIONAHA.110.007195

11. Farhat GN, Cauley JA. The link between osteoporosis and cardiovascular disease. *Clin Cases Miner Bone Metab*. 2008;5(1):19-34.

12. Benzinger P, Rapp K, König HH, et al. Risk of osteoporotic fractures following stroke in older persons. *Osteoporos Int*. 2015;26(4):1341-1349. doi:10.1007/s00198-014-3005-x

13. Chiang CH, Liu CJ, Chen PJ, et al. Hip fracture and risk of acute myocardial infarction: A nationwide study. *J Bone Miner Res*. 2013;28(2):404-411. doi:10.1002/jbmr.1714

14. Ojha N. *Myocardial Infarction*. StatPearls Publishing LLC.; 2022.

15. Branch NSC and O. Osteoporosis. National Institute of Arthritis and Musculoskeletal and Skin Diseases. Published April 7, 2017. Accessed March 19, 2023. https://www.niams.nih.gov/health-topics/osteoporosis

16. Emami AJ, Toupadakis CA, Telek SM, Fyhrie DP, Yellowley CE, Christiansen BA. Age Dependence of Systemic Bone Loss and Recovery Following Femur Fracture in Mice. *J Bone Miner Res*. 2019;34(1):157-170. doi:10.1002/jbmr.3579

17. Manolagas SC, Jilka RL. Bone Marrow, Cytokines, and Bone Remodeling — Emerging Insights into the Pathophysiology of Osteoporosis. *N Engl J Med*. 1995;332(5):305-311. doi:10.1056/NEJM199502023320506

18. Lello S, Capozzi A, Scambia G. Osteoporosis and cardiovascular disease: an update. *Gynecol Endocrinol*. 2015;31(8):590-594. doi:10.3109/09513590.2015.1041908

19. Rodríguez-Olleros Rodríguez C, Díaz Curiel M. Vitamin K and Bone Health: A Review on the Effects of Vitamin K Deficiency and Supplementation and the Effect of Non-Vitamin K Antagonist Oral Anticoagulants on Different Bone Parameters. *J Osteoporos*. 2019;2019:2069176. doi:10.1155/2019/2069176

20. Menezes AR, Lamb MC, Lavie CJ, DiNicolantonio JJ. Vitamin D and atherosclerosis. *Curr Opin Cardiol*. 2014;29(6):571-577. doi:10.1097/HCO.0000000000000108

21. Lips P, van Schoor NM. The effect of vitamin D on bone and osteoporosis. *Best Pract Res Clin Endocrinol Metab*. 2011;25(4):585-591. doi:10.1016/j.beem.2011.05.002

22. Laird E, Ward M, McSorley E, Strain JJ, Wallace J. Vitamin D and Bone Health; Potential Mechanisms. *Nutrients*. 2010;2(7):693-724. doi:10.3390/nu2070693

23. de la Guía-Galipienso F, Martínez-Ferran M, Vallecillo N, Lavie CJ, Sanchis-Gomar F, Pareja-Galeano H. Vitamin D and cardiovascular health. *Clin Nutr Edinb Scotl*. 2021;40(5):2946-2957. doi:10.1016/j.clnu.2020.12.025

24. Meng F, Wang W, Ma J, Lin B. Parathyroid hormone and risk of heart failure in the general population. *Medicine (Baltimore)*. 2016;95(40):e4810. doi:10.1097/MD.0000000000004810

25. Manolagas SC. Role of cytokines in bone resorption. *Bone*. 1995;17(2, Supplement 1):S63-S67. doi:10.1016/8756-3282(95)00180-L

26. Kimble RB, Bain S, Pacifici R. The Functional Block of TNF but Not of IL-6 Prevents Bone Loss in Ovariectomized Mice. *J Bone Miner Res*. 1997;12(6):935-941. doi:10.1359/jbmr.1997.12.6.935

27. Romas E, Martin TJ. Cytokines in the pathogenesis of osteoporosis. *Osteoporos Int*. 1997;7(3):47-53. doi:10.1007/BF03194342

28. McLean RR. Proinflammatory cytokines and osteoporosis. *Curr Osteoporos Rep*. 2009;7(4):134-139. doi:10.1007/s11914-009-0023-2

29. Ong SB, Hernández-Reséndiz S, Crespo-Avilan GE, et al. Inflammation following acute myocardial infarction: Multiple players, dynamic roles, and novel therapeutic opportunities. *Pharmacol Ther*. 2018;186:73-87. doi:10.1016/j.pharmthera.2018.01.001

30. Fatkhullina AR, Peshkova IO, Koltsova EK. The Role of Cytokines in the Development of Atherosclerosis. *Biochem Biokhimiia*. 2016;81(11):1358-1370. doi:10.1134/S0006297916110134

31. Boyce BF, Xing L. The RANKL/RANK/OPG pathway. *Curr Osteoporos Rep*. 2007;5(3):98-104. doi:10.1007/s11914-007-0024-y

32. Anagnostis P, Karagiannis A, Kakafika AI, Tziomalos K, Athyros VG, Mikhailidis DP. Atherosclerosis and osteoporosis: age-dependent degenerative processes or related entities? *Osteoporos Int*. 2009;20(2):197-207. doi:10.1007/s00198-008-0648-5

33. Baldwin MJ, Policha A, Maldonado T, et al. Novel association between bone mineral density scores and the prevalence of peripheral artery disease in both sexes. *Vasc Med*. 2017;22(1):13-20. doi:10.1177/1358863X16672740

34. Pennisi P, Russo E, Gaudio A, et al. The association between carotid or femoral atherosclerosis and low bone mass in postmenopausal women referred for osteoporosis screening. Does osteoprotegerin play a role? *Maturitas*. 2010;67(4):358-362. doi:10.1016/j.maturitas.2010.07.013

35. Shen Z, Kuang S, Zhang M, et al. Inhibition of CCL2 by bindarit alleviates diabetes-associated periodontitis by suppressing inflammatory monocyte infiltration and altering macrophage properties. *Cell Mol Immunol*. Published online July 16, 2020. doi:10.1038/s41423-020-0500-1

36. Ohtsuji M, Lin Q, Okazaki H, et al. Anti-CD11b antibody treatment suppresses the osteoclast generation, inflammatory cell infiltration, and autoantibody production in arthritis-prone FcγRIIB-deficient mice. *Arthritis Res Ther*. 2018;20(1):25. doi:10.1186/s13075-018-1523-1

37. Chen X, Zhi X, Pan P, et al. Matrine prevents bone loss in ovariectomized mice by inhibiting RANKL-induced osteoclastogenesis. *FASEB J*. 2017;31(11):4855-4865. doi:10.1096/fj.201700316R

38. Yuan H, Zelkha S, Burkatovskaya M, Gupte R, Leeman SE, Amar S. Pivotal role of NOD2 in inflammatory processes affecting atherosclerosis and periodontal bone loss. *Proc Natl Acad Sci*. 2013;110(52):E5059-E5068. doi:10.1073/pnas.1320862110

39. Zhao F, Emami AJ, De Jesus NM, et al. Loss of bone mass and trabecular microstructure of vertebrae and femur following myocardial infarction in mice. Published online 2016.

40. Ito T. PAMPs and DAMPs as triggers for DIC. *J Intensive Care*. 2014;2(1):65. doi:10.1186/s40560-014-0065-0

41. Rock KL, Kono H. The Inflammatory Response to Cell Death. *Annu Rev Pathol Mech Dis*. 2008;3(1):99-126. doi:10.1146/annurev.pathmechdis.3.121806.151456

42. Lenz A, Franklin GA, Cheadle WG. Systemic inflammation after trauma. *Injury*. 2007;38(12):1336-1345. doi:10.1016/j.injury.2007.10.003

43. Dutta P, Courties G, Wei Y, et al. Myocardial infarction accelerates atherosclerosis. *Nature*. 2012;487(7407):325-329. doi:10.1038/nature11260

44. Osipov B, Emami AJ, Christiansen BA. Systemic Bone Loss After Fracture. *Clin Rev Bone Miner Metab*. 2018;16(4):116-130. doi:10.1007/s12018-018-9253-0

45. Zhang C, Zhu J, Jia J, et al. Effect of Single Versus Multiple Fractures on Systemic Bone Loss in Mice. *J Bone Miner Res*. Published online December 10, 2020:jbmr.4211. doi:10.1002/jbmr.4211

46. Triposkiadis F, Karayannis G, Giamouzis G, Skoularigis J, Louridas G, Butler J. The Sympathetic Nervous System in Heart Failure. *J Am Coll Cardiol*. 2009;54(19):1747-1762. doi:10.1016/j.jacc.2009.05.015

47. Ziegler KA, Ahles A, Wille T, Kerler J, Ramanujam D, Engelhardt S. Local sympathetic denervation attenuates myocardial inflammation and improves cardiac function after myocardial infarction in mice. *Cardiovasc Res*. 2018;114(2):291-299. doi:10.1093/cvr/cvx227

48. Jiao K, Niu L, Xu X, et al. Norepinephrine Regulates Condylar Bone Loss via Comorbid Factors. *J Dent Res*. 2015;94(6):813-820. doi:10.1177/0022034515577677

49. Motyl KJ, DeMambro VE, Barlow D, et al. Propranolol Attenuates Risperidone-Induced Trabecular Bone Loss in Female Mice. *Endocrinology*. 2015;156(7):2374-2383. doi:10.1210/en.2015-1099

50. Khosla S, Drake MT, Volkman TL, et al. Sympathetic β1-adrenergic signaling contributes to regulation of human bone metabolism. *J Clin Invest*. 2018;128(11):4832-4842. doi:10.1172/JCI122151

51. Takeda S, Elefteriou F, Levasseur R, et al. Leptin Regulates Bone Formation via the Sympathetic Nervous System. *Cell*. 2002;111(3):305-317. doi:10.1016/S0092-8674(02)01049-8

52. Udagawa N, Takahashi N, Akatsu T, et al. Origin of osteoclasts: mature monocytes and macrophages are capable of differentiating into osteoclasts under a suitable microenvironment prepared by bone marrow-derived stromal cells. *Proc Natl Acad Sci*. 1990;87(18):7260-7264. doi:10.1073/pnas.87.18.7260

53. Väänänen HK, Laitala-Leinonen T. Osteoclast lineage and function. *Arch Biochem Biophys*. 2008;473(2):132-138. doi:10.1016/j.abb.2008.03.037

54. Zhou Y, Deng HW, Shen H. Circulating monocytes: an appropriate model for bone-related study. *Osteoporos Int*. 2015;26(11):2561-2572. doi:10.1007/s00198-015-3250-7

55. Zhang L, Liu YZ, Zeng Y, et al. Network-based proteomic analysis for postmenopausal osteoporosis in Caucasian females. *PROTEOMICS*. 2016;16(1):12-28. doi:10.1002/pmic.201500005

56. Xiao KW, Li JL, Zeng ZH, et al. Monocytes affect bone mineral density in pre- and postmenopausal women through ribonucleoprotein complex biogenesis by integrative bioinformatics analysis. *Sci Rep*. 2019;9(1):17290. doi:10.1038/s41598-019-53843-6

57. Homeister JW, Lucchesi BR. Complement Activation and Inhibition in Myocardial Ischemia and Reperfusion Injury. :24.

58. Beltrame MH, Catarino SJ, Goeldner I, Boldt ABW, de Messias-Reason IJ. The Lectin Pathway of Complement and Rheumatic Heart Disease. *Front Pediatr*. 2015;2:148. doi:10.3389/fped.2014.00148

59. Yasojima K, Schwab C, McGeer EG, McGeer PL. Human Heart Generates Complement Proteins That Are Upregulated and Activated After Myocardial Infarction. *Circ Res*. 1998;83(8):860-869. doi:10.1161/01.RES.83.8.860

60. Guo RF, Ward PA. Role of C5a in Inflammatory Responses. *Annu Rev Immunol*. 2005;23(1):821-852. doi:10.1146/annurev.immunol.23.021704.115835

61. De Hoog VC, Timmers L, Van Duijvenvoorde A, et al. Leucocyte expression of complement C5a receptors exacerbates infarct size after myocardial reperfusion injury. *Cardiovasc Res*. 2014;103(4):521-529. doi:10.1093/cvr/cvu153

62. van der Pals J, Koul S, Andersson P, et al. Treatment with the C5a receptor antagonist ADC-1004 reduces myocardial infarction in a porcine ischemia-reperfusion model. *BMC Cardiovasc Disord*. 2010;10(1):45. doi:10.1186/1471-2261-10-45

63. Weber B, Lackner I, Knecht D, et al. Systemic and Cardiac Alterations After Long Bone Fracture: *SHOCK*. Published online March 2020:1. doi:10.1097/SHK.0000000000001536

64. Munenaga S, Ouhara K, Hamamoto Y, et al. The involvement of C5a in the progression of experimental arthritis with Porphyromonas gingivalis infection in SKG mice. *Arthritis Res Ther*. 2018;20(1):247. doi:10.1186/s13075-018-1744-3

65. Kovtun A, Bergdolt S, Hägele Y, et al. Complement receptors C5aR1 and C5aR2 act differentially during the early immune response after bone fracture but are similarly involved in bone repair. *Sci Rep*. 2017;7(1):14061. doi:10.1038/s41598-017-14444-3

66. Bergdolt S, Kovtun A, Hägele Y, et al. Osteoblast-specific overexpression of complement receptor C5aR1 impairs fracture healing. Garcia Aznar JM, ed. *PLOS ONE*. 2017;12(6):e0179512. doi:10.1371/journal.pone.0179512

67. Ignatius A, Schoengraf P, Kreja L, et al. Complement C3a and C5a modulate osteoclast formation and inflammatory response of osteoblasts in synergism with IL-1β. *J Cell Biochem*. 2011;112(9):2594-2605. doi:10.1002/jcb.23186

68. Tu Z, Bu H, Dennis JE, Lin F. Efficient osteoclast differentiation requires local complement activation. *Blood*. 2010;116(22):4456-4463. doi:10.1182/blood-2010-01-263590

69. De Jesus NM, Wang L, Herren AW, et al. Atherosclerosis exacerbates arrhythmia following myocardial infarction: Role of myocardial inflammation. *Heart Rhythm*. 2015;12(1):169-178. doi:10.1016/j.hrthm.2014.10.007

70. Rueden CT, Schindelin J, Hiner MC, et al. ImageJ2: ImageJ for the next generation of scientific image data. *BMC Bioinformatics*. 2017;18(1):529. doi:10.1186/s12859-017-1934-z

71. Schindelin J, Arganda-Carreras I, Frise E, et al. Fiji: an open-source platform for biological-image analysis. *Nat Methods*. 2012;9(7):676-682. doi:10.1038/nmeth.2019

72. Bouxsein ML, Boyd SK, Christiansen BA, Guldberg RE, Jepsen KJ, Müller R. Guidelines for assessment of bone microstructure in rodents using micro-computed tomography. *J Bone Miner Res*. 2010;25(7):1468-1486. doi:10.1002/jbmr.141

73. Jepsen KJ, Silva MJ, Vashishth D, Guo XE, van der Meulen MC. Establishing Biomechanical Mechanisms in Mouse Models: Practical Guidelines for Systematically Evaluating Phenotypic Changes in the Diaphyses of Long Bones:

ASSESSING BIOMECHANICAL MECHANISMS IN MOUSE LONG BONES. *J Bone Miner Res*. 2015;30(6):951-966. doi:10.1002/jbmr.2539

74. Fu L, Patel MS, Bradley A, Wagner EF, Karsenty G. The Molecular Clock Mediates Leptin-Regulated Bone Formation. *Cell*. 2005;122(5):803-815. doi:10.1016/j.cell.2005.06.028

75. Maassen AP. The influence of adrenalectomy on the growth of rats. *Arch Int Pharmacodyn Ther*. 1952;88(4):473-481.

76. Chenu C. Glutamatergic innervation in bone. *Microsc Res Tech*. 2002;58(2):70-76. doi:10.1002/jemt.10120

77. Ducy P, Amling M, Takeda S, et al. Leptin Inhibits Bone Formation through a Hypothalamic Relay: A Central Control of Bone Mass. :11.

78. Moore RE, Smith CK, Bailey CS, Voelkel EF, Tashjian AH. Characterization of beta-adrenergic receptors on rat and human osteoblast-like cells and demonstration that beta-receptor agonists can stimulate bone resorption in organ culture. *Bone Miner*. 1993;23(3):301-315. doi:10.1016/s0169-6009(08)80105-5

79. Togari A, Arai M, Mizutani S, Mizutani S, Koshihara Y, Nagatsu T. Expression of mRNAs for neuropeptide receptors and beta-adrenergic receptors in human osteoblasts and human osteogenic sarcoma cells. *Neurosci Lett*. 1997;233(2-3):125-128. doi:10.1016/s0304-3940(97)00649-6

80. Kellenberger S, Muller K, Richener H, Bilbe G. Formoterol and isoproterenol induce c-fos gene expression in osteoblast-like cells by activating beta2-adrenergic receptors. *Bone*. 1998;22(5):471-478. doi:10.1016/s8756-3282(98)00026-x

81. Majeska RJ, Minkowitz B, Bastian W, Einhorn TA. Effects of beta-adrenergic blockade in an osteoblast-like cell line. *J Orthop Res Off Publ Orthop Res Soc*. 1992;10(3):379-384. doi:10.1002/jor.1100100310

82. Elefteriou F, Ahn JD, Takeda S, et al. Leptin regulation of bone resorption by the sympathetic nervous system and CART. *Nature*. 2005;434(7032):514-520. doi:10.1038/nature03398

83. Kondo H, Takeuchi S, Togari A. β-Adrenergic signaling stimulates osteoclastogenesis via reactive oxygen species. *Am J Physiol Endocrinol Metab*. 2013;304(5):E507-515. doi:10.1152/ajpendo.00191.2012

84. Whitsett JA, Burdsall J, Workman L, Hollinger B, Neely J. beta-Adrenergic receptors in pediatric tumors: uncoupled beta 1-adrenergic receptor in Ewing's sarcoma. *J Natl Cancer Inst*. 1983;71(4):779-786.

85. Nuntapornsak A, Wongdee K, Thongbunchoo J, Krishnamra N, Charoenphandhu N. Changes in the mRNA expression of osteoblast-related genes in response to

beta(3)-adrenergic agonist in UMR106 cells. *Cell Biochem Funct*. 2010;28(1):45-51. doi:10.1002/cbf.1617

86. Takeuchi T, Tsuboi T, Arai M, Togari A. Adrenergic stimulation of osteoclastogenesis mediated by expression of osteoclast differentiation factor in MC3T3-E1 osteoblast-like cells. *Biochem Pharmacol*. 2001;61(5):579-586. doi:10.1016/S0006-2952(00)00591-8

87. Bonnet N, Benhamou CL, Beaupied H, et al. Doping dose of salbutamol and exercise: deleterious effect on cancellous and cortical bones in adult rats. *J Appl Physiol*. 2007;102(4):1502-1509. doi:10.1152/japplphysiol.00815.2006

88. Bonnet N, Benhamou CL, Brunet-Imbault B, et al. Severe bone alterations under beta2 agonist treatments: bone mass, microarchitecture and strength analyses in female rats. *Bone*. 2005;37(5):622-633. doi:10.1016/j.bone.2005.07.012

89. Motyl KJ, Bishop KA, DeMambro VE, et al. Altered thermogenesis and impaired bone remodeling in Misty mice. *J Bone Miner Res Off J Am Soc Bone Miner Res*. 2013;28(9):1885-1897. doi:10.1002/jbmr.1943

90. Baek K, Bloomfield SA. β-Adrenergic Blockade and Leptin Replacement Effectively Mitigate Disuse Bone Loss. *J Bone Miner Res*. 2009;24(5):792-799. doi:10.1359/jbmr.081241

91. Collins S, Daniel KW, Petro AE, Surwit RS. Strain-specific response to beta 3-adrenergic receptor agonist treatment of diet-induced obesity in mice. *Endocrinology*. 1997;138(1):405-413. doi:10.1210/endo.138.1.4829

92. de Souza CJ, Burkey BF. Beta 3-adrenoceptor agonists as anti-diabetic and anti-obesity drugs in humans. *Curr Pharm Des*. 2001;7(14):1433-1449. doi:10.2174/1381612013397339

93. White CL, Ishihara Y, Dotson TL, Hughes DA, Bray GA, York DA. Effect of a beta-3 agonist on food intake in two strains of rats that differ in susceptibility to obesity. *Physiol Behav*. 2004;82(2-3):489-496. doi:10.1016/j.physbeh.2004.04.059

94. Xiao C, Goldgof M, Gavrilova O, Reitman ML. Anti-obesity and metabolic efficacy of the β3-adrenergic agonist, CL316243, in mice at thermoneutrality compared to 22°C. *Obes Silver Spring Md*. 2015;23(7):1450-1459. doi:10.1002/oby.21124

95. Tjandra PM, Paralkar MP, Osipov B, et al. Systemic bone loss following myocardial infarction in mice. *J Orthop Res*. Published online October 6, 2020:jor.24867. doi:10.1002/jor.24867

96. Debrunner M, Schuiki E, Minder E, et al. Proinflammatory cytokines in acute myocardial infarction with and without cardiogenic shock. *Clin Res Cardiol Off J Ger Card Soc*. 2008;97(5):298-305. doi:10.1007/s00392-007-0626-5

97. Frangogiannis NG, Smith CW, Entman ML. The inflammatory response in myocardial infarction. *Cardiovasc Res*. 2002;53(1):31-47. doi:10.1016/S0008-6363(01)00434-5

98. Emmens RW, Wouters D, Zeerleder S, van Ham SM, Niessen HWM, Krijnen PAJ. On the value of therapeutic interventions targeting the complement system in acute myocardial infarction. *Transl Res*. 2017;182:103-122. doi:10.1016/j.trsl.2016.10.005

99. Kim GH, Mocco J, Hahn DK, et al. Protective Effect of C5a Receptor Inhibition after Murine Reperfused Stroke. *Neurosurgery*. 2008;63(1):122-126. doi:10.1227/01.NEU.0000335079.70222.8D

100. Wetsel RA, Fleischer DT, Haviland DL. Deficiency of the murine fifth complement component (C5). A 2-base pair gene deletion in a 5'-exon. *J Biol Chem*. 1990;265(5):2435-2440.

101. Wheat WH, Wetsel R, Falus A, Tack BF, Strunk RC. The fifth component of complement (C5) in the mouse. Analysis of the molecular basis for deficiency. *J Exp Med*. 1987;165(5):1442-1447. doi:10.1084/jem.165.5.1442

102. Ooi YM, Colten HR. Genetic defect in secretion of complement C5 in mice. *Nature*. 1979;282(5735):207-208. doi:10.1038/282207a0

103. Stimpfling JH, Reichert AE. Strain C57BL-10ScSn and its congenic resistant sublines. *Transplant Proc*. 1970;2(1):39-47.

104. Nilsson UR, Müller-Eberhard HJ. Deficiency of the fifth component of complement in mice with an inherited complement defect. *J Exp Med*. 1967;125(1):1-16. doi:10.1084/jem.125.1.1

105. Höpken UE, Lu B, Gerard NP, Gerard C. The C5a chemoattractant receptor mediates mucosal defence to infection. *Nature*. 1996;383(6595):86-89. doi:10.1038/383086a0

106. Klein L, Stevenson S, Shaffer JW, Davy D, Goldberg VM. Bone mass and comparative rates of bone resorption and formation of fibular autografts: Comparison of vascular and nonvascular grafts in dogs. *Bone*. 1991;12(5):323-329. doi:10.1016/8756-3282(91)90018-E

107. Carulli C, Innocenti M, Brandi ML. Bone Vascularization in Normal and Disease Conditions. *Front Endocrinol*. 2013;4:106. doi:10.3389/fendo.2013.00106

108. Nobuto T, Suwa F, Kono T, et al. Microvascular Response in the Periosteum Following Mucoperiosteal Flap Surgery in Dogs: Angiogenesis and Bone Resorption and Formation. *J Periodontol*. 2005;76(8):1346-1353. doi:10.1902/jop.2005.76.8.1346

109. Editor DT. Blood Supply to Femoral Head & Neck. Wheeless' Textbook of Orthopaedics. Published July 22, 2020. Accessed March 30, 2023. https://www.wheelessonline.com/joints/blood-supply-to-femoral-head-neck/

110. Editor DT. Blood Supply of the Spinal Cord. Wheeless' Textbook of Orthopaedics. Published July 22, 2020. Accessed March 30, 2023. https://www.wheelessonline.com/bones/blood-supply-of-the-spinal-cord/

111. Scola AM, Johswich KO, Morgan BP, Klos A, Monk PN. The human complement fragment receptor, C5L2, is a recycling decoy receptor. *Mol Immunol*. 2009;46(6):1149-1162. doi:10.1016/j.molimm.2008.11.001

112. Li R, Coulthard LG, Wu MCL, Taylor SM, Woodruff TM. C5L2: a controversial receptor of complement anaphylatoxin, C5a. *FASEB J Off Publ Fed Am Soc Exp Biol*. 2013;27(3):855-864. doi:10.1096/fj.12-220509

113. Birdsall HH, Green DM, Trial J, et al. Complement C5a, TGF-β1, and MCP-1, in Sequence, Induce Migration of Monocytes Into Ischemic Canine Myocardium Within the First One to Five Hours After Reperfusion. *Circulation*. 1997;95(3):684-692. doi:10.1161/01.CIR.95.3.684

114. Ma Y. Role of Neutrophils in Cardiac Injury and Repair Following Myocardial Infarction. *Cells*. 2021;10(7):1676. doi:10.3390/cells10071676

115. Berkley KJ, Zalcman SS, Simon VR. Sex and gender differences in pain and inflammation: a rapidly maturing field. *Am J Physiol-Regul Integr Comp Physiol*. 2006;291(2):R241-R244. doi:10.1152/ajpregu.00287.2006

116. Rathod K, Kapil V, Velmurugan S, et al. Sex differences in the inflammatory response and inflammation-induced vascular dysfunction. *The Lancet*. 2017;389:S20. doi:10.1016/S0140-6736(17)30416-6

117. Varghese M, Clemente J, Lerner A, et al. Monocyte Trafficking and Polarization Contribute to Sex Differences in Meta-Inflammation. *Front Endocrinol*. 2022;13. Accessed April 5, 2023. https://www.frontiersin.org/articles/10.3389/fendo.2022.826320